Applications of the Electric Potential Sensor for Healthcare and Assistive Technologies

Natasha Steinhausen

Submitted for the degree of Doctor of Philosophy

March 2014

Sensor Technology Research Centre

University of Sussex,

Falmer, Brighton, UK, BN1 9QT

Declaration

I hereby declare that this thesis has not been and will not be submitted in whole or in part to another University for the award of any other degree.

Natasha Steinhausen

UNIVERSITY OF SUSSEX

NATASHA STEINHAUSEN

APPLICATIONS OF THE ELECTRIC POTENTIAL SENSOR FOR HEALTHCARE AND ASSISTIVE TECHNOLOGIES

SUMMARY

The work discussed in this thesis explores the possibility of employing the Electric Potential Sensor for use in healthcare and assistive technology applications with the same and in some cases better degrees of accuracy than those of conventional technologies. The Electric Potential Sensor is a generic and versatile sensing technology capable of working in both contact and non-contact (remote) modes. New versions of the active sensor were developed for specific surface electrophysiological signal measurements. The requirements in terms of frequency range, electrode size and gain varied with the type of signal measured for each application. Real-time applications based on electrooculography, electroretinography and electromyography are discussed, as well as an application based on human movement.

A three sensor electrooculography eye tracking system was developed which is of interest to eye controlled assistive technologies. The system described achieved an accuracy at least as good as conventional wet gel electrodes for both horizontal and vertical eye movements. Surface recording of the electroretinogram, used to monitor eye health and diagnose degenerative diseases of the retina, was achieved and correlated with both corneal fibre and wet gel surface electrodes. The main signal components of electromyography lie in a higher bandwidth and surface signals of the deltoid muscle were recorded over the course of rehabilitation of a subject with an injured arm. Surface electromyography signals of the bicep were also recorded and correlated with the joint dynamics of the elbow. A related non-contact application of interest to assistive technologies was also developed. Hand movement within a defined area was mapped and used to control a mouse cursor and a predictive text interface.

Acknowledgements

It is with great pleasure and relief that I have arrived at this point, where I can acknowledge and thank all of those who have helped, supported and guided me along the way. Firstly I must thank Prof Robert Prance and Dr Helen Prance for their endless support through the ups and downs I have experienced throughout this work. I would also like to extend my thanks and appreciations to Martin Nock for his invaluable technical advice, both in the lab and on my bicycles.

Huge thanks must go to Andrew McAlley for the enormous amount of support over the years, especially during this last long haul where the thesis has been omnipresent!

To James Birchall, good times were had and good times were lost. Thanks for absolutely everything buddy. Phil Watson, you were a fantastic sounding board. Thanks for letting me ask so many questions that I did not need the answers to. Shrijit and Moustachio, it was a pleasure sharing an office with you both, thank you for all the laughs. Finally I would like to thank all of my friends and family who have been there for me over the years; I could not have done this without you.

Contents

List of Publications ..... **vii**

List of Figures ..... **viii**

List of Tables ..... **xv**

1 Introduction **1**

1.1 The Electric Potential Sensor *3*

1.2 Thesis Overview *10*

2 Position Sensing using the Ambient Electric Field **12**

2.1 Introduction *12*

2.2 One Dimensional Position Sensing *13*

2.2.1 Method 13

2.2.2 Results 15

2.3 Two Dimensional Position Sensing *17*

2.4 Mouse Control *24*

2.4.1 Usability Testing 26

2.5 Discussion and Future Work *28*

3 A Three Sensor Eye Tracking System based on Electrooculography (EOG) **30**

3.1 Introduction *30*

3.2 The Electrooculogram *31*

3.3 Method *33*

3.3.1 Results 36

3.4 Further Experiments *40*

3.4.1 Results 40

3.5 Calibration and Normalisation *42*

3.6 Feature Extraction *45*

3.7 Discussion and Future Work *48*

4 Surface Recording of an Evoked Potential: The Electroretinogram (ERG) **49**

4.1 Introduction *49*

4.2 The Electroretinogram *50*

4.3 Initial Experiments *53*

4.3.1 Method 53
4.3.2 Results 55

4.4 Further Experiments 61
4.4.1 Method 61
4.4.2 Results 61

4.5 Discussion and Future Work 66

5 Upper Limb Rehabilitation using Surface Electromyography (SEMG) and Real-Time Biofeedback 67

5.1 Introduction 67
5.1.1 SEMG Signal Characteristics 68
5.1.2 Biofeedback and Rehabilitation 69

5.2 Method 70
5.2.1 System 71
5.2.2 Procedure 73

5.3 Results 75

5.4 Discussion 79

6 SEMG Recordings of the Bicep Muscle During Fixed Trajectory Movements 81

6.1 Introduction 81

6.2 Method 82

6.3 Results 84

6.4 Discussion and Future Work 91

7 Conclusions 92

References 96

Appendices 107

Appendix A. EPIC Movement Sensor Data Sheet 107

Appendix B. LabVIEW Virtual-Instrument (VI) Program Code 112

Appendix C. Matlab Code 126

Appendix D. Additional Surface Electromyography Results 130

Appendix E. System Performance Characterisation 135
1 Statistical Hypothesis Testing 135
2 Benchmarking and Quality Assessment 137
3 Algorithm Performance Testing for Assistive Technology Applications 139

List of Publications

1. **N. Steinhausen**, *Wearable EOG Sensors for Assistive Technologies*, Presentation at the Postgraduate Conference on Biomedical Engineering and Medical Physics, University of Surrey, June 2013

2. **Natasha Steinhausen**, Helen Prance and Robert Prance*, Human Computer Interface based on the Eye Movement (EOG) Signals,* Presentation and paper at 11th Annual Conference for the Advancement of Assistive Technology, Maastricht, September 2011

3. **N. Steinhausen**, H. Prance, C. J. Harland, P. Watson, S.T. Beardsmore-Rust, R.J. Prance, *Active, insulated electrode sensors for measuring physiological parameters,* EPSRC KT-EQUAL consortium event, Bath, June 2010

4. Florian Hirth, Thorbjörn C. Buck, **Natasha Steinhausen** and Alexander W. Koch *Performance of a combined chromatic confocal microscope with thin film reflectometer*, Proc. SPIE 7729, Scanning Microscopy, 77291L, June 03, 2010, DOI: 10.1117/12.853517

List of Figures

Figure 1.1 Schematic block diagram of the Electric Potential Sensor.....4

Figure 1.2 Operational modes of the Electric Potential Sensor: (a) non-contact and (b) contact 5

Figure 1.3 Illustration of the Electric Potential Sensor that was used for electrophysiological sensing applications including electrode dimensions 6

Figure 1.4 Electric Potential Sensor block diagram demonstrating the employed configuration of filters and amplification.....7

Figure 1.5 Sensor gain-frequency measurements for (a) eye sensors and (b) muscle sensors..8

Figure 1.6 Sensor noise measurements for (a) eye sensors and (b) muscle sensors, peaks on the graphs represent 50 Hz mains noise and associated harmonics within the system ...9

Figure 2.1 Illustration of inference of a hand at position *d*, equidistance between two sensors positioned and d_A at d_B 14

Figure 2.2 Block diagram demonstrating the configuration of sensors, DAQ and associated software components.....15

Figure 2.3 Differential measurements between sensor *A* and *B* on the *x* axis, across the field of interest for 30 mm incremental hand positions 16

Figure 2.4 Differential measurements between sensor *A* and *B* (*y* axis), across the field of interest for 30 mm incremental hand positions 17

Figure 2.5 Configuration of four sensors on a two-dimensional plane for hand tracking experiments 18

Figure 2.6 Inferred hand position in the target tracking area for the four sensor configuration, hand was traced from left to right with the palm facing to the left at *y* axis positions of -0.6, 0 and -0.6.....19

Figure 2.7 Single sensor output RMS voltage measurements (*y* axis) across the field of interest for 30 mm incremental hand positions 20

Figure 2.8 Normalised and calibrated single sensor RMS output voltage measured for hand position varied over the y axis 21

Figure 2.9 Illustration of the five sensor configuration used for two-dimensional hand tracking experiments.....22

Figure 2.10 Flowchart illustrating the interpretation of normalised and calibrated sensor data in determining hand position.....23

Figure 2.11 Inferred hand position in the target tracking area for the five sensor configuration, hand was traced from left to right with the palm facing to the left at *y* axis positions of -0.6, 0 and -0.6.....24

Figure 2.12 Flowchart illustrating the interpretation of real-time hand position information in determining mouse cursor position 26

Figure 2.13 Screen shot of the Dynamic Keyboard used during usability testing of the real-time interface between hand position and mouse cursor control, developed by CanAssist [88].....27

Figure 3.1 Typical facial electrode positions for acquiring horizontal and vertical EOG signals 32

Figure 3.2 Illustration of three Electric Potential Sensors mounted to a headband, configured for acquiring horizontal and vertical EOG signals 34

Figure 3.3 Block diagram demonstrating the configuration of sensors, DAQ and the associated software components for acquiring horizontal and vertical EOG signals 35

Figure 3.4 Gaze position grid used during eye movement experiments; subjects were instructed to direct their gaze toward each of the dots as focal points.....36

Figure 3.5 Measured EOG signals for eye movements at 10° intervals between 0° and ±40°, with gaze returning to centre position after each movement, for horizontal eye movements (a) and vertical eye movements (b) 37

Figure 3.6 Change in EOG amplitude (step size) versus gaze position angular displacement for horizontal eye movements: left and right 38

Figure 3.7 Change in EOG amplitude (step size) versus gaze position angular displacement for vertical eye movements: up and down 39

Figure 3.8 Horizontal EOG amplitude versus gaze position angular displacement across eight subjects; blue line represents the lowest measured sensitivity, the red line represents the highest measured sensitivity 41

Figure 3.9 Vertical EOG amplitude versus gaze position angular displacement across eight subjects; blue line represents the lowest measured sensitivity, the red line represents the highest measured sensitivity 42

Figure 3.10 Calibration screen: during the calibration routine the user is instructed to make a series of eye movements between locations represented by the dots: left, right, down

and up, starting and ending at the central resting position in the middle of the screen. 43

Figure 3.11 EOG Signals recorded during a calibration routine: (a) Horizontal EOG, negative signal shows the eyes looking far left, positive shows eyes far right (b) Vertical EOG, negative is down, positive is up. 44

Figure 3.12 Flowchart showing how the calibration routine is implemented in software in order to normalise the real-time EOG signals.....45

Figure 3.13 Example EOG signals for typical eye movements occurring during human machine interaction, acquired by the Electric Potential Sensor: (a) Horizontal (b) Vertical 46

Figure 3.14 Flowchart showing how the feature extraction routine is implemented in software in order to identify characteristics of the real-time EOG signals 47

Figure 4.1 The basic waveform of the electroretinogram showing the a-wave arising from solely the rods and cones and the b-wave arising from cells of the retina , taken from [67].....50

Figure 4.2 a- and b-wave amplitude and time measurements of the basic ERG waveform, taken from [67] 51

Figure 4.3 Different types of corneal electrodes used for acquiring ERGs (a) Contact lens (b) Hook (c) Cotton wick with speculum and (d) DTL fibre, images taken from [67] 52

Figure 4.4 Block diagram demonstrating the configuration of sensors, LED stimulus, DAQ and the associated software components for acquiring ERG, including facial EPS placements 54

Figure 4.5 Comparison of photopic ERG signals resulting from a 5 Hz full-field LED stimulus measured by the EPS, DTL fibre and Ag-AgCl electrodes, signals averaged 50 times over a 200 ms period 56

Figure 4.6 Frequency domain measurement of the 5 Hz evoked potential with the eye closed (a) and open (b) in order to verify the signal 57

Figure 4.7 Implicit time indications on 5 Hz ERGs recorded from: the EPS (blue), DTL (green) and Ag-AgCl skin electrodes (red) 58

Figure 4.8 Comparison of implicit time measurements from photopic ERG signals resulting from a 30 Hz full-field LED stimulus, measured by the EPS, DTL fibre and Ag-AgCl electrodes, signals averaged 100 times over a 90 ms period.....59

Figure 4.9 Frequency domain measurement of the 30 Hz evoked potential with the eye closed (a) and open (b) in order to verify the signal 60

Figure 4.10 Comparison of implicit time measurements from photopic ERG signals resulting from a 30 Hz full-field LED stimulus, measured simultaneously by the EPS and DTL fibre electrodes, signals averaged 10 times over a 70 ms period 62

Figure 4.11 Frequency domain measurement of the 30 Hz evoked potential comparison between signals measured with a DTL fibre (a) and the EPS (b).....63

Figure 4.12 EPS measurement of five ERG responses to 1 Hz stimulus over 4.5 seconds 64

Figure 4.13 Comparison of non-averaged photopic ERG signals resulting from a 1 Hz full-field LED stimulus measured simultaneously by the EPS and DTL fibre electrodes 64

Figure 4.14 Comparison of implicit time measurements from photopic ERG signals resulting from a 1 Hz full-field LED stimulus, measured simultaneously by the EPS and DTL fibre electrodes 65

Figure 5.1 Illustration of how the EMG signal results from a summation of Action Potentials originating from the central nervous system, taken with permission from [61].....68

Figure 5.2 Block diagram demonstrating the configuration of sensors, DAQ and the associated software components for acquiring SEMG signals.....72

Figure 5.3 Real-time Biofeedback rehabilitation graphical user interface showing muscular activity for the left and right side of the body 72

Figure 5.4 Normal shoulder range of motion: (a) Flexion, from 0° to 180° (b) Abduction, from 0° to 180°, taken from [173].....73

Figure 5.5 EPS electrode placement for acquiring SEMG signals during rehabilitation exercises, taken from [174].....74

Figure 5.6 Comparison of normalised SEMG signals for right (injured) and left (healthy) shoulder muscles during a 30° abduction of the arms 76

Figure 5.7 Comparison of normalised SEMG signals for right (injured) and left (healthy) shoulder muscles during a 30° flexion of the arms 77

Figure 5.8 Comparison of the difference between the normalised SEMG amplitudes for the right and the left shoulder over the course of rehabilitation for a 30° abduction (a) and a 30° flexion (b) 78

Figure 5.9 Comparison of the difference between the normalised SEMG amplitudes for the right and the left shoulder over the course of rehabilitation for a 60° abduction (a) and a 60° flexion (b) 78

Figure 5.10 Comparison of the difference between the normalised SEMG amplitudes for the right and the left shoulder over the course of rehabilitation for a 90° abduction (a) and a 90° flexion (b) 79

Figure 6.1 Experimental model of the arm manipuladum apparatus 82

Figure 6.2 Configuration of the apparatus used to measure real-time physical joint deflection angles, including EPS placement locations used to measure real-time SEMG signals from the bicep, based on image taken from [181] 83

Figure 6.3 Graphical user interface showing real-time joint movement measurements, displayed to the subject during the limb dynamics experiment 84

Figure 6.4 Right arm data: (a) Rectified SEMG and normalised physical limb movement, to 18° target (b) RMS SEMG with a 500 ms window and normalised limb movement (c) Normalised SEMG as %MVIC 85

Figure 6.5 Right bicep normalised SEMG amplitudes (blue) and normalised physical limb movements (red) to target angles of (a) 18° (b) 36° (c) 54° (d) 72° and (e) 90° 86

Figure 6.6 Right bicep: Averaged normalised RMS SEMGs for x10 lower arm movements to different target angle 87

Figure 6.7 Normalised left and right bicep SEMG versus limb target angle 88

Figure 6.8 Right arm limb dynamics for fixed movement trajectory, x10 averages: (a) limb trajectory data (b) angular velocity (c) angular acceleration (d) joint torque 89

Figure 6.9 Peak joint torque developed during fixed trajectory movement versus limb target angle 90

Figure 6.10 Normalised SEMG amplitude versus peak joint torque developed during fixed trajectory movement: (a) Left arm (b) Right arm 90

Figure B1.1 Main LabVIEW code for one dimensional position sensing 113

Figure B1.2 LabVIEW program code for calculating sensor RMS voltage used for inferring hand position on a one dimensional plane 114

Figure B1.3 LabVIEW program code for normalised hand position determination on a one dimensional plane 114

Figure B1.4 Graph showing inferred hand position on one dimensional plane 114

Figure B1.5 LabVIEW program code for normalised hand position determination on a two dimensional plane 115

Figure B1.6 Graphical display of inferred hand position on two dimensional plane 115

Figure B1.7 Hand position sensing program front panel user interface 116

Figure B2.1 Main LabVIEW program code for acquiring and recording EOG signals 118

Figure B2.2 LabVIEW front panel display used during EOG eye-tracking program experiments 119

Figure B2.3 Eye-tracking LabVIEW sub-VI -"LOAD": Continuously loads real-time EOG signals until change in amplitude occurs signifying an eye movement. 120

Figure B2.4 Eye-tracking LabVIEW sub-VI - "TRACK": Changes in EOG amplitudes are loaded into a buffer in order to determine the magnitude of the eye movement. 120

Figure B2.5 Eye-tracking LabVIEW sub-VI - "EOG OUTPUT":Outputs the magnitude of the amplitude change that occurred during an eye movement once the eye movement is complete. 121

Figure B3.1 Main LabVIEW program code for acquiring and recording the electroretinogram (ERG) 123

Figure B3.2 LabVIEW front panel display for electroretinogram (ERG) experiments 123

Figure B4.1 Main LabVIEW program code for acquiring and recording SEMG signals 125

Figure C.1 Signal averaging and graphing MATLAB program code used for the 5 Hz stimulus ERG 127

Figure C.2 Signal averaging and graphing MATLAB program code used for the 30 Hz stimulus ERG 128

Figure C.3 Fast Fourier Transform calculation and graphing MATLAB program code user during ERG signal processing 129

Figure D.1 Comparison of normalised SEMG signals for right (injured) and left (healthy) shoulder muscles during a 60° abduction of the arms 131

Figure D.2 Comparison of normalised SEMG signals for right (injured) and left (healthy) shoulder muscles during a 60° flexion of the arms 131

Figure D.3 Comparison of normalised SEMG signals for right (injured) and left (healthy) shoulder muscles during a 90° abduction of the arms 132

Figure D.4 Comparison of normalised SEMG signals for right (injured) and left (healthy) shoulder muscles during a 90° flexion of the arms 132

Figure D.5 Left bicep normalised SEMG Amplitudes and physical limb movement to target angles of (a) 18° (b) 36° (c) 54° (d) 72° and (e) 90° 133

Figure D.6 Right bicep: Averaged RMS EMGs for x10 lower arm movements to each target angle 134

List of Tables

Table 1.1 Characteristic measured values of input impedances for eye and muscle sensors ...6

Table 1.2 Integrated noise voltage over the operating bandwidth represented in the graphs above for eye and muscle sensors 9

Table 2.1 Feedback scores reported by usability study group for real-time hand sensing system with mouse control and predictive text program 28

Table 3.1 Output results from the EOG feature extraction algorithm with the eye movement signals presented in Figure 3.13 as the input.....47

Table 4.1 Standard ERG measurements and stimuli, as set by ISCEV [60] 52

Table 4.2 Implicit time measurements from 5 Hz flash ERG 58

Table 4.3 Implicit time measurements from 30 Hz flicker ERG 60

Table 4.4 Implicit time measurements from 30 Hz flicker ERG 62

Table 4.5 Implicit time measurements from the 1 Hz flash ERG 65

Table 5.1 Maximum shoulder deflection angles, where no shoulder deformation occurred, during monitoring of rehabilitation exercises 75

Table E.1 Table outlining the chapters, specific repeated measurements and metrics that would be used to validate the EPS results using a statistical hypothesis test.....135

Table E.2 Table outlining the chapters, suggested systems for comparison and metrics that would be used to benchmark using a statistical hypothesis test.....137

1 Introduction

The UK is currently facing significant growth in the elderly population aged 65 and older, with an estimated 47% increase by the year 2026 [1]. Life expectancies in the UK have also risen tremendously with projected life expectancies rising to 94.2 for males and 97.2 for females by 2037 [2]. These two factors coupled with an increasing number of people wishing to spend their elderly years in the comfort of their own homes, are putting a tremendous strain onto resources [3]. Healthcare and monitoring is no longer situated solely in the clinical environment; there is a growing trend for these technologies to be available in the home. Quality of life is an important driving factor not only for the elderly but for disabled persons as well [1, 4]. Among both the elderly and disabled, the challenges of maintaining mobility and cognitive function make it increasingly difficult to remain living independently. As a result many are forced pay for home carers or to seek residence in clinical institutions in order to receive constant medical supervision. In efforts to minimise these situations many healthcare monitoring and assistive technologies (AT) have been developed. Advancements in the technologies must be such that the applications can easily be used by the general population with little to no instruction or medical background. Assistive technology and home health monitoring sensors find applications for monitoring temperatures, pressures, positions, and biological signals of patients. Sensors can play an important role in enhancing the safety and improving the quality of life in the healthcare arena. Sensors are increasingly being used in healthcare applications due to their accuracy, intelligence, capability, reliability, small size, and low power consumption.

Sensing systems for healthcare and assistive technologies can be broadly separated into three categories: monitoring, mobility and communication. Monitoring applications range from occupancy sensing [5-8] and fall detection for the elderly [9] to clinical observation of biological signals for use in diagnostics [10, 11] and rehabilitation [12-18]. Various mobility aid systems have been presented, including eye, brain and muscle controlled wheelchairs [19-25]. Mobility enhancement systems based on biological signals have been presented [26-29], where muscle signals are interfaced with robot exoskeletons aiming to encourage mobility following a stroke. Several eye controlled typing systems which aid communication have been developed [30-33], and there are already some commercially available systems [34].

Many of these sensing systems rely on electrophysiological signals. Electrophysiology describes the changes in electric potential which occur within the body as a result of various biochemical functions and can be measured as changes in voltages or currents at the surface of the body. These signal levels range from micro to millivolts in amplitude, and from quasi-DC up to 5 kHz. Essential requirements of sensors for biopotentials and movement sensing are the ability to separate small amplitude signals of interest, in low frequency bands, with several types of environmental and biological sources of interference. To achieve these qualities the sensors generally rely on high gain in differential mode, low common mode gain, high input impedance and low noise profiles. Conventional sensing techniques employ needle or surface electrodes which are placed in direct electrical contact with fibres or skin. Needle electrodes are highly invasive and hence not suitable for AT applications. Skin electrodes on the other hand have been highly regarded as a great advance in the technologies underpinning developments in consumer AT. They provide a cheap and easy to use method for acquiring electrophysiological signals directly from the skin with minimal invasiveness. There are two types of surface electrodes: wet and dry. Wet electrodes provide a resistive DC coupling to the source, in this case the human body, which provides great amplification capabilities at the low-end of the required bandwidth. However there are significant drawbacks due to the effects of DC drift. There are also limiting factors with regards to long term monitoring; the use of conductive gels means that signal levels will degrade over time as the gel dries out. Several forms of dry electrodes exist which do not require the use of conductive gels: metal-plate, textile and spiked. These however can suffer negative effects on signal qualities if changes in contact body impedances occur, resulting from sweat, body hair and temperature changes [35, 36].

Another sensing technique that has been successful does not rely on a resistive contact between skin and electrode and instead capacitively couples to surface potentials, through a thin insulating dielectric layer [35, 37]. The insulation layer provides a high resistance between the subject and electrode, creating a capacitive coupling between them. A thin insulating layer is required in order to create a large capacitance necessary for a strong coupling to the source. Since acquiring signals from this type of sensor is not reliant on a resistive skin contact, skin preparation is not necessary and changes in contact resistance will have no effect. They can however still suffer the effects of movement artefacts and charge sensitivity [38]. This type of insulated electrode has been around since 1967, where the electrode was a plate of anodised aluminium and the dielectric was provided by aluminium oxide [39]. Advancements have been made in this sensing technology over the years, several research papers have been published on capacitively coupled sensors acquiring high quality electrocardiograms (ECGs) [40, 41] and

electroencephalograms (EEGs) [40, 42]. A direct comparison of simultaneous ECG and EEG measurements between capacitively coupled electric potential sensors and wet electrodes was presented with evidence suggesting a high correlation of data; however no details of the insulating capacitive coupling layer were provided [40]. A multi-channel USB powered system comprising of 15 capacitively coupled electrodes has also demonstrated a high correlation when compared to wet surface electrodes while recording ECGs. This system states that the insulating layer is comprised of a thin plastic layer, however no thickness or plastic composition details were included in the report [41]. Soft dry foam has been used as the insulating layer while acquiring EEG measures. The electrodes were mounted on a cap; however this did not provide adequate contact for high quality EEG signals. In this instance, there was not enough applied pressure, but when the electrodes were held firmly against the scalp successful measurements of the EEG signal were achieved [42].

A capacitively coupled Electric Potential Sensor (EPS) is the basis of the work presented here. The EPS overcomes the limitations presented by wet and dry DC electrodes, as discussed above, and has been successfully applied to the non-invasive monitoring of high resolution electrophysiological signals [43]. High quality surface recordings of electrooculograms (EOGs), electromyograms (EMGs), electrocardiograms (ECGs) and electroencephalograms (EEGs) have been demonstrated [44-52]. It has also been possible to use the EPS as an electric field meter to detect human movement from the changes within the ambient electric field [53-55].

1.1 The Electric Potential Sensor

The EPS is a generic electric field sensing technology that was designed, developed and patented at the University of Sussex [44, 56]. This thesis will discuss a range of possible applications concerned with assistive and healthcare technologies, employing various configurations of the EPS. The EPS technology has been developed using an ultra-high impedance amplifier design technique coupled with a capacitive input electrode structure, with the aim of allowing a broad range of measurement approaches. The sensors are capable of detecting changes in an electric field passively, causing no disturbances to said field. This non-disruptive capability is due to the high input impedance and capacitive electrode at the input of the sensor. Effective input impedances typically as high as 10^{15} Ω and 10^{-16} F have been achieved through the use of several types of positive feedback, guarding and active electrode techniques. The EPS design maintains a stable DC bias point and hence does not

suffer the effects of DC drift. Figure 1.1 shows a block diagram based schematic of the EPS, including the positive feedback techniques employed to achieve the input impedance boost.

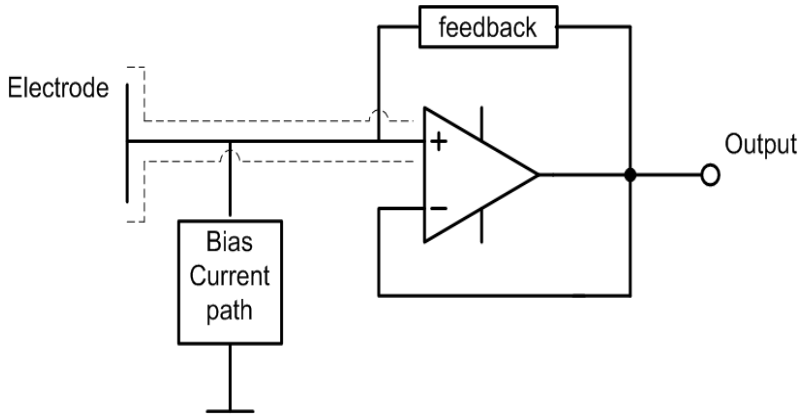

Figure 1.1 Schematic block diagram of the Electric Potential Sensor

Depending on specifications such as bandwidth, gain and input impedance, the EPS is capable of measuring a range of physical properties. These capabilities include measurements of biological signals, movement signals, material properties and charge detection. Operational bandwidths depend on the amplifier design, noise performance and coupling conditions. In various versions, the sensors can operate from <1 mHz to >100 MHz. Two modes of operation are possible: contact and non-contact [43] (shown in Figure 1.2). In contact mode, these electrodes are capacitively coupled probes, where the sensor input is coupled through a defined capacitance to a known source. When configured in non-contact mode, the electrode is considered an electric field probe, where the coupling capacitance is not well defined and there is physical space between the sensor and source. In this mode the sensor performance depends on a combination of the leakage capacitance between the probe and ground and the front end input capacitance of the sensor. The sensor operates by measuring the displacement current created by a change in electric field. This change will vary in amplitude whether working in contact or non-contact mode with the sensor, and hence requirements of the sensor will change with respect to gain and input impedance.

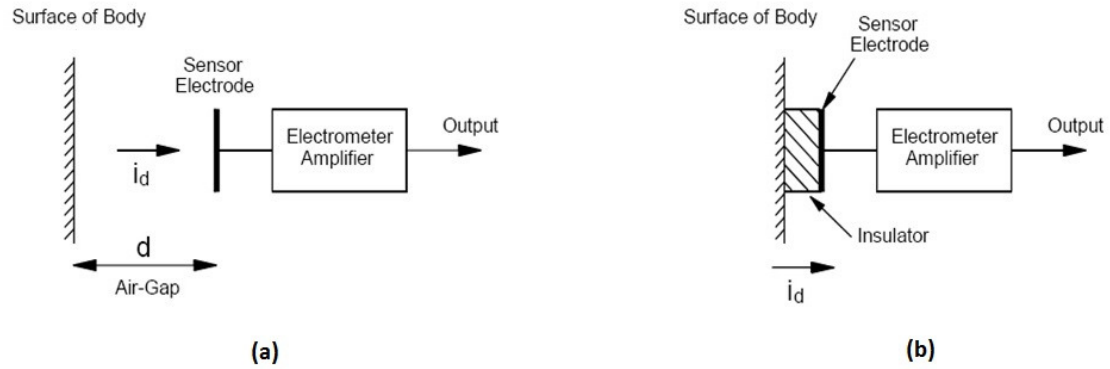

Figure 1.2 Operational modes of the Electric Potential Sensor: (a) non-contact and (b) contact

The application discussed in chapter 2 employs a commercially available EPS, developed under licence to University of Sussex by Plessey Semiconductors [57]. In this case the sensor is configured in non-contact mode. Full sensor details can be found Appendix A.

When monitoring biological signals in contact mode, the EPS is configured such that it is in electrical isolation from the skin via a thin insulator at the surface of the electrode; hence there is no requirement for cutaneous electrical contact. Changes in voltage at the skin are monitored by sensing the displacement current that arises due to the strong capacitive nature of the sensor input. Two different sensors were designed in order to acquire biological signals: specifically, eye signals and muscle signals. The sensors have identical physical properties, shown in Figure 1.3. They comprise of circular anodised titanium electrodes, 5 mm in diameter surrounded by guarding making the full sensor contact diameter 10 mm. The amplitude and frequency spectrum of each type of signal investigated made the requirements for each sensor different.

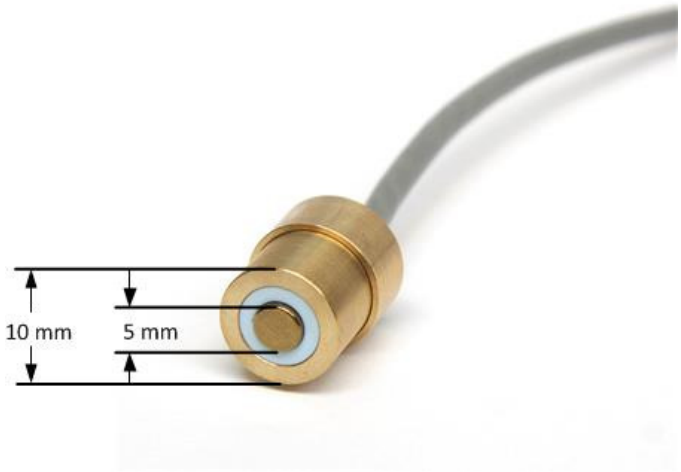

Figure 1.3 Illustration of the Electric Potential Sensor that was used for electrophysiological sensing applications including electrode dimensions

Characterisation of the sensors required several measurements, including input impedance, gain and noise profiles. Input impedances were determined with measurements of frequency response at the sensor output, with a signal applied at the input through a known coupling capacitance. The input impedance of the sensor is expressed as a separate input resistance and capacitance, which together create a high pass filter. Extracting the corner frequency of the high pass roll-off enables determinations of R_{in} and C_{in}. A further in-depth description of these measurements can be found in the literature [58]. Input impedance measurement results for the sensors, specifically for eye and muscle signal acquisition, are shown in Table 1.1.

Table 1.1 Characteristic measured values of input impedances for eye and muscle sensors

	$\boldsymbol{R_{in}}$	$\boldsymbol{C_{in}}$
Eye sensors	52.7 GΩ	7.54 pF
Muscle sensors	0.7 GΩ	11.15 pF

The eye signals presented in this thesis range in frequency between 1 Hz and 40 Hz, with typical amplitudes in the microvolt range [59, 60]. Muscle signals available at the skin typically range from micro to millivolts and their main power spectrum lies between 10 Hz and 250 Hz. However EMG sensors typically allow for a much greater bandwidth [61-63].

Figure 1.4 shows a block diagram for the sensors. Both sensors provide a gain of x114, which is provided by two stages of amplification. The eye sensors have a bandwidth from 0.1 Hz to 86 Hz and the muscle sensors have a bandwidth from 10 Hz to 3 kHz. The sensor bandwidth is determined by a first order bandpass filter consisting of resistor and capacitor pairs, where values of *R* and *C* were chosen based on transfer function associated with first order filters [$fc = (2\pi RC)^{-1}$].

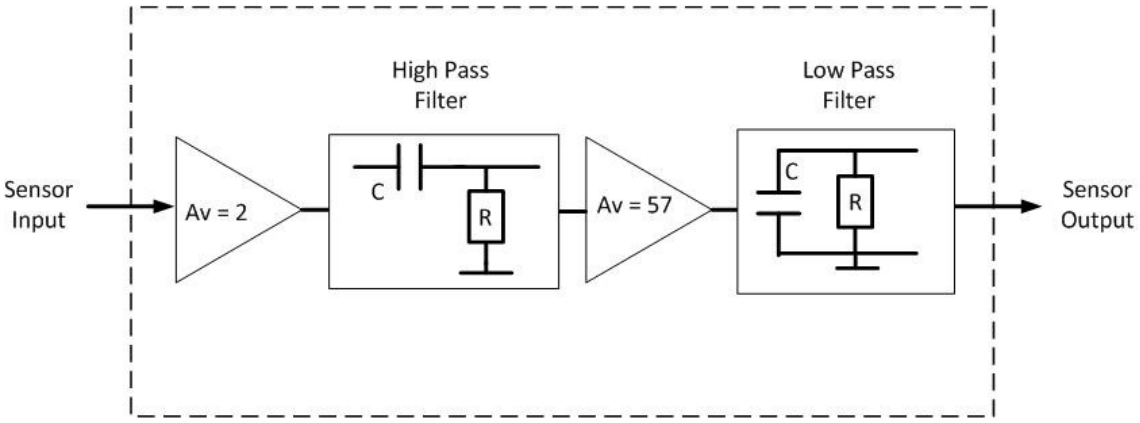

Figure 1.4 Electric Potential Sensor block diagram demonstrating the employed configuration of filters and amplification

Gain-frequency measurements for both sensors were achieved by injecting a signal through a conductive rubber pad on the input electrode. A swept sine measurement was carried out, results of which can be seen in Figure 1.5.

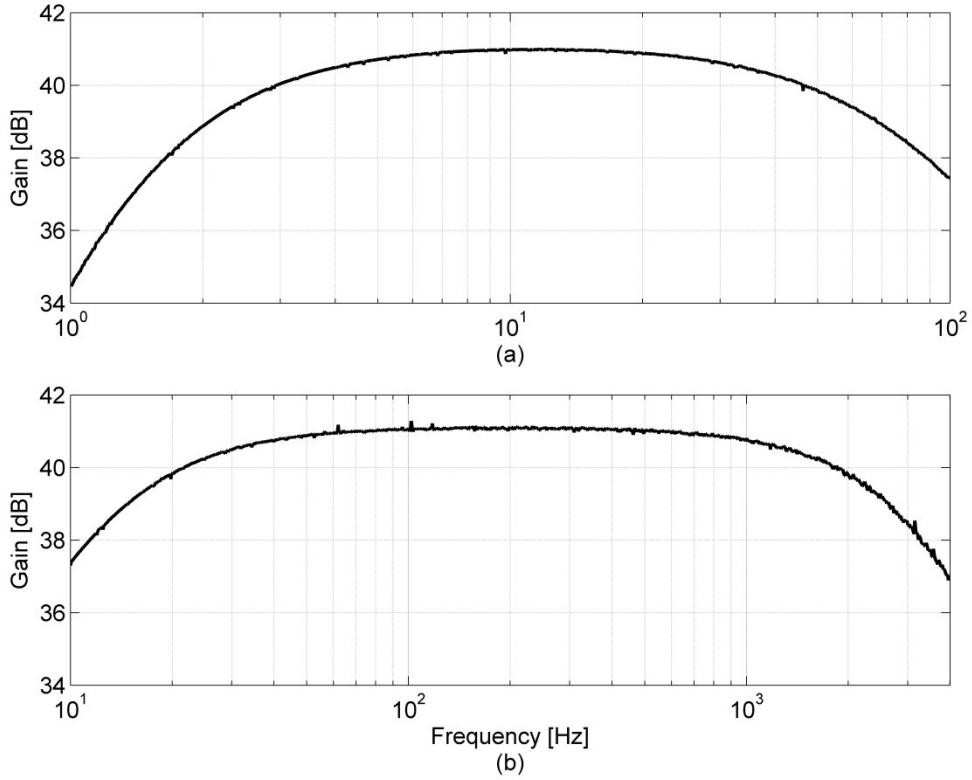

Figure 1.5 Sensor gain-frequency measurements for (a) eye sensors and (b) muscle sensors

Figure 1.6 shows sensor noise measurements as spectral densities, which represent both thermal and current noise. The peaks that are present on both graphs represent 50 Hz mains noise and the associated harmonics. Noise measurements of the sensors were carried out by grounding the input electrode through the conductive rubber and observing noise levels at the output of the sensor. This represents a measurement scenario which is similar to the situation encountered when measuring on body electrophysiological signals. The conductive rubber sheet mimics the surface of the skin in several ways; it is flexible and has a conductivity of ~100 Ω/square. This provides a more realistic estimation of the system noise than conventional short circuit voltage or open circuit current noise measurement techniques that can be found in the literature [58].

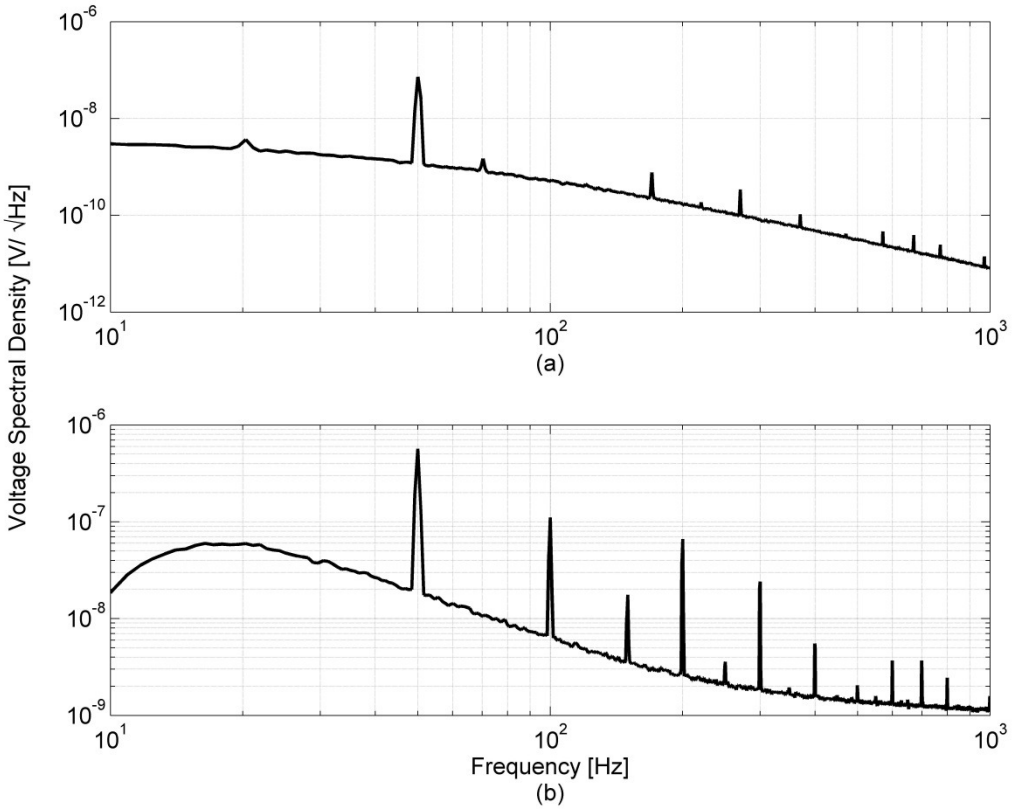

Figure 1.6 Sensor noise measurements for (a) eye sensors and (b) muscle sensors, peaks on the graphs represent 50 Hz mains noise and associated harmonics within the system

Table 1.2 Integrated noise voltage over the operating bandwidth represented in the graphs above for eye and muscle sensors

Eye Sensors	154 nV in 85.9 Hz Δf
Muscle Sensors	2.34 µV in 2990 Hz Δf

Integrated noise voltages over the sensor bandwidth are presented in Table 1.2. Results include a x1.57 bandwidth factor for the first order bandpass filter within the sensors. Results show that the noise levels presented by the sensors are far less than the expected signal levels of the biological signals arising from the eyes and muscles, which range from micro to millivolts in amplitudes. This noise can be reduced by employing additional filters, either in hardware or software, as they have lower bandwidth factors [64].

1.2 Thesis Overview

This section provides an overview of the work presented in this thesis and highlights the aspects which contribute original contributions to the field. These include the design, construction and testing of bespoke Electric Potential Sensors for use in contact mode, as discussed in the previous section. These EPS were designed for specific signal requirements as in chapters 3 and 4 for acquiring electrophysiological signals arising from the eyes (EOG and ERG) and in chapters 5 and 6 for acquiring signals arising from the muscles (EMG). In each instance, I also designed and developed the associated data acquisition, signal processing and user interface systems for a variety of healthcare and assistive technology applications. For the non-contact movement sensing application discussed in chapter 2, the commercially available EPIC[1] sensors were used. My contributions to this application were to integrate the sensors into a complete system. This involved the configuration of the sensors, and the data acquisition and signal processing systems as well as interfacing to a third party predictive text GUI.

Chapter 2 presents a full non-contact movement sensing application whereby perturbations of the ambient electric field are measured and used to infer hand positions within a defined space. Full coverage sensing is achieved employing a commercially available Electric Potential Sensor. Similar applications exist, however they are based on alternate technologies such as infrared and video sensing [65, 66]. The perturbation signals acquired by the EPS are then interfaced with a real-time position determination algorithm that maps the physical location of a hand within the sensing area to on-screen mouse cursor locations. The mouse cursor, controlled by the user, is interfaced to a predictive text program such that non-contact typing capabilities are achieved.

The remaining chapters are focussed on contact applications specifically based on electrophysiological signals. Chapter 3 presents the first demonstration of an EOG eye tracking system using electric potential sensors. A number of systems utilised this type of electrophysiological signal, however typical EOG sensing applications employ five facial electrodes for full directional eye tracking [20] whereas the system presented here provides full coverage EOG eye tracking using only three facial sensors.

---

[1] EPIC sensor provided by Plessey Semiconductors Ltd

The EPS has already been proven capable of acquiring an evoked potential arising from the brain, the electroencephalogram [52]. In chapter 4 monitoring of another type of evoked potential, the electroretinogram (ERG) which arising from the retina, is investigated. This is the first demonstration of this type of signal acquisition using the EPS. Many sensing technologies exist to acquire this type of signal; all employ DC electrodes, most of which are invasive, requiring electrodes to be placed in the eye cavity [67]. Signals acquired using the EPS are directly compared to some of these conventional electrodes and systems.

The results of a series of experiments related to muscle monitoring on both injured and healthy subjects are given in chapter 4 and chapter 5. The EPS has been used previously to demonstrate SEMG signal acquisition from the forearm [47]. Chapter 4 investigates the use of the EPS for use in a real-time biofeedback rehabilitation program. The system was used to monitor the SEMG signals from the right and left deltoid muscle during a course of rehabilitation. SEMG rehabilitation monitoring and biofeedback systems exist, however they are based on wet-gel electrodes [68, 69]. Chapter 5 aims to correlate SEMG signals from the bicep with the peak angular torque developed on a fixed trajectory motion. Many kinematic studies have been carried out in a similar manner but have, again, only employed wet-gel electrodes [70-75].

As will be shown, using the EPS has noted benefits in each of these cases. In particular the commercial potential of the technology due to the ease of use, through not requiring skin preparation, no need for electrode replacement or reapplication of conductive gels.

2 Position Sensing using the Ambient Electric Field

2.1 Introduction

Position and movement sensing applications are wide ranging: systems include occupancy monitoring for energy efficiency [76], smart homes [5, 76] and care of the elderly [6-9] to security and offender management [77]. Of particular interest with respect to assistive technologies are hand position and gesture sensing applications [65, 66, 78-81]. Hand tracking can be achieved by employing many different technologies, these include wearable sensors such as accelerometers [79, 80] and bending sensors [82], external sensors including video cameras [66, 78], infrared proximity sensors [65] and electric field sensors [81]. Due to its commercial availability, the most prevalent technology used in hand tracking systems is the use of video; however it comes with drawbacks in terms of overall usability. These systems require the user to stand directly in front of the sensing area, with the hand placed in a position easily detected by the camera. If the ambient light changes, a rapid hand movement occurs or other skin coloured objects are detected within the scene, the system will cease to operate as desired [66]. Infrared reflection techniques suffer the same disadvantages, although they can be minimised by increasing the number of infrared receivers used, however this increases costs and the working range is still small compared to that of video tracking systems [65]. While wearable sensors can overcome these disadvantages, they come with drawbacks of their own. They require the user to wear electronic sensors, which need either lengthy cables or batteries to provide power. When running on batteries, they will be limited to the usable timeframe of the battery life [83]. The use of electric field sensors has been well known since Leon Theremin's musical instrument [84]. There was a large pause in the development of this technology, up until the 1990's, when researchers wanted to overcome the problems discussed above and the field sensing technologies became more affordable [85]. Electric field sensing has advantages over the other technologies. It does not rely on line-of-sight, and thus can detect movement within any light or dark space. The sensors rely solely on detecting changes in electric fields, the processing power and data storage necessary are far smaller than that of infrared and video systems [85]. This method of hand tracking does not

require the user to wear any type of sensor, although a system has been developed where the user wears an electrode array [81]. Small scale, 5 to 150 square centimetre applications exist consisting of a transmitter and a receiver electrode, where a signal is induced into the tracking area creating a dipole field. The signal strength at the receiver varies as the hand moves further into the field; using this configuration, absolute position sensing is achievable [85]. While this technology overcomes many of the problems associated with video, infrared and wearable tracking technologies, it increases power consumption and electronic complexity for the transmitting and receiving electrodes [86].

The Electric Potential Sensor has already been proven capable of recognizing human movement passively by detecting changes in the amplitude of the ambient 50 Hz electric field [54, 55], with no requirement for an induced electric field. Absolute position sensing was achieved in room size space, again only using perturbations arising from human movement in the 50 Hz ambient electric field [53]. These experiments were carried out in the United Kingdom, where electricity is delivered at 50 Hz and hence it is the prevalent frequency in the ambient field making it highly exploitable in this setting. If these experiments were carried out elsewhere, the frequency of the ambient field might differ. This chapter investigates the scalability of the EPS position sensing system for use as a hand tracking application.

2.2 One Dimensional Position Sensing

2.2.1 Method

In the case of the EPS absolute position sensing [53], an assumption was made that the object of interest was conducting and in contact with the earth. This assumption allowed for the realisation that as the earthed conductor, or human subject moved around, distortion to the ambient electric field would be significant. Due to the ultra-high input impedance of the EPS it can be consider as an ideal voltage meter, such that it has no effect on the ambient electric field lines. Then as the conducting object approaches and then moves away, the sensor output should vary in amplitude by the near field fall off relationship of $1/d$, where d is the distance between the sensor and the conducting object. This same assumption can be applied for a hand position sensing experiment: hand position may then be inferred by the respective amplitudes of RMS voltage at the output of sensors *A* and *B* as shown in Figure 2.1.

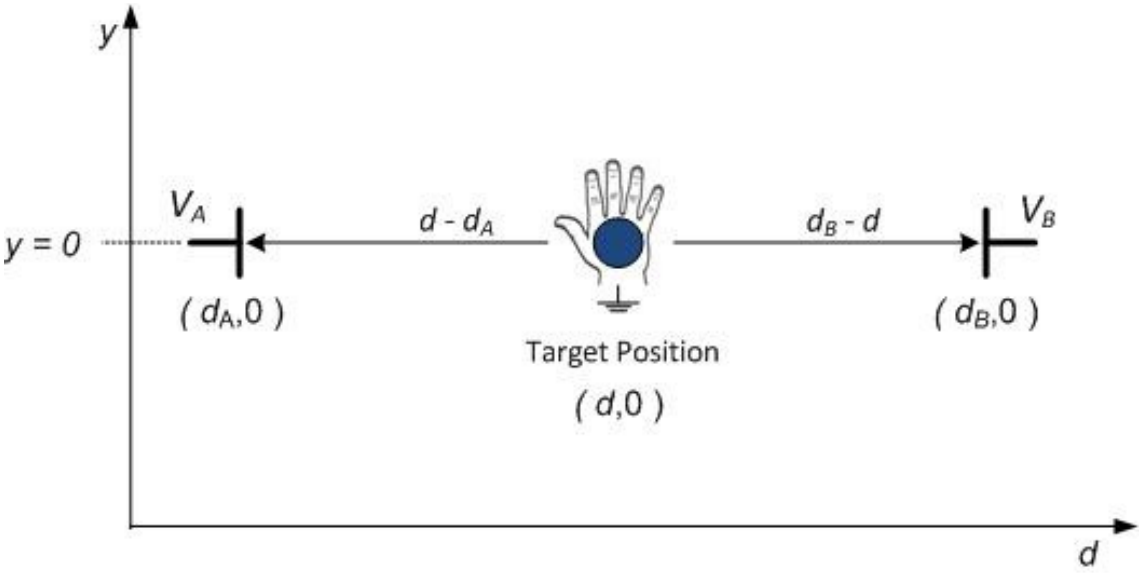

Figure 2.1 Illustration of inference of a hand at position *d*, equidistance between two sensors positioned and d_A at d_B

The voltage at sensor outputs *A* and *B* are then defined by Equations (2.1)

$$V_A = \frac{k_A}{d - d_A} \qquad V_B = \frac{k_B}{d_B - d} \tag{2.1}$$

where V_A and V_B are the RMS output voltages of the sensors, k_A and k_B are normalisation constants. If the sensors are placed symmetrically such that $d_B = -d_A$ the two simultaneous equations can be solved for d:

$$d \propto \frac{k_A V_B - k_B V_A}{2 V_A V_B} \tag{2.2}$$

Constants k_A and k_B are determined by taking a measurement of the ambient 50 Hz signal with no conducting presence in the sensor test area. This equation can be further simplified since for small deviations about the origin, the denominator product will be approximately constant:

$$d \propto V_B - V_A \tag{2.3}$$

Based on this theoretical approach, an experiment was designed to measure hand position in an active area 300 mm in length. Two Electric Potential Sensors were used for this experiment. The sensors provided x10 amplification over a bandwidth from 30 Hz to 20 kHz, see Appendix A for the data sheet. The outputs of the sensors were at a rate of 5 kSamples per second into 16-bit signals by a National-Instruments USB-6212 real-time data acquisition card. LabVIEW [87] was used to apply a 3rd order Butterworth bandpass software filter to each channel, with a bandwidth from 48 Hz to 52 Hz. The narrow bandwidth was chosen since we were only interested in the perturbations of the 50 Hz ambient field. The custom GUI was designed to view RMS displacement voltages occurring when a hand was placed in the active measurement area. Figure 2.2 shows a block diagram of the experimental set up. Real-time data was also recorded to data files for further off-line processing. LabVIEW program code can be found in Appendix B1.

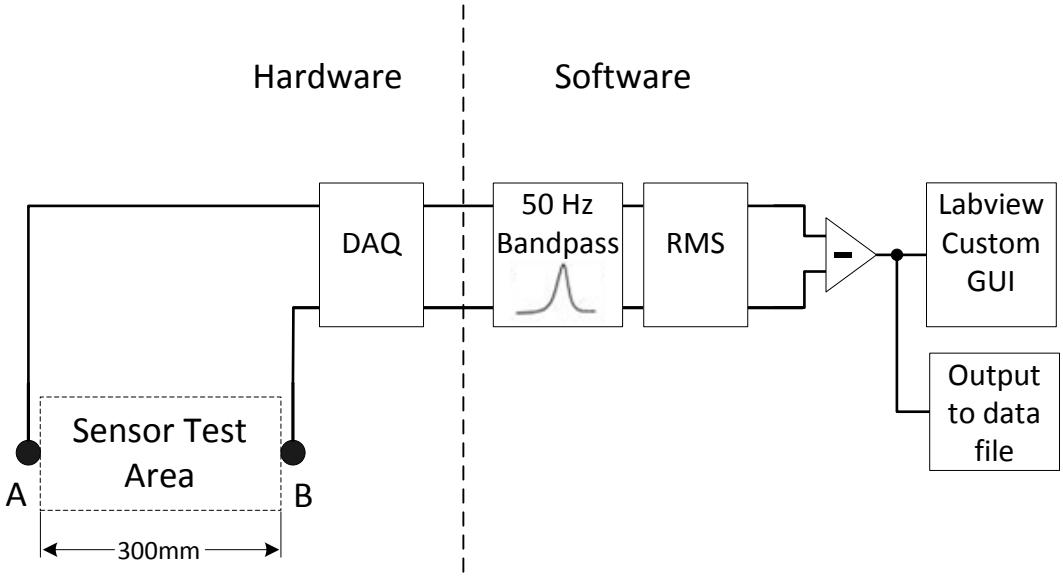

Figure 2.2 Block diagram demonstrating the configuration of sensors, DAQ and associated software components

2.2.2 Results

Results shown in Figure 2.3 correspond to a hand movement from left to right (Sensor *A* towards Sensor *B*) in the test area at 30 mm increments. The hand was placed in the sensor

area with the palm facing to the side, with the sensing area positioned parallel to the body. Since the sensors were normalised to the ambient electric field, the position equidistant from both sensors *A* and *B* corresponds to the origin, zero millimetres.

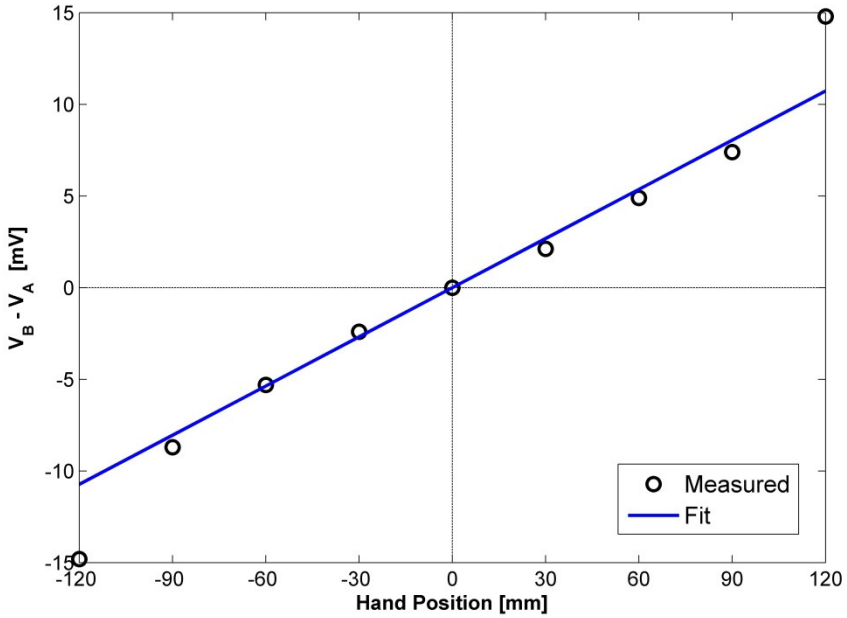

Figure 2.3 Differential measurements between sensor *A* and *B* on the *x* axis, across the field of interest for 30 mm incremental hand positions

The results show a linear relationship between ±90 mm, with a standard deviation of 5 mm. The increase in amplitude change at the extremities of sensor test area result due to the proximity of the hand to the sensors. As the hand approaches the sensor, the reduction of the 50 Hz amplitude corresponds to the region where a steeper gradient is evident on the $1/d$ curve.

Similar measurements were taken for the *y* axis; with the sensor test area rotated 90° such that it was positioned perpendicular to the body. The hand, palm facing towards the body, was placed at 30 mm increments moving from sensor *A* to sensor *B*. Sensor *B* was positioned such that it was closer to the body of the subject than sensor *A*. Results are shown in Figure 2.4: it can be seen that when the hand is closer to sensor *A*, a similar change in sensitivity occurs with the hand in close proximity to the sensor as in the *x* axis experiment. When the hand is brought closer to sensor *B* and subsequently closer to the body, the sensitivity of the sensor is reduced, this is due to the proximity of the large conducting body behind the sensor. Similar to

the *x* axis results, the *y* axis results show a linear relationship between ±90 mm, with a standard deviation of 15.23 mm.

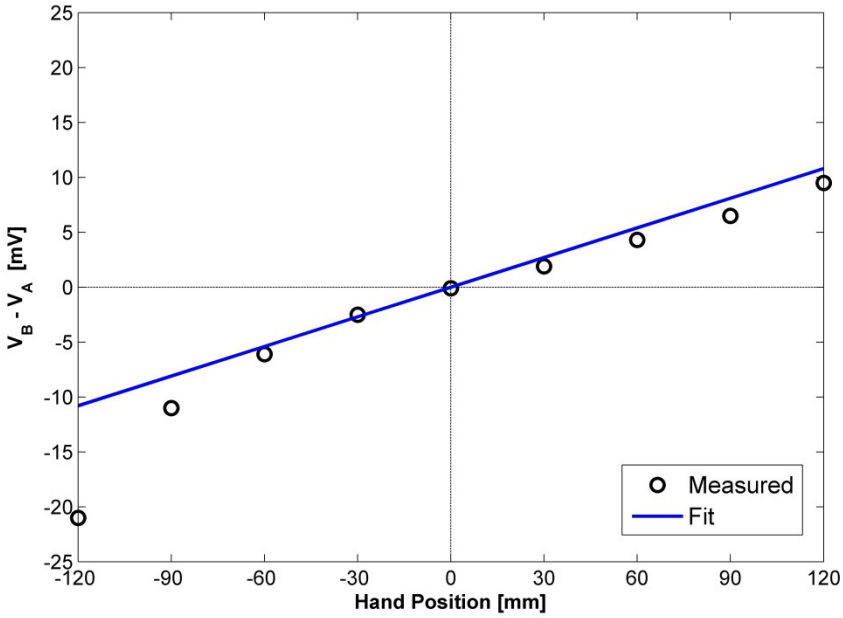

Figure 2.4 Differential measurements between sensor *A* and *B* (*y* axis), across the field of interest for 30 mm incremental hand positions

2.3 Two Dimensional Position Sensing

With the experimental relationship between target position and differential output investigated and supported by the results on both dimensions *x* and *y*, the next logical step was to combine the two axes to create a two dimensional hand sensing area. The immediate thought was to configure an area to support the triangulation of hand position using two pairs of sensors (Figure 2.5), each pair defining a measurement axis.

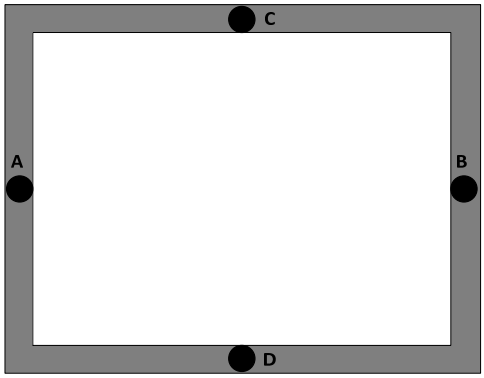

Figure 2.5 Configuration of four sensors on a two-dimensional plane for hand tracking experiments

A two point calibration technique was used in order to normalise the system. First measurements of the ambient electric field with no conducting objects in the target area were taken to determine constants k for each sensor. Since the sensors were normalised to the ambient electric field, the position equidistant from both sensors pairs *A*,*B* and *C,D* corresponds to the origin. The user was then instructed to place their hand midpoint between sensor pair *A,B* and sensor pair *C,D,* the origin. This centre point measurement is taken as half of the sensor maximum amplitudes for normalisation, this assumption is viable due to the linear relationship between hand position and differential sensor voltage output seen previously in Figure 2.3 and Figure 2.4. Normalised target position was then displayed graphically on a custom LabVIEW Graphical User Interface (GUI), the program code and GUIs can be found in Appendix B1. Initial observations using this configuration were that the sensitivity was limited; this was due to the fact that the hand is not an ideal target. The hand has complex geometric properties and is attached to an arm; it is not just an earthed conducting object within the target area. When the hand was moved around the target area, there were positions where the arm would saturate one of the sensors, mainly sensor *D*, closest to the body, resulting in inaccurate estimations of target position. There were also issues inferring target position in the four corners, since the hand was not placed between either of the deterministic sensor pairs. Figure 2.6 shows the resulting position vectors inferred by the four sensor configuration, when the hand was traced across the sensing area, from left to right, at three intervals. The intervals relate to normalised *y* positions, +0.6, 0 and -0.6, at the centre of the palm.

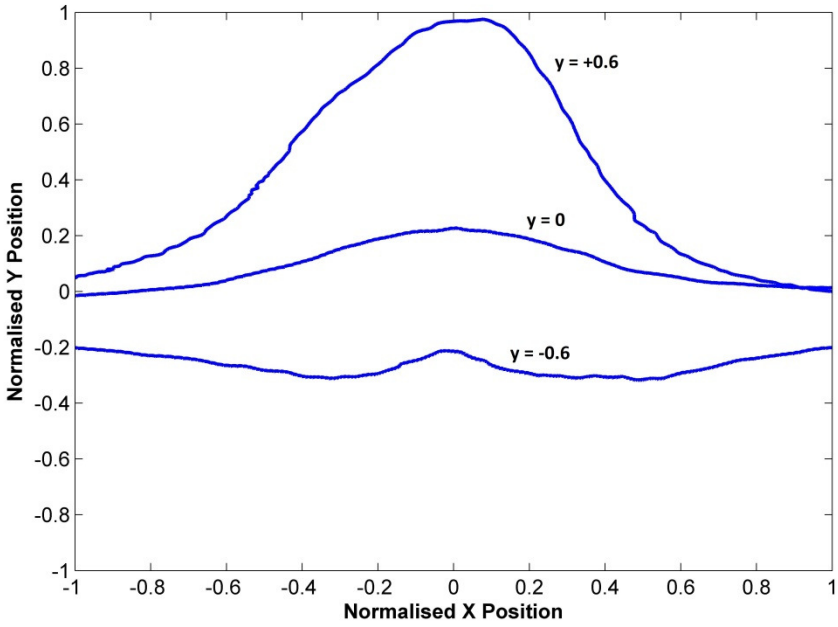

Figure 2.6 Inferred hand position in the target tracking area for the four sensor configuration, hand was traced from left to right with the palm facing to the left at *y* axis positions of -0.6, 0 and -0.6.

To overcome the issues presented by the four sensor configuration, the use of a single y axis sensor was investigated. Figure 2.7 shows the results of a single sensor, one dimension experiment where the hand was moved away from the sensor at 30 mm increments. The sensing area was positioned directly in front of the user, with the palm was facing towards the body.

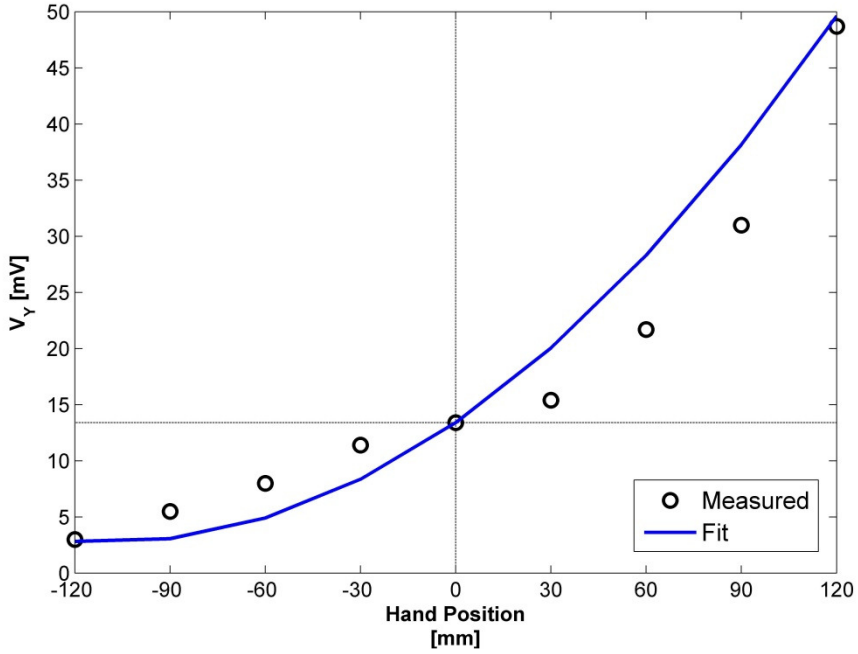

Figure 2.7 Single sensor output RMS voltage measurements (*y* axis) across the field of interest for 30 mm incremental hand positions

The results show a clear $1/d$ reduction in RMS field voltage using a single sensor, with a standard deviation of 20.88 mm. While this is not a linear response as is evident using the differential measurements, it is still a useful relationship. The use of a single sensor has the advantage that disturbances outside of the sensing area will have little to no effect on the hand sensing system. Thus a person moving around behind or beside the user will not cause interference to the system. In order to exploit the single sensor response to hand movements a more complex position determination technique was required in order to provide a close approximation to a linear relationship between hand position and sensor voltage. The single sensor was calibrated in the same way as the differential pair, with two points measured: first, the ambient field to determine k, second, the hand was placed at centre point in the target area. This measurement was taken to be half the sensor maximum voltage for the sensing area. The normalised signal of the single sensor response is centred on positive one, swinging between the limits of zero and two. For appropriate position inference, this must be centred about zero corresponding to the origin of the sensing area; the scaling was achieved by subtracting one from the normalised sensor value. The positive portion of the signal was capable of adequate coverage of the sensor area; however the negative portion needed additional scaling to reach the bottom extremity of the sensing area. It was found that an

additional scaling of times four was sufficient to cover the sensing distance required. Full vertical coverage was achieved by employing the following relationships:

$$y > 0: \quad y_{pos} = {}^{V_Y}\!/_{(2 \times V_{Y_{CENTRE}})} - 1 \tag{2.4}$$

$$y < 0: \quad y_{pos} = 4 \times ({}^{V_Y}\!/_{(2 \times V_{Y_{CENTRE}})} - 1) \tag{2.5}$$

Figure 2.8 shows the results of normalising and calibrating the single sensor response from Figure 2.7 using the relationships described by Equations (2.4) and (2.5). We can see the results are comparable to a linear model, with a standard deviation of 11.19 mm.

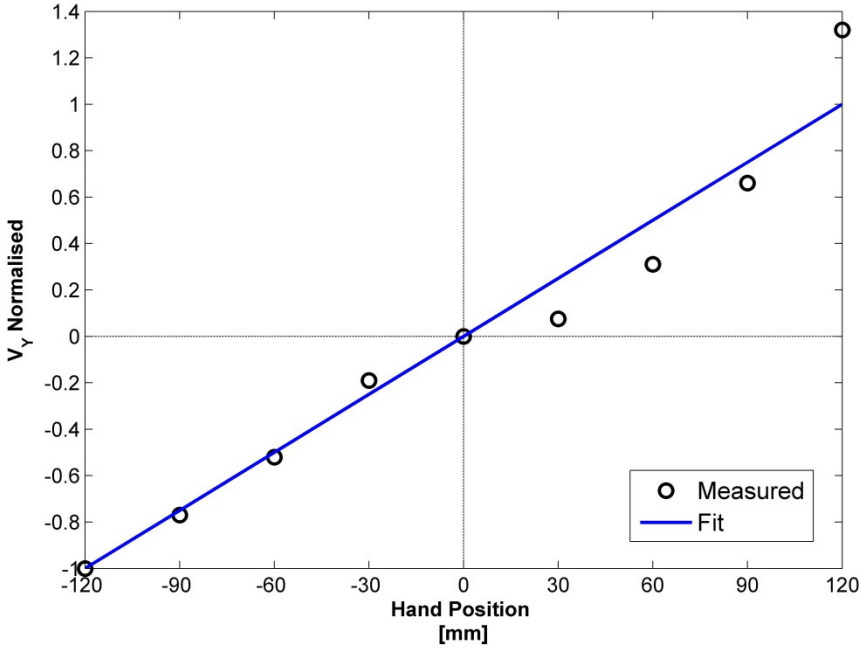

Figure 2.8 Normalised and calibrated single sensor RMS output voltage measured for hand position varied over the y axis

After achieving suitable results for inferring hand position using a single sensor an improved two-dimensional sensor configuration was developed, shown in Figure 2.9. Three single *y* axis

sensors were employed, in conjunction with a pair of differential sensors for *x* axis position detection; the full coverage sensing area was 300 mm by 250 mm.

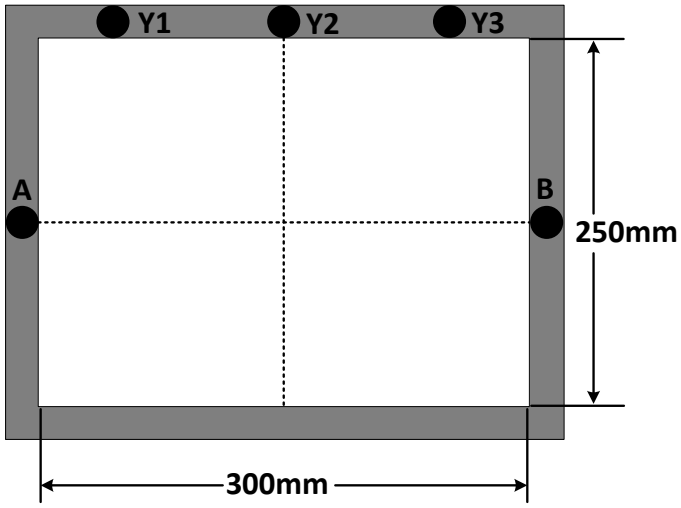

Figure 2.9 Illustration of the five sensor configuration used for two-dimensional hand tracking experiments

Calibration of the system was achieved by the same two point calibration technique described previously. An amplitude priority algorithm was developed to accomplish accurate position determination for full coverage over the sensing area. Full coverage was achieved; the sensing area was segmented into four quadrants in order to determine the absolute position of the hand.

Figure 2.10 shows the control algorithm flowchart outlining the priority method, the corresponding LabVIEW program code can be found in Appendix B1. The amplitude priority algorithm works as follows: if the *x* position is negative, then only sensor *Y1* or *Y2* can infer hand position on the *y* axis. When the *x* position is positive, only sensor *Y2* or *Y3* can infer *y* position. The vertical sensors are scaled as per Equations (2.4) and (2.5) based on whether the hand is in a positive or a negative *y* position. Normalised hand position was graphically displayed on a custom LabVIEW GUI (see Appendix B1).

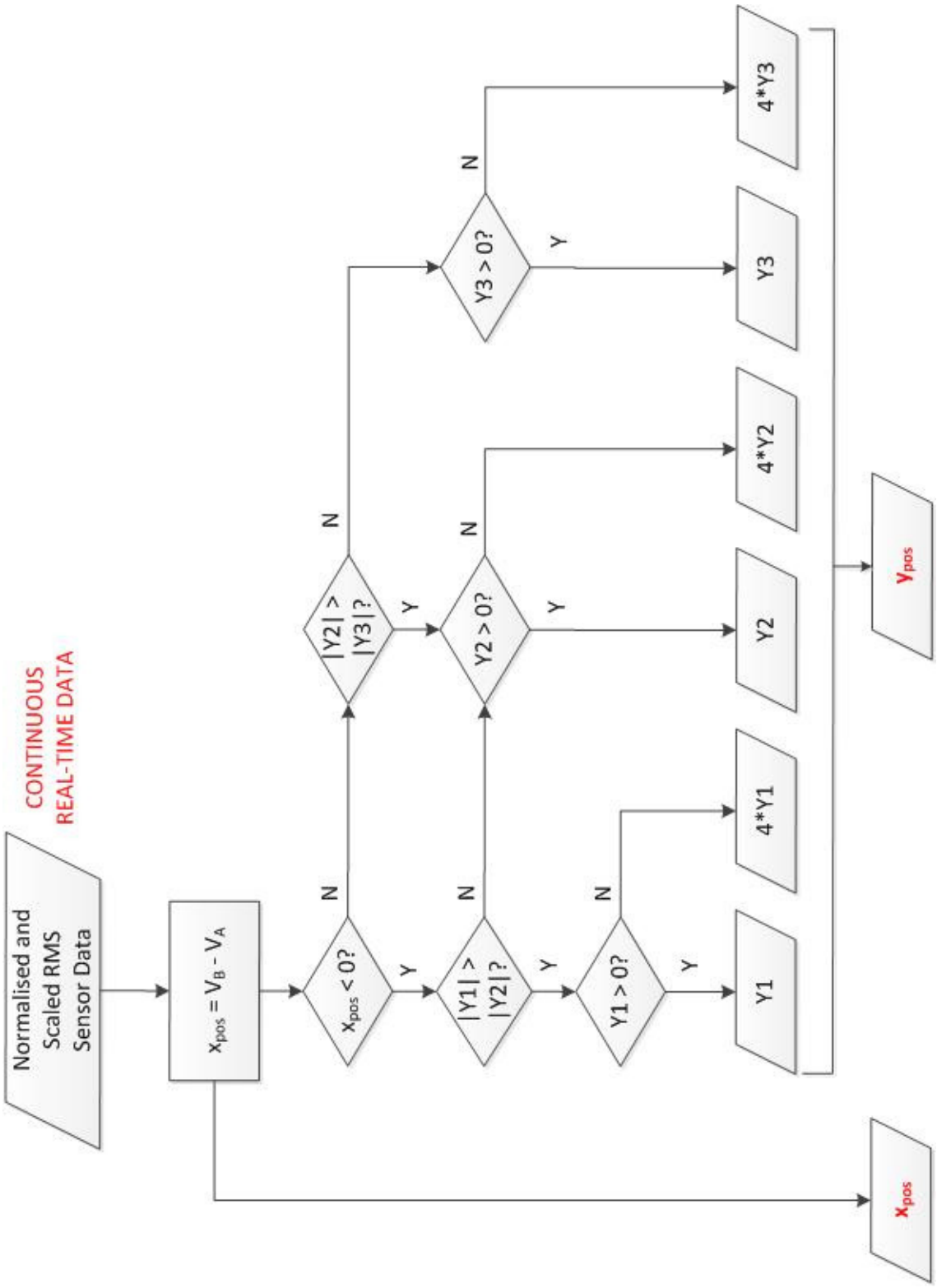

Figure 2.10 Flowchart illustrating the interpretation of normalised and calibrated sensor data in determining hand position

Figure 2.11 shows the resulting position vectors inferred by the five sensor configuration, when the hand was traced across the sensing area, from left to right, at three intervals. The intervals relate to normalised *y* positions, +0.6, 0 and -0.6, at the centre of the palm. It can be seen from the graph that there is a clear cross-over point between the positive and negative *x* halves of the sensing area. It should be noted that the appearance of noise on the signals is due to using single sensors on the *y* axis: the noise increases as the hand is positioned further from the sensors. This common mode noise does not appear in the four sensor configuration due to the differential measurements. The trace at +0.6 on the *y* axis shows some non-linearity which is consistent with the relationship shown in Figure 2.8.

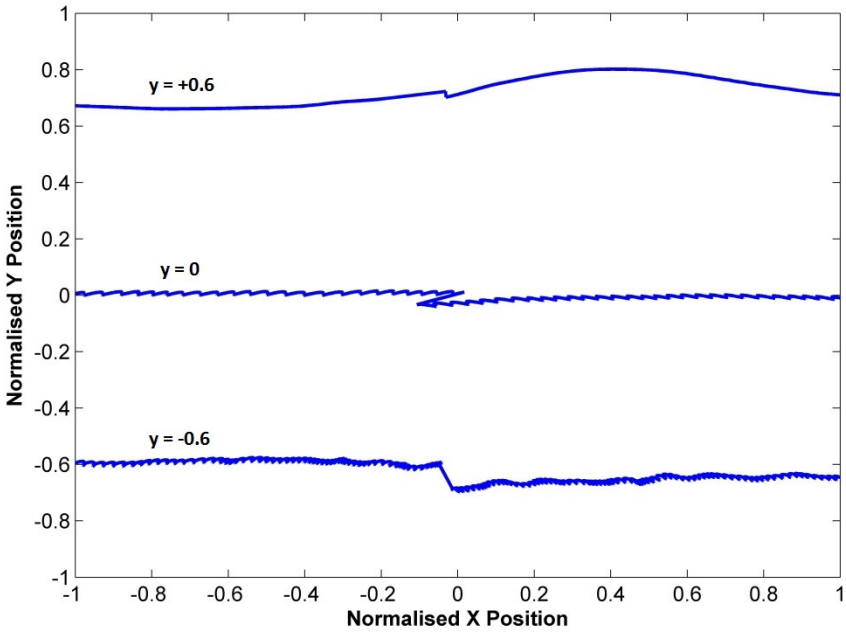

Figure 2.11 Inferred hand position in the target tracking area for the five sensor configuration, hand was traced from left to right with the palm facing to the left at *y* axis positions of -0.6, 0 and -0.6.

2.4 Mouse Control

To finalise the hand tracking system for use as an AT application, control over a mouse cursor was preferred over a graphical representation of hand position. LabVIEW allows for communication with the computer operating system such that mouse cursor movement and click functionality can be controlled. The first requirement for scaling the *x,y* positions into

pixel locations was to determine the screen resolution of the device being used, this was accomplished using LabVIEW. Once determined, the *x,y* position was re-scaled to lie within a range between zero and one, then multiplied by the screen resolution resulting in an on-screen pixel location. Generating a mouse click event was achieved by holding the cursor, or hand, in a sensitive area for the correct amount of time. The sensitive area was scalable such that it could change with pixel resolutions on different machines, with optimum results achieved with the active click pixel area between 50 and 100 square pixels. The time required to hold the position to initiate a mouse click was 500 ms. These variables could be changed for more or less resolution. Figure 2.12 shows the program flowchart for controlling the mouse cursor.

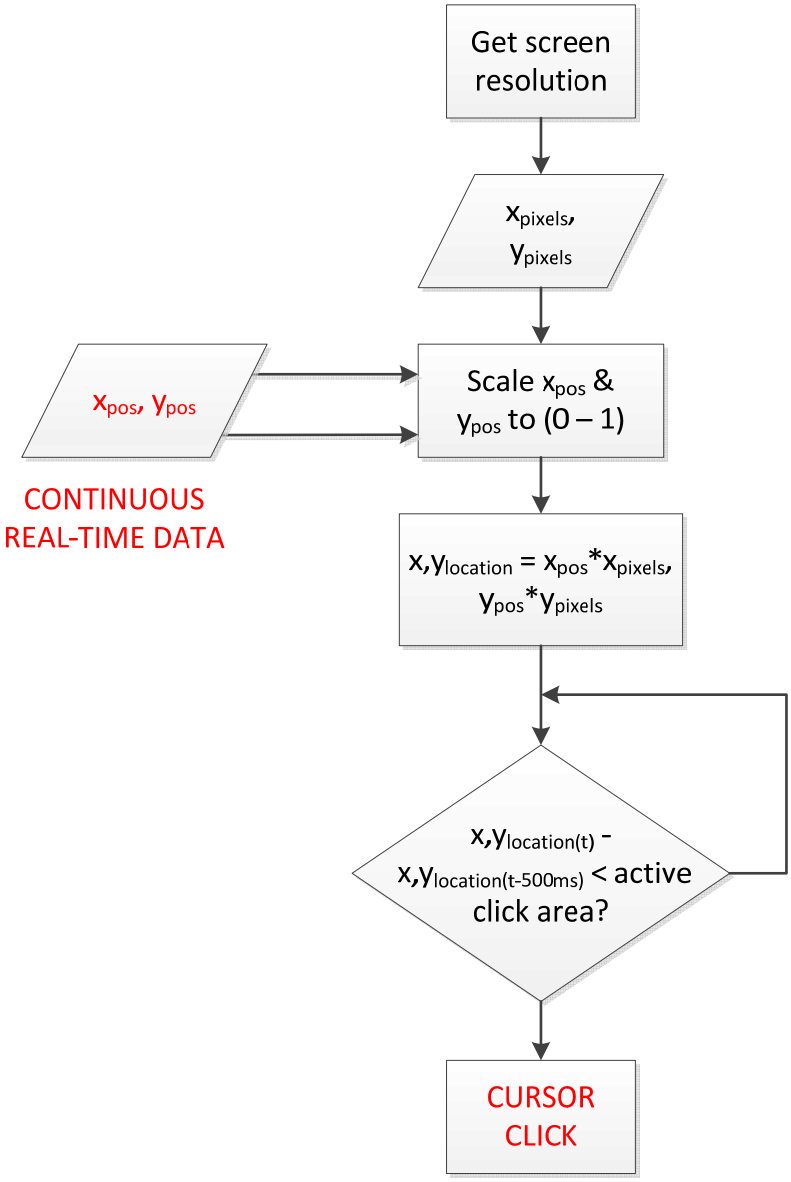

Figure 2.12 Flowchart illustrating the interpretation of real-time hand position information in determining mouse cursor position

2.4.1 Usability Testing

Due to the complex physical properties of the hand it is difficult to quantify errors for this system, thus a usability study was carried out. A group of 15 University of Sussex students; male and female, varying between ages 20 and 45, volunteered to try the hand tracking system. The usability test consisted of using the mouse control interface and a large icon predictive text typing program, the predictive text program was called Dynamic Keyboard and

is shown in Figure 2.13. Click sensitivity was set to 100 square pixels and the click time was set to 500 ms. All tests were carried out in an open laboratory.

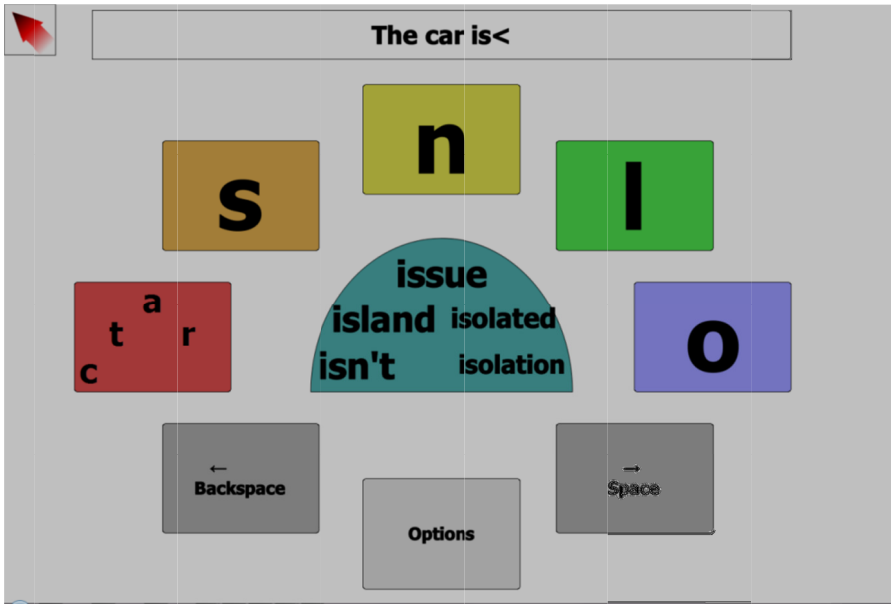

Figure 2.13 Screen shot of the Dynamic Keyboard used during usability testing of the real-time interface between hand position and mouse cursor control, developed by CanAssist [88]

Students were given a short demo of the mouse control system with instructions on how the mouse click functionality was implemented. The system was calibrated to the user and they were given as much time as they needed to be comfortable with the interface and the Dynamic Keyboard functionality. Three students were standing up when using the system, the remaining students sat in a chair and either positioned themselves directly in front of the sensing area or slightly to the side. The task was first to spell 'hello' with no errors, and the second task was to spell the sentence 'the car is red'. Users were asked to rate the system numerically between one and five (1=very easy, 5=very difficult) for overall ease of use in terms of 'Learning', 'Control', and 'Comfort'. All users were also asked some questions on the cursor coverage area, the click sensitive area and the click event timing requirement. Results of the usability test are tabulated below. All users were able to spell 'hello' with no errors in under one minute, the sentence was a more difficult task with 75% of users taking up to five minutes to complete, while the remaining 25% were unable to complete or gave up on the task. All users commented that spelling out a sentence with their hand hovering for mouse

functionality caused tiredness in their arm. Additionally, all users agreed that the click sensitive area and time could be decreased once familiar with the functionality of the system.

Table 2.1 Feedback scores reported by usability study group for real-time hand sensing system with mouse control and predictive text program

	Score					
Metric	**1**	**2**	**3**	**4**	**5**	**Total**
Learning			5	7	3	77.3%
Control		2	6	5	2	69.3%
Comfort	7	4	3	1		37.3%

Total score for each of the categories was determined by multiplying each score by the number of users who chose the score. A maximum of 75 points is available for each category. From the results we can see that most of the users were happy with the learning process and the control of the system; however comfort of use of the system scored very low.

2.5 Discussion and Future Work

In this chapter it has been demonstrated that the EPS is capable of a small scale hand position sensing application using an entirely passive measurement technique, by sensing changes to the ambient electric field. It has been shown that on a single axis hand position can easily be determined by a pair of sensors and a simple differential measurement. A two-dimensional hand tracking system was presented using two orthogonal differential sensor pairs, which presented some impractical limitations that were discussed. A single sensor solution was presented, and although the sensor response was non-linear with respect to hand position, it was still a viable relationship to exploit for hand position sensing within a small area. Agreeable results were achieved using a five sensor configuration: a differential pair for horizontal position detection, and three single y-axis sensors for vertical detection. Full coverage hand tracking over a 300 mm by 250 mm space was achieved in an open laboratory environment.

A method for controlling the mouse cursor was presented which was interfaced with a large icon predictive text typing software. Results of the usability test showed that the mouse

cursor control system was easy to learn and use. It also showed that ease of use increased over time. However, in general it was thought that this was not an ideal substitute for a mouse due to the need to hover a hand in the sensing area. This valuable feedback will lead onto further work on the system to incorporate gesture recognition capability where the hand would not have to complete complex and discrete movements for functionality.

Further validation studies are essential if this technology is to be taken into the consumer space. Statistical benchmarking analysis methods are discussed in Appendix E which could be undertaken alongside further in-depth usability studies to increase the appeal of this novel sensing application.

3 A Three Sensor Eye Tracking System based on Electrooculography (EOG)

3.1 Introduction

The study of eye movements has been around since long before the technological advances of the modern PC. Initial studies, dating back to the late 19th century, used highly invasive techniques involving mechanical contacts with the eye. In the early 1900's, methods were developed to track eye movements less invasively by observing light reflections from the cornea. Throughout the 1900's, eye tracking was used passively for observation purposes only, it was not until the development of minicomputers that the necessary resources were available to track eye movements in real-time and hence lead to human computer interactions based on eye movements [32].

Eye tracking is the method used to monitor eye movements with respect to head position. It is also used to determine where one is looking (the gaze point). Commonly used eye tracking techniques can be broadly separated into four categories: contact lens, pupil or corneal reflection, image-based video-oculography (VOG) and electrooculography (EOG) [89]. Two main types of eye movements are observed through these technologies: smooth pursuits and saccadic movements. Smooth pursuit movements are slow eye movements which occur when gaze is fixed on a moving target [90]. Saccades are fast eye movements that occur when a person quickly changes their visual target. These fast movements typically last between 30 and 120 ms [31]. Depending on how far the eyes move, the amplitude of the saccade is proportional to the angular distance moved. Fixations, where the eye is stable and fixed on an object, are typically observed following a saccade; these can last between 200 and 600 ms [91].

Contact lens eye tracking is one of the most precise methods; however it requires the subject to have a device such as a coil or a mirror attached to a contact lens inserted into the eye. This method has extremely high accuracies, down to 0.08° [92]; however it is extremely invasive and thus inappropriate for use in assistive technologies (AT). Pupil and corneal reflection is achieved by either using infrared or video cameras directed at the eye in order to capture

reflected light. The amount of light reflected back to a receiver relates to the position of the eye. Accuracies range from 0.5° to 2° for both horizontal and vertical eye movements [59, 92]. This technique is not as invasive as the contact lens method; however it requires a direct unobstructed line of sight to the naked eye, and accuracies suffer for subjects who wear glasses. The subject must not move, and the measuring apparatus must be directly in front of the eye, both of these factors make this type of eye tracking unsuitable for AT applications. Image based techniques (VOG) use cameras and complex algorithms to determine gaze positions. Accuracies have been quoted from 0.5° to 2° [92], but additional cameras and/or tracking techniques must be incorporated to the system to achieve such accuracies [93, 94]. VOG systems are the least invasive of the four groups and are often used for human observation studies [95, 96]; however there are significant drawbacks in terms of processing power for high quality images, lengthy calibration routines and the need for recalibration if the user moves or ambient light levels change. An eye controlled mouse based on VOG is commercially available, but it has a very high cost, typically $7000 (~£4616) [34]. The most prevalent eye tracking technology used for AT is the electrooculogram (EOG). It is slightly more invasive than VOG as it requires electrodes to be attached to the face around the eyes. However, the cost and the amount of processing power required are the least of all the categories of eye tracking. This eye tracking technique requires simple measurements that can be taken with the head in any position. Comparable accuracies to the above technologies have been published [19, 46, 97]. The following section provides details on these accuracies, how the EOG is measured and a brief review of AT applications based on EOG signals.

3.2 The Electrooculogram

The EOG is a signal resulting from a differential measurement across an eye or both eyes, either on a horizontal or a vertical plane. The front of the eye, the cornea, is at a positive potential with respect to the back of the eye, the retina. When the eyes move a change in electric potential results, this is due to the electrostatic field surrounding them. As the eyes rotate, the electrostatic dipole rotates with them, thus the displacement voltage can be measured across the eyes for both vertical and horizontal eye movements. Historically this was done using a system of many DC electrodes placed around the eyes, depending on how much detail was required from the EOG signals [59]. The more electrodes used the more precise detail on eye position is achievable. Recorded potentials are small, usually in the microvolt range, and have been quoted between 15 μV and 200 μV [59] and 50 μV to 3500 μV

[98]. Results vary due to electrode type, position and differences in individual biopotentials or physiological make up. It is possible to record the monopolar behaviour of the eye with the electrode positioned at a distance from the eye up to three times its diameter [99], which dictates a practical limitation for this technique. Electrodes positioned closer to the eye will resolve larger potential differences arising from the eye movement. In any case of electrode placement within the limitation, eye behaviour has been proven to be linear in the range of ±70° [59]; this sensitivity is highly stable in the range of ±40°, becoming progressively worse at greater excursions. Sensitivities have been measured between 4 µV/degree and 20 µV/degree, with a trade-off between sensitivity and number of electrodes [59]. In practice horizontal sensitivities are more stable than vertical sensitivities due to muscle movements and eyelid interferences. These linear characteristics of EOG signals make them an easily exploitable physiological signal for use in AT applications.

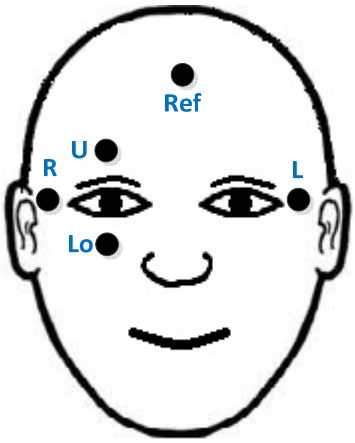

Figure 3.1 Typical facial electrode positions for acquiring horizontal and vertical EOG signals

Typical EOG systems use five wet gel electrodes [19, 30, 100-102], two on either side of the eyes (L) and (R) positioned equidistant from the centre of the eye for horizontal measurements. Two electrodes are used for vertical measurements, one above an eye (U) and the second below that same eye (Lo). The fifth electrode is a reference electrode (Ref) and is placed on an electrically isolated position on the subject's body, such as the forehead, neck or earlobe. The frequency range in which the EOG signals lie is from DC to 40 Hz, thus the need for an isolated point of reference. This is used to minimize system noise from other physiological signals such as EMG and EEG that lie in the same frequency range.

When using the EOG signals for AT applications, user experience, in terms of comfort and ease of use, is invaluable. Therefore a minimum number of electrodes are desirable, reducing visual obstruction and preparation time. Earlier eye typing studies show a high usability experience with low learning times [30, 100]; however the use of five electrodes is not conducive to comfort as one electrode is placed on the lower eye lid. A solution to the under eyelid electrode was presented [97], where EOG gaze detection was achieved by attaching two arrays of wet gel electrodes to a pair of headphones. In this experiment accuracies were not very good; horizontal and vertical accuracies were quoted as 4.4° and 8.3° respectively. While this system leaves the eyes unobstructed, it will suffer the effects of DC drift and long term signal degradation from the electrodes drying out. Excellent levels of control of a wheelchair have been achieved [19, 98], with the highest degree of accuracy in the detection of saccadic movement being 2° [19]. However, the wet gel electrodes used are not suitable for long term use since they dry out and can also cause skin irritation. Three electrode systems have been investigated, including a wheelchair control system [23]. However this system relied only on acquiring horizontal EOG signals for left and right directional control, with the third sensor serving only as a reference. The remaining control system was based on electromyography.

The system designed and discussed in the remainder of this chapter relies on three electrodes to detect both horizontal and vertical EOG signals.

3.3 Method

A three Electric Potential Sensor configuration was used; the sensors were spring mounted to a headband for easy application. The physical arrangement of the sensors can be seen in Figure 3.2. Two sensors are positioned on both sides of the eyes at the temples, and the third sensor is placed in the centre of the forehead. By using this configuration the need for additional facial electrodes was eliminated. This arrangement could easily be transferred onto a pair of glasses or goggles providing the required skin contact points for adequate signal detection.

Figure 3.2 Illustration of three Electric Potential Sensors mounted to a headband, configured for acquiring horizontal and vertical EOG signals

The sensors used for these experiments have been described in Chapter 1. Internally the sensor hardware consists of a two stage amplifier providing x114 amplification to the EOG signals acquired at the skin. There is a first order bandpass filter in the sensor, providing a bandwidth from 0.1 Hz to 86 Hz. The output signals from the sensors were taken to a control box with additional variable amplification and anti-aliasing filtering before being converted from analog to 16-bit digital signals by a National-Instruments USB-6212 real-time data acquisition card. LabVIEW software was used to acquire the data and perform all subsequent signal processing; program code is shown in Appendix B2. Data was sampled at 20 kSamples per second, then a software 3rd order 40 Hz Butterworth lowpass filter was applied to each data channel prior to extracting the EOG signals, thus eliminating any unwanted noise due to movement artifacts or EMG signals. The 40 Hz lowpass filter was chosen since all of the signal power and useful information in EOG signals lies below this frequency, it also attenuates any mains noise. The horizontal signal was determined by using a simple differential measurement, right sensor (R) minus the left sensor (L). The vertical signal was resolved by a differential measurement between the centre sensor (C) and reference signal created by adding the right sensor (R) to the left sensor (L). Figure 3.3 shows the block diagram of the entire system. A smoothing filter was applied to the final EOG signals in LabVIEW before displaying on the custom graphical user interface (GUI). The signals were also recorded to data files for further interpretation and off-line graphical representation.

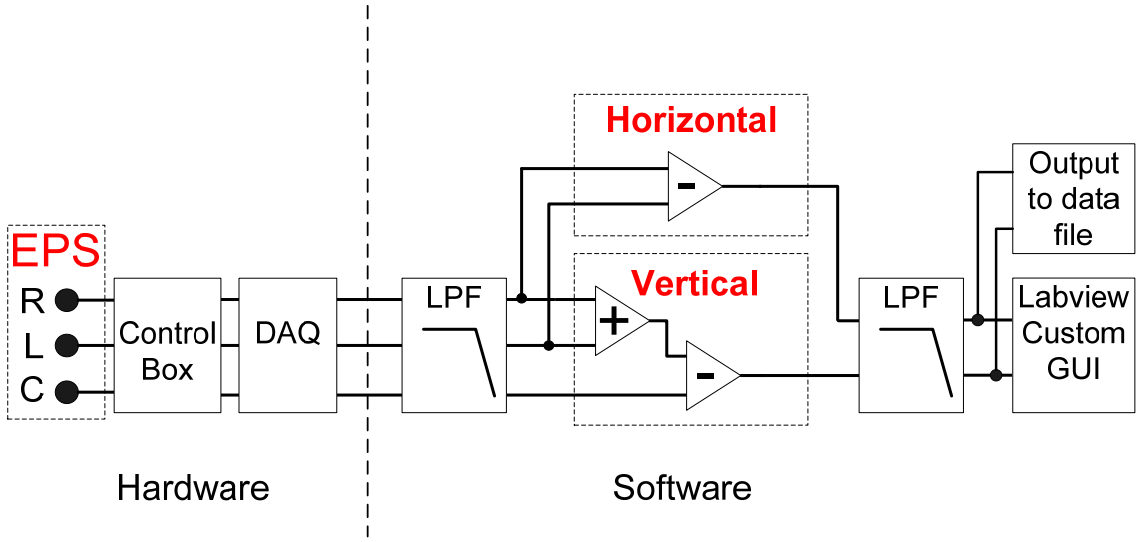

Figure 3.3 Block diagram demonstrating the configuration of sensors, DAQ and the associated software components for acquiring horizontal and vertical EOG signals

An experiment was designed in order to measure EOG signals over a gaze range of ±40° on both the horizontal and vertical planes. Initial experiments were carried out on a single user in an open laboratory environment. A series of horizontal and vertical eye movements were made, gaze was directed to circles positioned at 10°, 20°, 30° and 40° to the left from centre, returning to the centre position after each excursion. The procedure was repeated with the same eye movements to the right, up and down from centre. Figure 3.4 shows the gaze position grid used during the experiments. The position grid used was on a flat surface, thus the gaze points are not linearly spaced on the diagram. Each point corresponds to the angle the eye had to rotate in order to alter the gaze position.

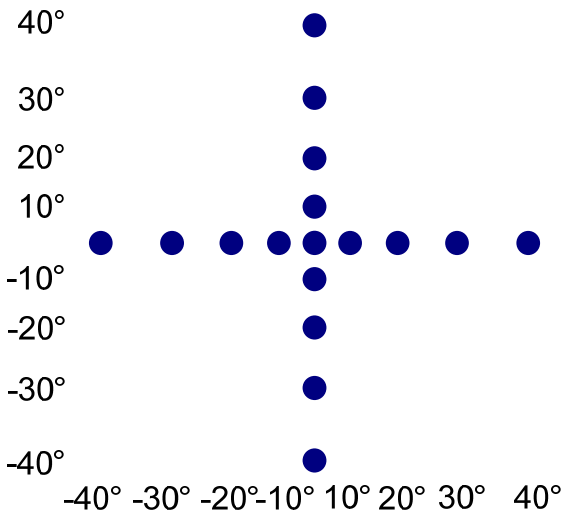

Figure 3.4 Gaze position grid used during eye movement experiments; subjects were instructed to direct their gaze toward each of the dots as focal points

3.3.1 Results

Both the recorded horizontal and vertical EOG signals were plotted using MATLAB [103]. In Figure 3.5(a), data is presented for eye movements to the left of centre position followed by eye movements to the right of centre position. Figure 3.5(b) shows the vertical EOG signals for eye movements up, then down from centre position. The initial falling edge in Figure 3.5(a) at three seconds is the saccadic eye movement recorded corresponding to the gaze angle of 10° to the left of centre. Each subsequent falling edge increases in amplitude until the gaze direction is shifted to the right of centre (at 12 seconds). It should be noted that the decay in signal amplitude seen directly after the saccade is associated with gaze fixations; the decay is due to the capacitive nature of sensors electrode coupled to the skin.

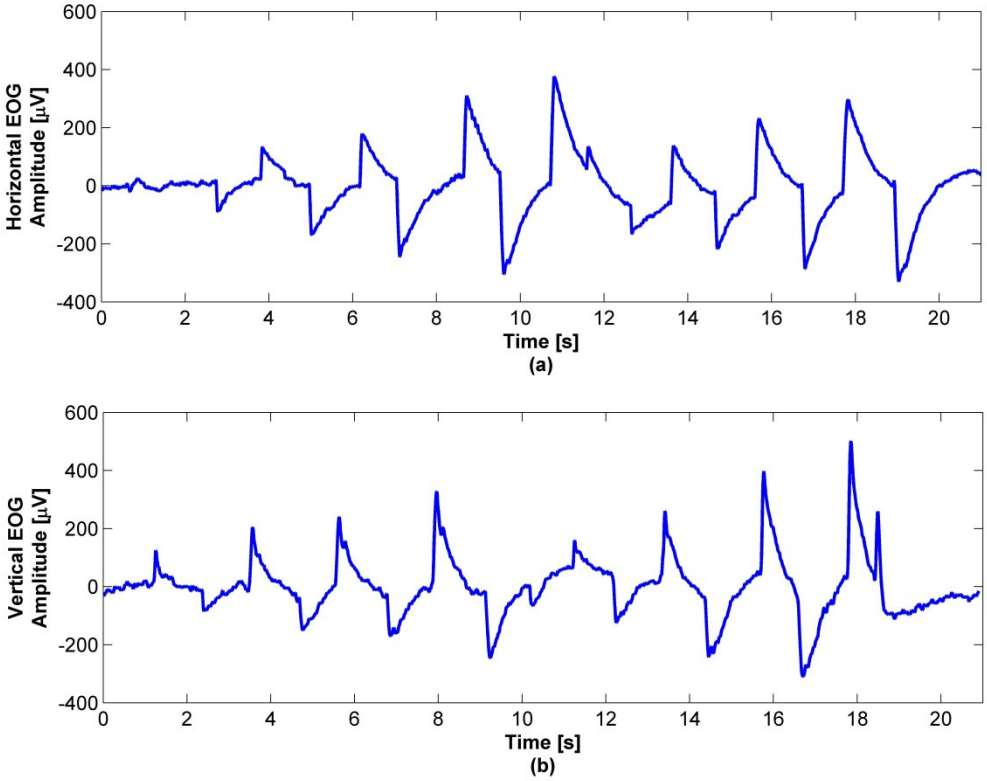

Figure 3.5 Measured EOG signals for eye movements at 10° intervals between 0° and ±40°, with gaze returning to centre position after each movement, for horizontal eye movements (a) and vertical eye movements (b)

It is easily seen from these graphs that as gaze angle increases EOG amplitude also increases and that a relationship between EOG amplitude and gaze position exists. In order to identify the relationship between EOG and gaze angle, the step change in amplitude is plotted against eye displacement. Figure 3.6 shows this relationship for both the left and right eye movements. The data is highly correlated with a linear relationship between the step change and gaze angle over the entire range of ±40°. There is also good agreement between the left and right data sets. From this data, the accuracy of the measured saccadic movements is 1° for the horizontal data.

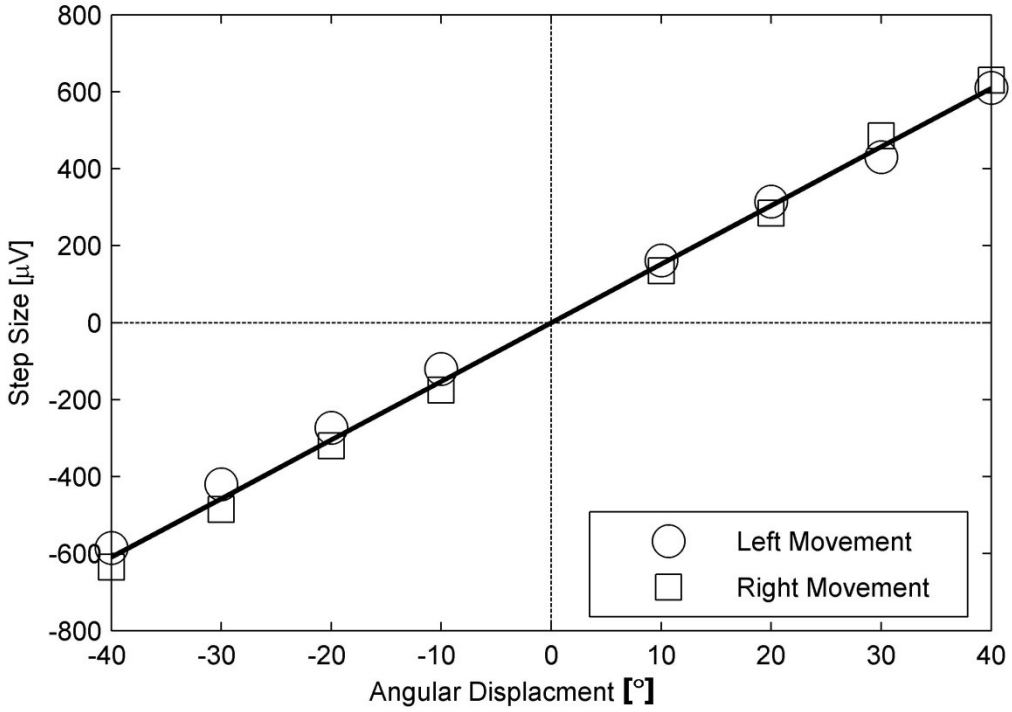

Figure 3.6 Change in EOG amplitude (step size) versus gaze position angular displacement for horizontal eye movements: left and right

Figure 3.7 shows the corresponding data set for the vertical axis where the gaze angles up to ±40° are plotted against the step change in EOG amplitude of the measured saccades. Again there is a strong correlation and a linear relationship between the saccadic amplitudes and angles, for this subject, over the entire range. However it should be highlighted that the accuracy for the vertical data is not as good as for the horizontal with an accuracy of 2.5°. This is in agreement with much published literature that also finds the vertical is less linear at the extremities of vision, usually past 30° of eye deflection [19, 59, 98].

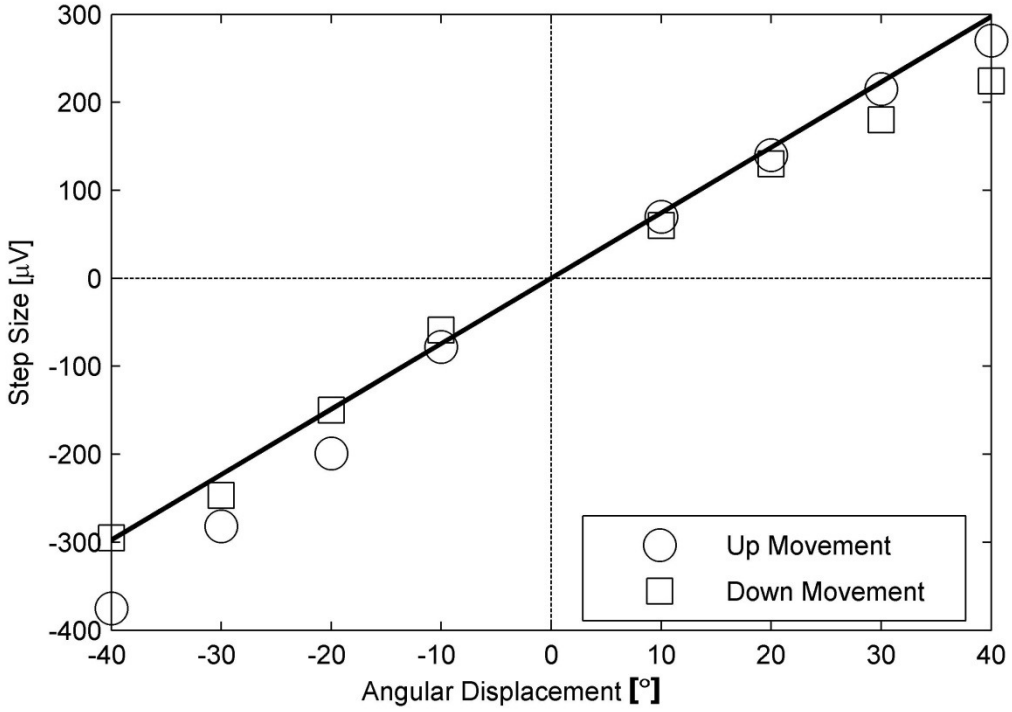

Figure 3.7 Change in EOG amplitude (step size) versus gaze position angular displacement for vertical eye movements: up and down

These initial experiments yielded sensitivities for the horizontal and vertical eye movements of 10.3 µV/degree and 9.9 µV/degree, with standard deviations of 2.6° and 5.6° respectively. These sensitivities fall within range of published findings [59, 98]. A measure of system noise was taken during this experiment, the user was directed to hold the central gaze position in order to observe the resting potentials generated at the sensor inputs. Noise in the system is attributed to both electronic noise in the sensor and any muscle noise picked up by the sensors. The muscle noise is limited due to the system bandwidth. Throughout this experiment the system noise level was less than 10 µV, which is less than the level of sensitivities in these experiments.

3.4 Further Experiments

An EOG controlled system cannot be developed based on a single set of sensitivity measurements from one individual. Thus to determine the potential capability of the EPS for an EOG based AT application the above experiment was repeated across a range of male and female subjects, ranging in age between 25 and 60. All experiments were carried out in an open laboratory environment. Some users wore glasses during the experiment, some wore contact lenses and others had no eye sight problems at all. Users were instructed to place the head band with the EOG sensors on their own heads with no assistance so that the electrodes were on the situated on their temples and forehead. The users were positioned in front of the gaze position grid shown in Figure 3.4 and instructed to make a series of horizontal and vertical eye movements, directing their gaze to the circles at 10°, 20°, 30° and 40° to the left from centre, starting at centre and returning to the centre position after each excursion. Each user was asked to repeat the procedure with the same eye movements to the right, up and down from centre. Each subject carried out three trials on each gaze direction in order to investigate the repeatability of measurements. Each trial was recorded to data files for further interpretation.

3.4.1 Results

The step change in amplitude at each 10° increment in eye position for each subject was extracted from the trial data. Then the relationship between EOG amplitude with respect to eye gaze position was analysed. Figure 3.8 shows the experimental results for the horizontal data for all eight users. It is clear from the graph that a linear relationship holds across a range of users; however the EOG data varies in sensitivities. In this case it was found the maximum sensitivity was 16.6 μV/degree (red line), compared to the minimum change of 4.7 μV/degree (blue line). The deviation from the linear best fit model averaged at 0.8° with the average accuracy of less than 1°.

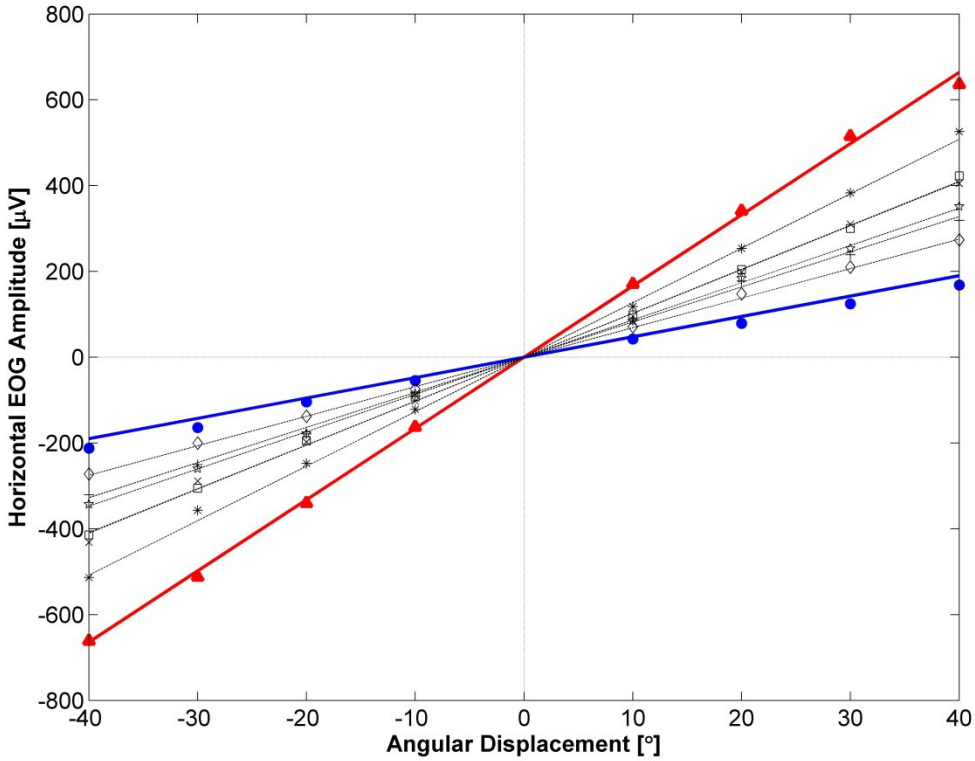

Figure 3.8 Horizontal EOG amplitude versus gaze position angular displacement across eight subjects; blue line represents the lowest measured sensitivity, the red line represents the highest measured sensitivity

Similar results were achieved on the vertical plane: the deviation from the linear best fit model was 2.6° and the average resolution was 2°. The corresponding minimum change in EOG signal amplitude per degree of eye displacement was 3.52 µV/degree (blue line), and the maximum was 9.86 µV/degree (red line) as seen in Figure 3.9.

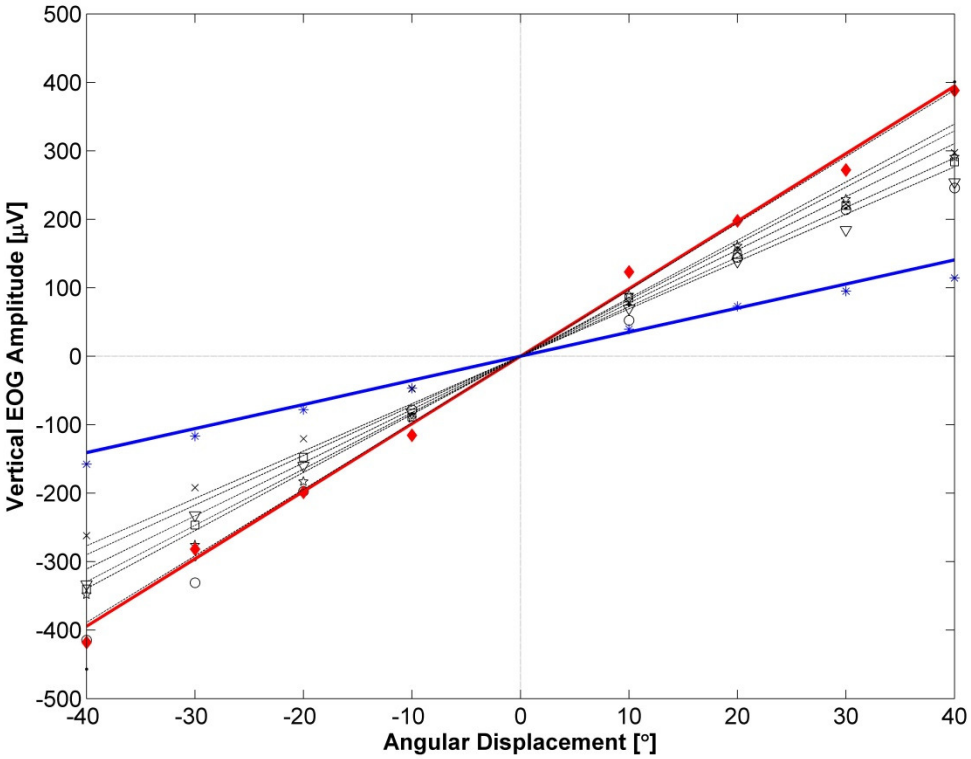

Figure 3.9 Vertical EOG amplitude versus gaze position angular displacement across eight subjects; blue line represents the lowest measured sensitivity, the red line represents the highest measured sensitivity

System noise level was also assessed during this experiment, as the users held the central gaze position so that the resting potentials generated at the sensor inputs could be observed. Noise levels during these observations for all users never exceeded 10 µV.

Results across the subjects show the linear relationship between EOG saccades and angular displacement of the eye holds true. In order to exploit this relationship the EOG signals must be normalised such that these variations do not disrupt levels of control within an AT system. A calibration routine was developed and will be discussed in the following section.

3.5 Calibration and Normalisation

When the headband (Figure 3.2) is initially applied, the sensors need around one second to settle to a constant level due to the time constant associated with the high input impedance. Once a constant level below the noise threshold is achieved the calibration routine will run

automatically. The routine consists of a circle that moves to several locations on the screen. The gaze locations relate to maximum eye deflections on both the horizontal and vertical planes that are required for the system. Figure 3.10 shows the positions of the circle on screen.

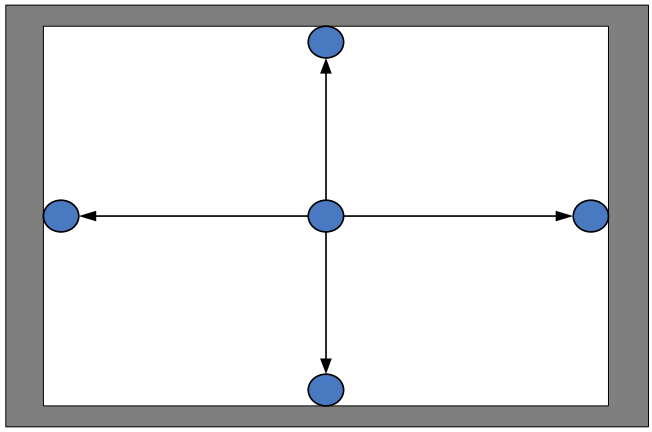

Figure 3.10 Calibration screen: during the calibration routine the user is instructed to make a series of eye movements between locations represented by the dots: left, right, down and up, starting and ending at the central resting position in the middle of the screen.

Figure 3.11 shows a typical EOG signal for both the horizontal and vertical eye movements recorded during the calibration routine. We can see there is no cross talk between signals; they are completely independent from one another. The peak signal excursion is used to compute the deviation from the screen centre point. The amplitude of these peaks will depend on the position of the electrodes and the position of the user with respect to the screen. The signal to noise for the vertical signals is clearly lower than the horizontal, consistent with the lower angular resolutions seen, both with this method and others reported in the literature.

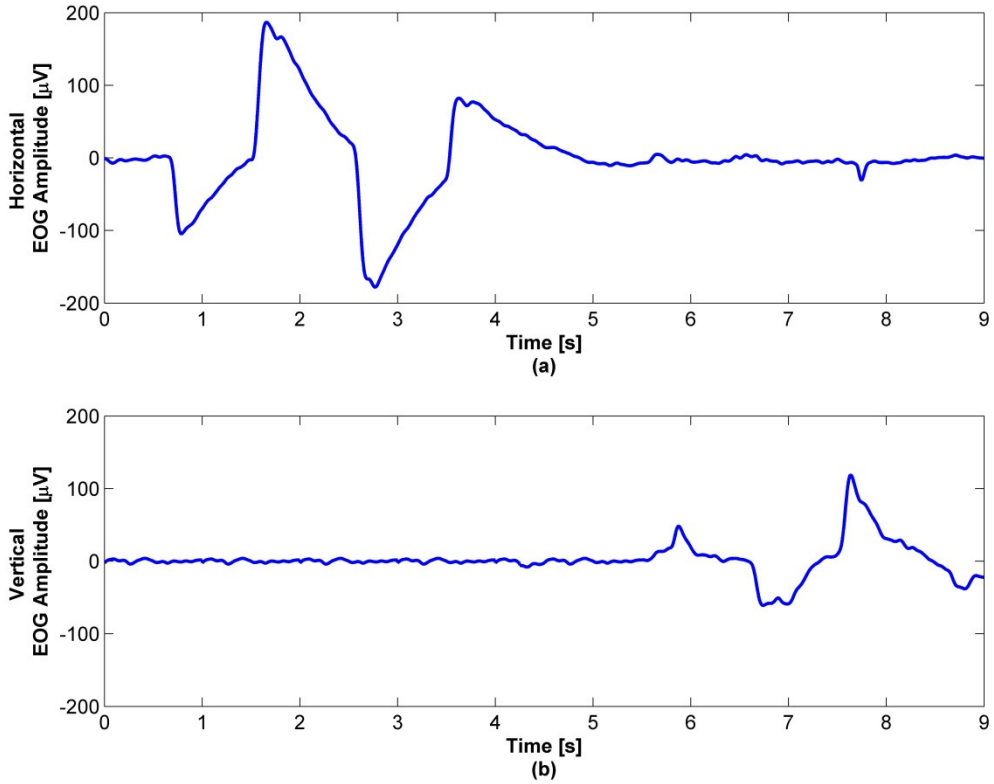

Figure 3.11 EOG Signals recorded during a calibration routine: (a) Horizontal EOG, negative signal shows the eyes looking far left, positive shows eyes far right (b) Vertical EOG, negative is down, positive is up.

During the calibration routine, the real-time EOG signals are buffered in software until the routine comes to the end. At the end of the routine, the user will have completed maximum eye deflections for the system, and these maximum deflections can be used to normalise the EOG signals for use in an AT system. Depending on the position of the user, the maximum and minimum deflections might not be the same: if a user is slightly to the right of the origin, the left deflection will be larger than the right. The same relationship will hold for the vertical plane. Thus in order to normalise any saccadic eye movements they must be normalised to their individual maximum and minimum values, corresponding to gaze locations far right, left, up and down. Figure 3.12 shows the flow chart demonstrating how the calibration routine runs in order to obtain maximum and minimum EOG values for both the horizontal and vertical planes.

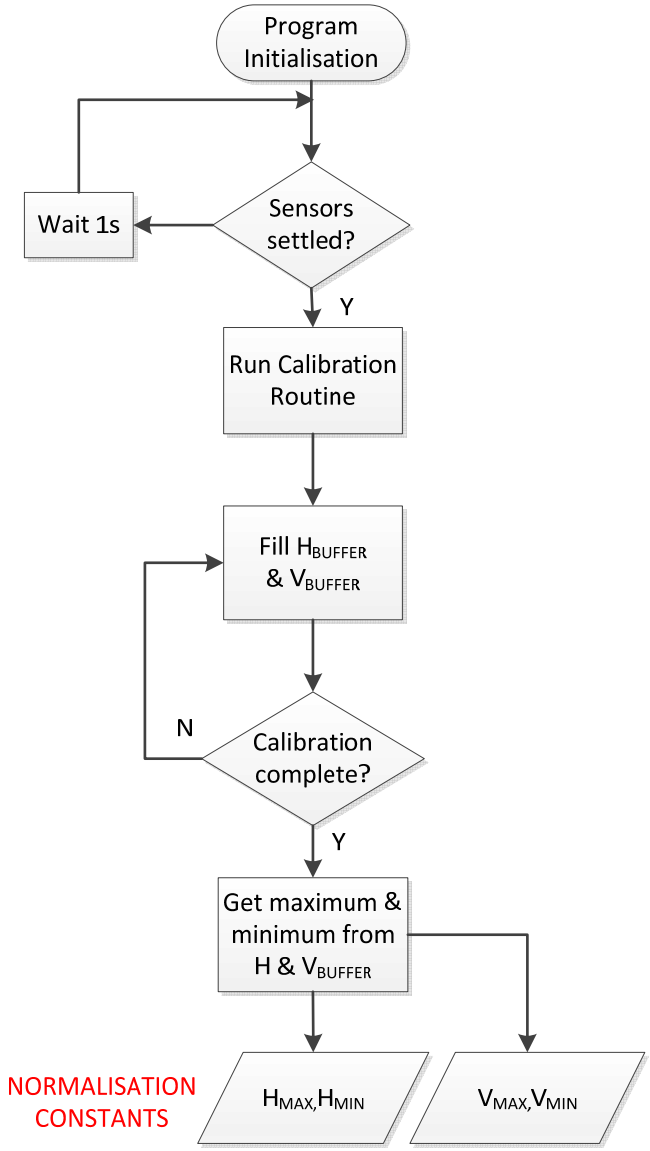

Figure 3.12 Flowchart showing how the calibration routine is implemented in software in order to normalise the real-time EOG signals

3.6 Feature Extraction

It is important that valid features of an EOG signal can be extracted for use in an AT system. Valid features of the EOG signal are the saccadic changes in EOG amplitude corresponding to changes in gaze locations as well as eye blinks which have not been discussed until this point. Eye blinks are another exploitable characteristic of EOG signals that make it exceptional for use in AT systems. Blinks are a combination of EMG signals and vertical saccades; they are greater in amplitude than the maximum amplitude on the vertical plane arising from intentional eye movements and they are much shorter in duration than normal saccadic eye movements. A

typical eye blink consists of a quick rise and fall in amplitude, the entire process lasting between 100 and 200 ms [104]. Since the characteristics of blinks differ greatly from saccades, they can easily be used as a control signal such as mouse clicks [33, 100]. Figure 3.13 shows EOG signals for some eye movements that occur during human computer interaction.

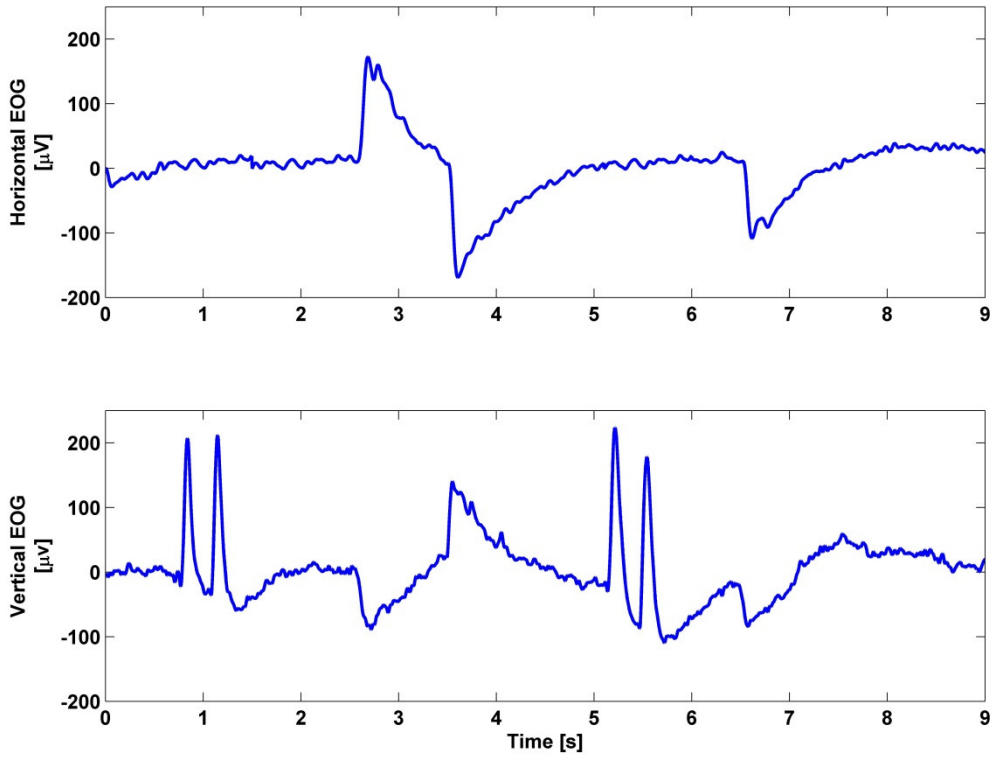

Figure 3.13 Example EOG signals for typical eye movements occurring during human machine interaction, acquired by the Electric Potential Sensor: (a) Horizontal (b) Vertical

The data seen in Figure 3.13 was recorded using LabVIEW; the real-time signals were fed into a feature extracting algorithm, the flowchart for which is shown in Figure 3.14. The algorithm determines the amplitude of the saccades and thus the change in gaze angle and direction of eye movement made by the user. It also determines if the user blinks. Features are extracted by identifying a valid saccade, which is one that has occurred if the change in amplitude lasts longer than 30 ms, as discussed in Section 3.1. The saccades are divided by the maximums determined during calibration: the results are values normalised to ±1. Blinks are also identified by this timing threshold, but are further identified by their amplitude being greater than maximum vertical deflection.

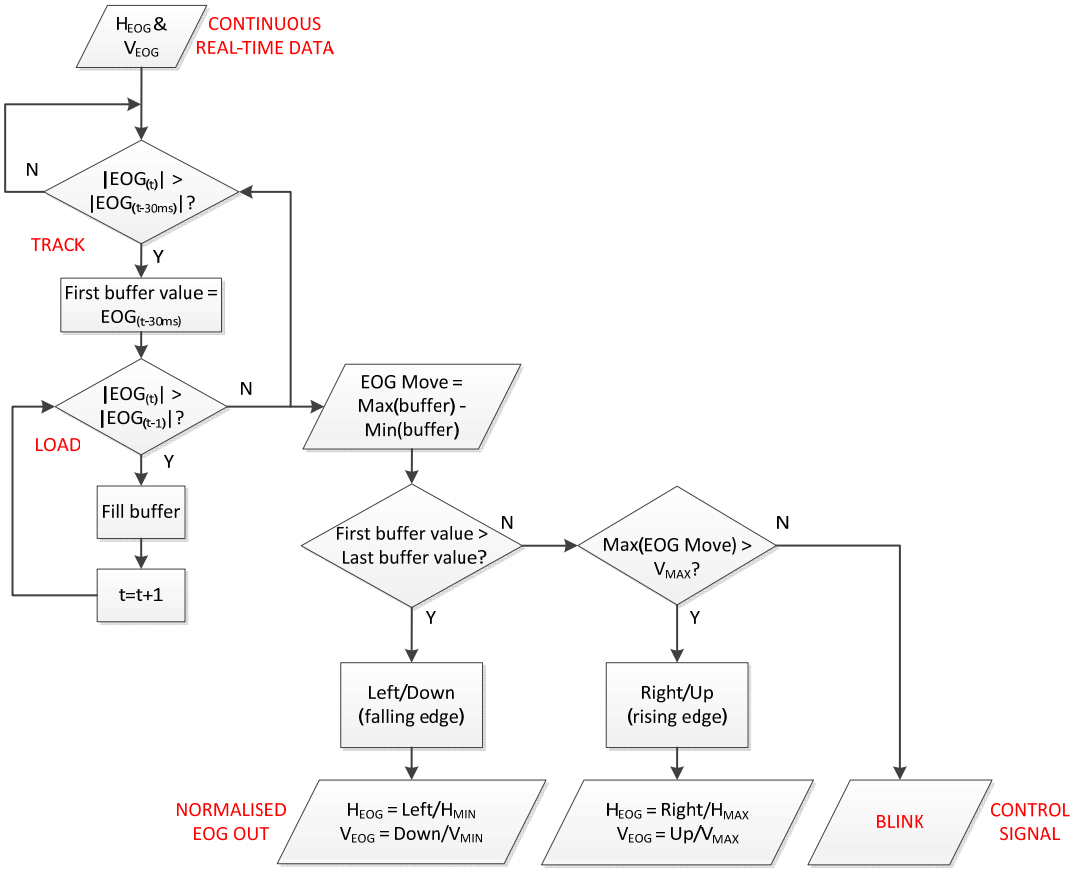

Figure 3.14 Flowchart showing how the feature extraction routine is implemented in software in order to identify characteristics of the real-time EOG signals

The output from the feature extraction algorithm for the sequence of eye movements in Figure 3.13 is outlined as a time series in Table 3.1.

Table 3.1 Output results from the EOG feature extraction algorithm with the eye movement signals presented in Figure 3.13 as the input

Time (seconds)	Horizontal EOG	Vertical EOG	Gaze Indication
0 to 2.5	No changes > 30ms	2x Blinks	Control Signal
2.5	Rising edge	Falling edge	Right and Down
2.5 to 3.5	No change > 30ms	No change > 30ms	Fixation
3.5	Falling edge	Rising edge	Left and Up
3.5 to 5	No change > 30ms	No change > 30ms	Fixation
5 to 6	No change > 30ms	2x Blinks	Control Signal
6.5	Falling edge	Falling edge	Left and Down
6.5 to 9	No change > 30ms	No change > 30ms	Fixation

3.7 Discussion and Future Work

Experimental work within this chapter has demonstrated the ability to acquire high quality, repeatable EOG signals across a variety of subjects using three Electric Potential Sensors. It has been shown that with the configuration used, EOG signals are comparable in resolution and linearity with systems previously published requiring more than three electrodes [19, 97]. Users were required to put on the apparatus themselves, minimizing preparation time. With little instruction all were capable of placing the head band in a position that was appropriate for adequate EOG signal acquisition.

The linearity of EOG signals with respect to eye displacement throughout all of the trials shows that these EOG signals are highly suitable for use in AT applications. However, due to the variability in sensitivities it is necessary to incorporate calibration and normalisation techniques so that any user can benefit from the same control algorithms.

A method for calibrating and normalising the EOG signals was described. This technique demonstrates how to overcome the variability in individual eye movements. Once normalised to ±1, the eye movements detected within a system can be converted for any control algorithm. Systems can involve scaling eye movements into pixel locations, or they can be used as binary control inputs or state machine variable control inputs. A feature extraction method was also presented that discriminated between valid saccadic eye movements as well as eye blinks. It was shown that blinks are an easily exploitable attribute of the eyes and subsequently the EOG signals since they occur only on the vertical and display different characteristics than those of simple eye movements. Blinks can then be used for control signals such as mouse clicks or binary on/off control instructions etc.

This first demonstration of an EPS based EOG eye tracking system has served as proof of principal. Appendix E details methodologies that would be employed for future work in order to verify the systems statistical significance and benchmark against other technologies. A method has also been presented that would be employed to test the effectiveness and reliability of the feature extraction algorithm (Appendix E.3).

Applications opportunities based on these EOG signal acquisition, calibration and feature extraction techniques could easily be applied to any system where an assistive technology is based on human interaction, including communication and mobility control systems.

4 Surface Recording of an Evoked Potential: The Electroretinogram (ERG)

4.1 Introduction

Previous chapters have described some biopotentials and the capability of the Electric Potential Sensors to acquire high quality, repeatable signals non-invasively and directly from the skin. The EPS has already been proven capable of acquiring high quality EEG signals, both in contact mode and remote mode [52]. It is for this reason that the School of Optometry and Vision Sciences Research Group[2] [105] at Cardiff University approached the Sensor Technology Research Centre to investigate whether the Electric Potential Sensor was capable of acquiring electroretinograms. The electroretinogram (ERG) is a type of visually evoked potential arising from the retina in response to a light stimulus and will be described in detail in the following section.

Visually evoked responses are a change in electric potential within the body caused by the central nervous system arising from an external visual stimulus. These responses are used primarily to measure the functional integrity of the visual pathways from retina via the optic nerves to the visual cortex of the brain. These responses differ from the previously discussed biopotential, EOG, whereby they cannot be controlled; they can only arise with the application of a visual stimulus. Evoked potentials tend to be very small in amplitude, typically in the range of hundreds of microvolts to millivolts [106, 107]. This feature of evoked potentials makes them difficult to acquire. Low noise highly sensitive electrodes are required to resolve these signals over other electrophysiological activity within the body. Signal averaging techniques must be employed to extract any useful information from these signals. Signal averaging is necessary and simple to achieve. Since evoked responses follow an applied stimulus that is often periodic, signals can then be averaged with respect to the stimuli [106, 107].

[2] I would like to acknowledge Dr Alison Binns and Dr Tom Margrain for providing the equipment and expertise required to run the experiments carried out in order to acquire standard ERG signals with the conventional systems described.

4.2 The Electroretinogram

The electroretinogram (ERG) is the measurement of light induced electrical responses of different cell types in the eye, more specifically cells within the retina. Flashes of light of different colours or patterns are directed at a chemically dilated pupil; the cellular response is then recorded by electrodes. ERG recording is a widely used ocular electrophysiological test allowing assessment of eye health problems that may arise in both the rods and cones in the outer retina as well as associated pathways in the middle and inner layers of the retina [108-111]. Figure 4.1 shows the most common human ERG response, containing the a-wave and the b-wave, elicited from a full field flash of light. This stimulus is called Ganzfeld stimulation which spans the whole visual field so that gaze direction is unimportant [67, 112].

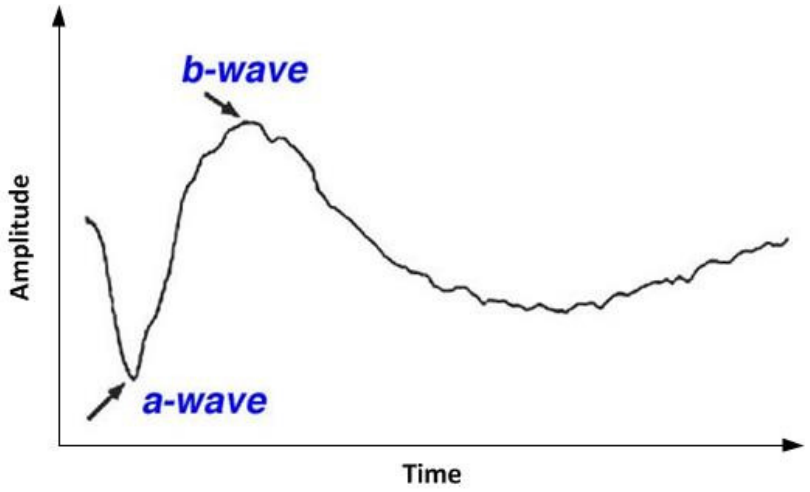

Figure 4.1 The basic waveform of the electroretinogram showing the a-wave arising from solely the rods and cones and the b-wave arising from cells of the retina , taken from [67]

Sufficiently bright stimuli will elicit an ERG containing the a-wave (the initial negative deflection) followed by the b-wave (positive deflection). The leading edge of the a-wave is produced by the photoreceptors (rods and cones) [113], while the remaining portions of the response are produced by a mixture of cells within the retina [67]. The ERG parameters that are customarily measured in an ophthalmic clinic for electrodiagnosis are amplitudes and timings of the a-wave and b-wave, shown in Figure 4.2.

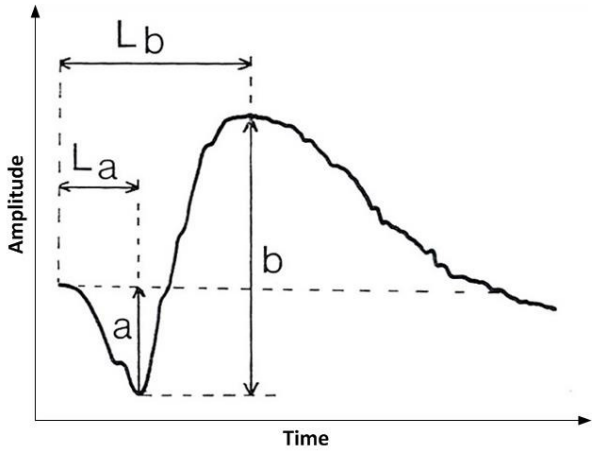

Figure 4.2 a- and b-wave amplitude and time measurements of the basic ERG waveform, taken from [67]

The a-wave amplitude (a) is measured from a baseline monitored before the light stimulus is applied, to the trough of the negative wave. The b-wave amplitude (b) is measured from the trough of the a-wave to the peak of the b-wave. While these are important parameters of the ERGs composition, they vary greatly with the type of recording electrode used [114, 115]. The temporal properties of the ERG are independent of the type of recording electrode used. These properties are defined by the time-to-peak (implicit time) of the a-wave and the b-wave. These times (L_a and L_b) are measured from the stimulus onset to the respective troughs and peaks; results will vary depending on stimulus rate and intensity and the state of eye adaptation. The eye can be light or dark adapted, yielding photopic and scotopic ERGs respectively [116]. These features of the ERG make it a useful tool when monitoring the neurological status of a patient; ERGs can be monitored when a patient is either awake or anesthetised. Abnormal shapes and latencies found in an ERG can lead to a diagnosis of various degenerative diseases of the eyes [110, 111, 117], such as Age-related Macular Degeneration (AMD) [118]. In 1989 a basic protocol was standardised [119] such that ERG recordings carried out across the world could be comparable. This standard was outlined and is maintained by the International Society for Clinical Electrophysiology of Vision (ISCEV) [60]. ISCEV outlines recommendations for five

retinal evoked responses for evaluation, all named according to conditions of eye adaptation. An outline of these standard measurements can be found in Table 4.1.

Table 4.1 Standard ERG measurements and stimuli, as set by ISCEV [60]

	Measurement	Rate of Stimulus	Indications
1	Dark-adapted ERG (Scotopic)	0.5Hz – 2 Hz Flash	Rod response
2		Typically 10 Hz	Combined rod and cone response
3		Typically 15 Hz	Oscillatory potentials, arising from the amacrine cells [67]
4	Light-adapted ERG (Photopic)	0.5 Hz – 2 Hz Flash	Cone response
5		30 Hz Flicker	Cone response

These recorded ERGs result from measuring the electrical response from an eye electrode with respect to a reference electrode which is placed either on the forehead or on the temple. Several different types of DC electrodes are used for acquiring ERGs; some of the most common are shown in Figure 4.3.

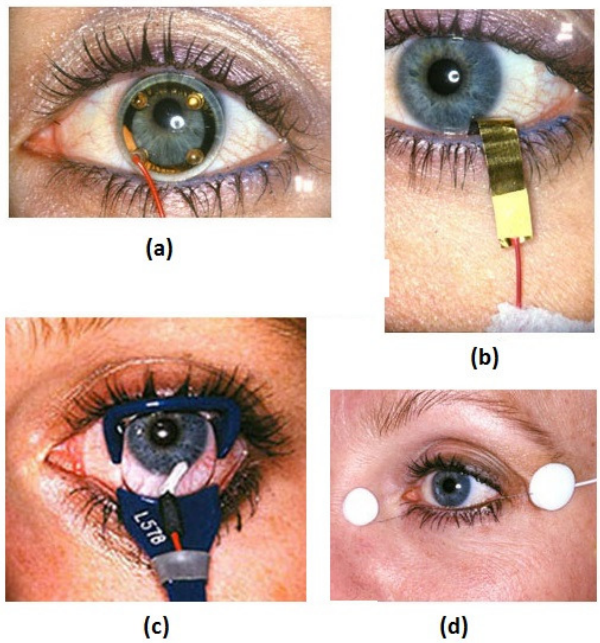

Figure 4.3 Different types of corneal electrodes used for acquiring ERGs (a) Contact lens (b) Hook (c) Cotton wick with speculum and (d) DTL fibre, images taken from [67]

As can be seen, all of these recording electrodes are highly invasive which is not ideal for primary investigations of the retinal function, especially for those of children [114, 120, 121]. ERGs have been recorded using Ag-AgCl electrodes placed on the orbital ring around the eye, and while this recording technique is preferable when investigating children or people averse to having electrodes placed in their eyes, factors such as the electrode position and eye lid movements can degrade the skin ERG. Using Ag-AgCl electrodes requires skin preparation; conductive gels and the electrodes must be taped on to the eye lid. These time dependent factors mean that an incorrectly placed electrode must be repositioned, which may further upset a patient [109, 121]. Adequate ERG signal detection with the Electric Potential Sensor could overcome these factors limiting skin electrodes, since no skin preparation is required when using the EPS and it can be held in place without the use of an adhesive.

It should be noted that the experiments described here follow the clinical procedures outlined by ISCEV [119] for light-adapted ERG recordings. The experimental subject was the same throughout all experiments. The stimuli apparatus was run by a professionally trained Optometry specialist from the School of Optometry and Vision Sciences at Cardiff University [105], the same operator was used during each experiment. These specialists were also responsible for positioning the electrodes correctly, including the EPS, for all of the experimental work. Throughout the experiments, the specialists operated their own data acquisition systems, my contribution was to operate the data acquisition system I designed specifically for acquiring the ERG signals with the EPS (Figure 4.4). The aim of the experiments was to achieve a comparison of the quality of signal acquisition capabilities of the EPS versus conventional techniques. Temporal parameters acquired from the EPS are compared against those from some standard electrodes used for recording ERG signals [122]. All subsequent data processing and analysis presented was my contribution to this work with no assistance from Cardiff University. Results presented do not include any medical analysis.

4.3 Initial Experiments

4.3.1 Method

Initial experiments were carried out in a darkened screened room; the use of a screened room was employed to minimize the effects of environmental noise on the sensors. The subject was given a drop of tropicamide to dilate the pupil, which was light adapted for 10 minutes. Stimuli

were generated with a miniature Ganzfeld LED stimulator, details of which can be found in [123, 124]. The stimulator was held between two and five centimeters from the eye; further details about the stimulator and the experimental protocol can be found in [118]. Two Electric Potential Sensors were used to acquire the ERG signals: one was held below the eye on the lower lid and the second acted as a reference electrode placed on the forehead. The electrode and system configuration can be seen in Figure 4.4.

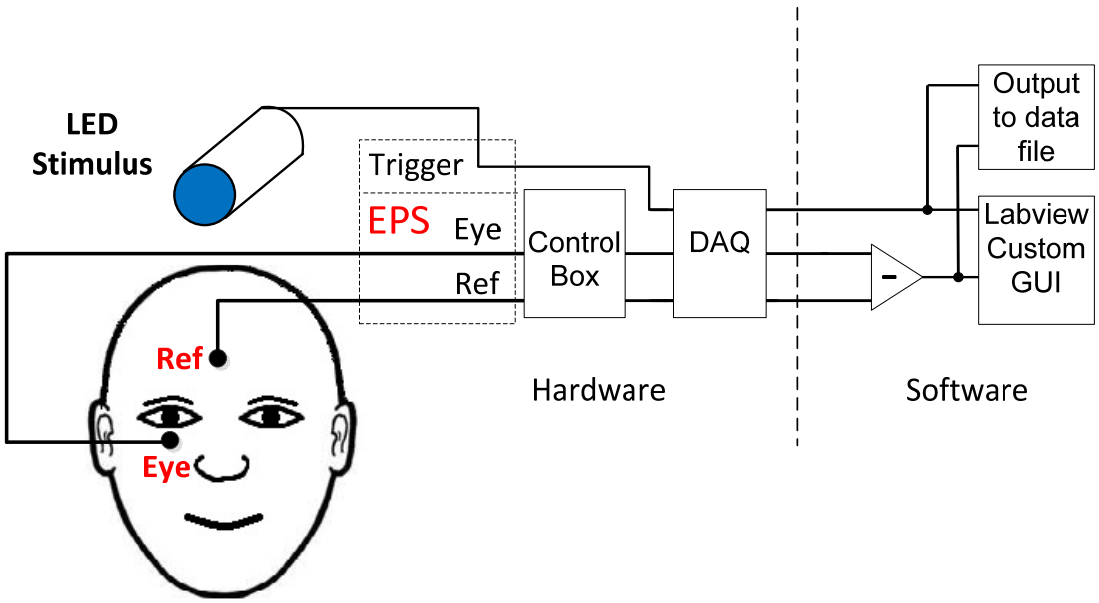

Figure 4.4 Block diagram demonstrating the configuration of sensors, LED stimulus, DAQ and the associated software components for acquiring ERG, including facial EPS placements

The sensors used for these experiments are the same sensors that were used for acquiring EOG signals, which have been described in Chapter 2. The output signals from the sensors were taken through a control box with an additional ten times amplification and anti-aliasing filtering before being converted at 20 kSamples per second from analog to 16-bit digital signals by a National-Instruments USB 6212 real-time data acquisition card. LabVIEW software was used to acquire and record the data, the program code is shown in Appendix B3. The signal processing required a simple differential measure of the eye electrode (Eye) minus the reference electrode (Ref). The trigger signal from the light stimulus was also recorded so that off line averages could be computed.

4.3.2 Results

Experimental results are presented here for two different stimuli; both are from a light-adapted left eye. The photopic cone responses from 5 Hz and 30 Hz full-field LED stimulation with maximum pupillary dilation are discussed. Five data sets for each of the two different stimuli frequencies were taken with the EPS in order to determine mean and standard deviations for implicit time measurements, as discussed in Section 4.2. Results of the EPS recordings, taken from the darkened screened room, are compared to recordings that had been previously collected using conventional electrodes on the same subject having been prepared in the same way. This data, provided by Cardiff University, was acquired using DTL fibre electrodes as well as Ag-AgCl skin electrodes [122] in an open laboratory. Placement of the Ag-AgCl electrodes was the same as that used for the EPS (Figure 4.4). An Ag-AgCl electrode was taped to the forehead to act as the ground electrode; both the under eyelid skin electrode and the DTL fibre electrode were referenced to a skin electrode taped to the temple adjacent to the eye under investigation, in this case the left eye. These ERGs were digitised at 1000 samples per second into 16-bit signals by an industry standard evoked potential monitoring system, Medelec Synergy EP [125]. The digitised signals were then filtered by the accompanying software: a first order highpass and a second order lowpass filter provided a bandwidth of 1 Hz to 100 Hz. MATLAB was used to graph all ERGs and to post-process the recorded EPS signals, which included signal averaging and down sampling from 20 kSamples per second to match the standard of 1000 samples per second. Program code is provided in Appendix C. The data provided by Cardiff University were specified as ERGs resulting from an Amber LED stimulation, as in the literature [118]. However it should be noted that this detail is inaccurate since there are no Amber LEDs in the Mini-Ganzfeld stimulator, the Amber was created by mixing spectral components from White, Red, Green and/or Blue [123, 124].

4.3.2.1 5 Hz Response

A 5 Hz stimulus is non-standard with regard to ISCEV, but it was chosen for initial experiments to ensure electrical activity within the eye had time to return to the baseline before the next stimulus was presented. Figure 4.5 shows a comparison of the EPS data recorded in the screened room and the ERGs acquired using conventional recording electrodes whilst applying an amber 5 Hz full-field flash stimulus. Averages were computed over a 200 ms window, with the trigger signal used to align the EPS data with the DTL and skin electrode recordings.

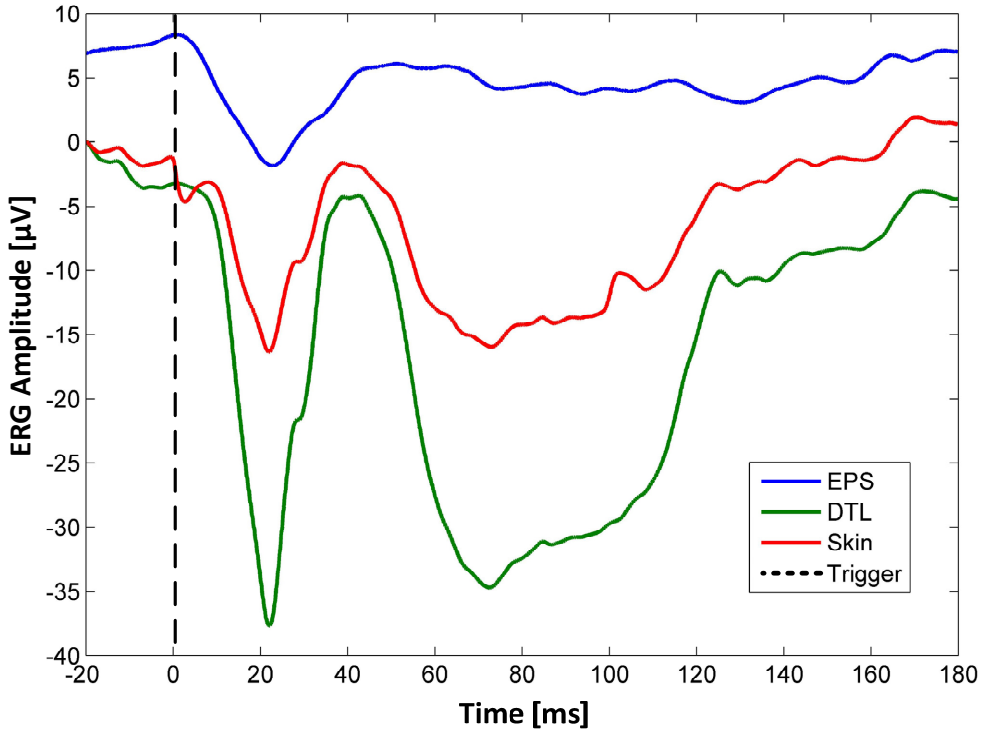

Figure 4.5 Comparison of photopic ERG signals resulting from a 5 Hz full-field LED stimulus measured by the EPS, DTL fibre and Ag-AgCl electrodes, signals averaged 50 times over a 200 ms period

It can be seen from the graph that the EPS acquired a response from the 5Hz stimulus with a similar shape to those acquired with the DTL fibre and skin electrodes, although smaller in peak to peak amplitude with a small DC offset. The difference in amplitudes can be attributed to the non-invasive capacitive nature of EPS coupling to the skin as well as the differences in electrode types, as discussed in the literature [120, 126, 127]. In order to verify that this signal was indeed the evoked response, the subject was asked to close their eye during a recording cycle; this was taken as the control data to determine if the ERG was a valid response detected by the EPS. Fourier analysis was performed on two sets of non-averaged data, one with the eye closed and the second with the eye open, Figure 4.6 shows the results of this frequency domain analysis on a ten second long data set.

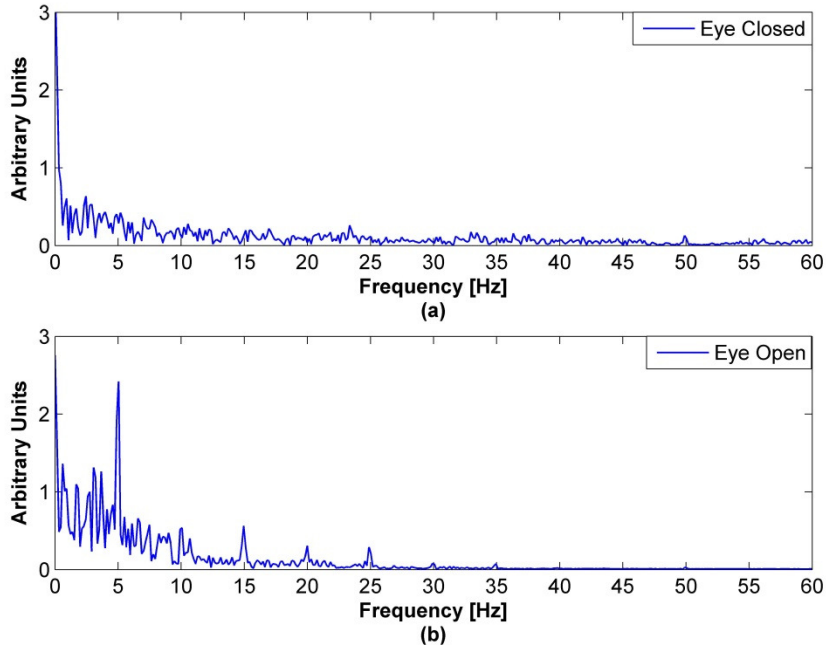

Figure 4.6 Frequency domain measurement of the 5 Hz evoked potential with the eye closed (a) and open (b) in order to verify the signal

It can clearly be seen from the above graph that a strong 5 Hz component as well as the expected harmonics are present in the data when the eye is open and none of these components are present when the eye is closed, thus verifying that we have indeed acquired the 5 Hz evoked response from the retina.

Further time domain analysis was carried out on the ERGs; Figure 4.7 shows indications of the a- and b-Wave implicit time (L_a and L_b) for all three electrode recordings. Table 4.2 outlines the measured means and standard deviations for comparison.

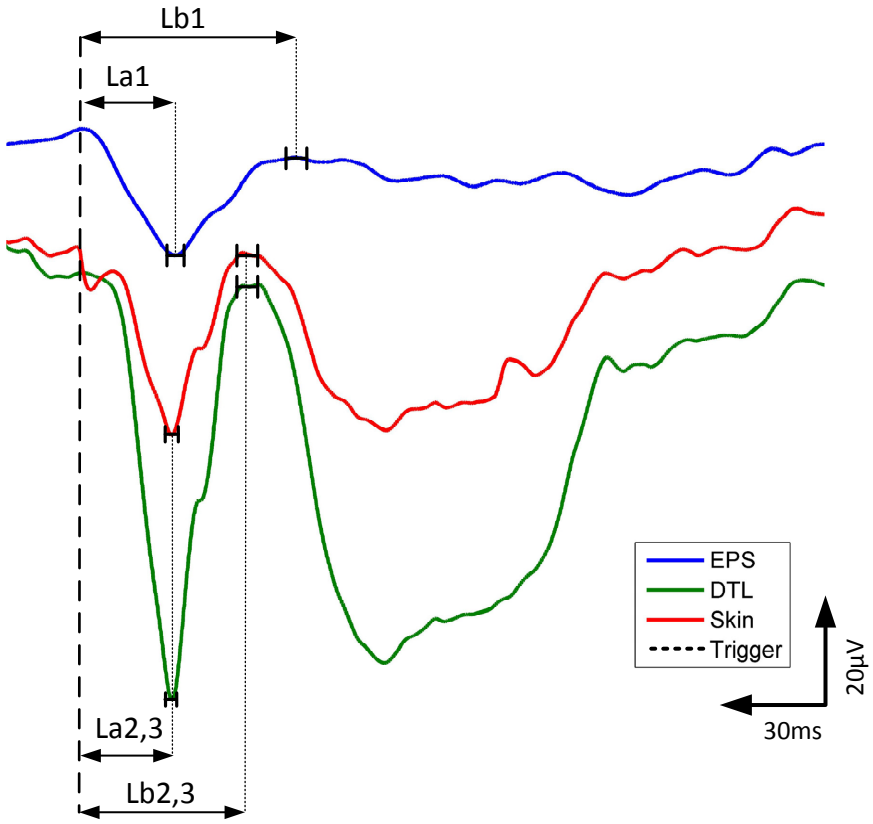

Figure 4.7 Implicit time indications on 5 Hz ERGs recorded from: the EPS (blue), DTL (green) and Ag-AgCl skin electrodes (red)

Table 4.2 Implicit time measurements from 5 Hz flash ERG

	Implicit Time (mean ± SD)	
Electrode Type	L_a (a-wave)	L_b (b-wave)
EPS	25 ± 2.2 ms	44.7 ± 3.6 ms
DTL	22 ± 0.5 ms	38.6 ± 1.1 ms
Skin (Ag-AgCl)	22.2 ± 0.7ms	39.2 ± 1.4ms

Good results in implicit time have been observed, and the EPS measurements agree with previously published results [118]. The longer observed implicit times on the EPS can also be attributed to the filtering effects of the AC coupling at the capacitively coupled input of the sensor.

4.3.2.2 30 Hz Response

Figure 4.8 shows a comparison of the EPS data recorded in the screened room and the flicker ERGs acquired using conventional recording electrodes for an amber 30 Hz full-field stimulus. Three cycle averages were computed over a 90 ms window; the trigger signal was used to align the EPS data with the DTL and skin electrode recordings. In this case the initial trigger occurs at the time of zero seconds, the implicit time is then measure from the trigger point to the first peak in ERG amplitude, as indicated on the graph. The results are in agreement for implicit time measurements; there is still evidence of some signal smearing on the EPS, which again can be attributed to the capacitive nature of the sensor input. Numerical measures (mean and standard deviation) of implicit time for each ERG recording can be found in Table 4.3.

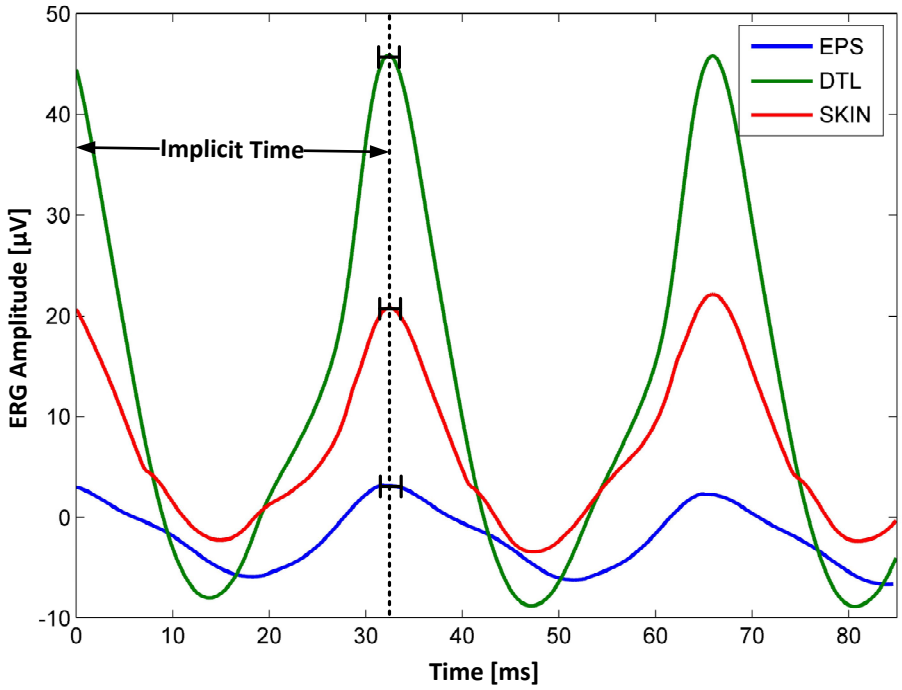

Figure 4.8 Comparison of implicit time measurements from photopic ERG signals resulting from a 30 Hz full-field LED stimulus, measured by the EPS, DTL fibre and Ag-AgCl electrodes, signals averaged 100 times over a 90 ms period

Table 4.3 Implicit time measurements from 30 Hz flicker ERG

Electrode Type	Implicit Time (mean ± SD)
EPS	32.9 ± 2.7 ms
DTL	32.3 ± 1.4 ms
Skin (Ag-AgCl)	32.5 ± 1.6 ms

Once again similar results of implicit time measurements have been observed and all results agree with previously published values [116, 128, 129].

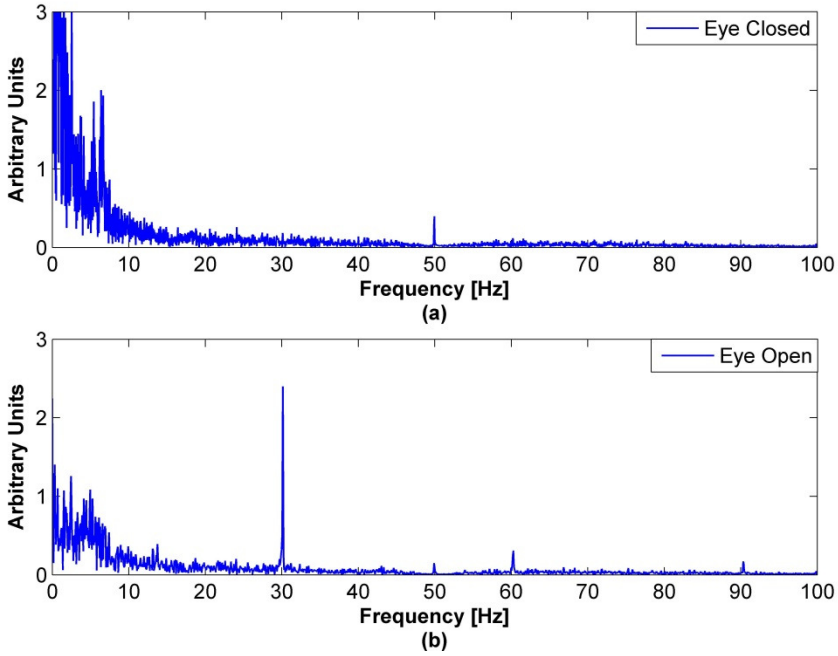

Figure 4.9 Frequency domain measurement of the 30 Hz evoked potential with the eye closed (a) and open (b) in order to verify the signal

Figure 4.9 shows the results of the Fourier analysis of two ten-second data sets. One is a control set where the eye under investigation was closed while the stimulus was applied, compared to a data set recorded when the eye was open while the stimulus was applied. We can see a clear 30 Hz frequency component is present when the eye was open, and none at all when the eye was closed, thus verifying we have detected the cone response from a 30 Hz visual stimulus.

4.4 Further Experiments

4.4.1 Method

Following on from the successful ERG signal acquisition in a screened environment, experiments were moved to a typical ophthalmology open laboratory set up at Cardiff University. The same subject was used and was prepared in the same way as previously discussed in Section 4.3.1. The EPS electrode placement and software configurations remained unchanged (Figure 4.4). The aim of the secondary experiments was a direct comparison between EPS and DTL fibre during simultaneous recordings, therefore the subject was required to have two pairs of recording electrodes applied during the experiments. The DTL fibre was inserted into the lower lid of the eye under investigation (left); it was referenced to an Ag-AgCl skin electrode taped to the temple adjacent to the eye. Data acquired from the DTL fibre electrode was at 1000 samples per second into 16 bit digital signals by an industry standard evoked potential monitoring system, Medelec Synergy EP [125]. The digitised signals were filtered by the accompanying software: a first order highpass and a second order lowpass filter providing a bandwidth of 0.1Hz to 100Hz. MATLAB was used to graph all ERGs and to post-process the recorded EPS signals. This included signal averaging and down sampling from 20 kSamples per second to match the standard of 1000 samples per second. Program code is provided in Appendix C.

4.4.2 Results

Experimental results are presented here for two different stimuli, both from the light-adapted left eye. Photopic cone responses from a 1 Hz full-field and 30 Hz flicker white LED stimulation with maximum pupillary dilation are discussed. In both cases the stimulator was held between two and five centimeters from the eye. Five data sets for each of the two different stimuli were taken in order to determine mean and standard deviations for timing parameters, as discussed in Section 4.2.

4.4.2.1 30 Hz Response

Figure 4.10 shows ERGs resulting from the 30 Hz flicker stimulus; both DTL fibre and EPS data recorded simultaneously are compared. Table 4.4 specifies the numerical results (mean and standard deviation) of the implicit time measurements.

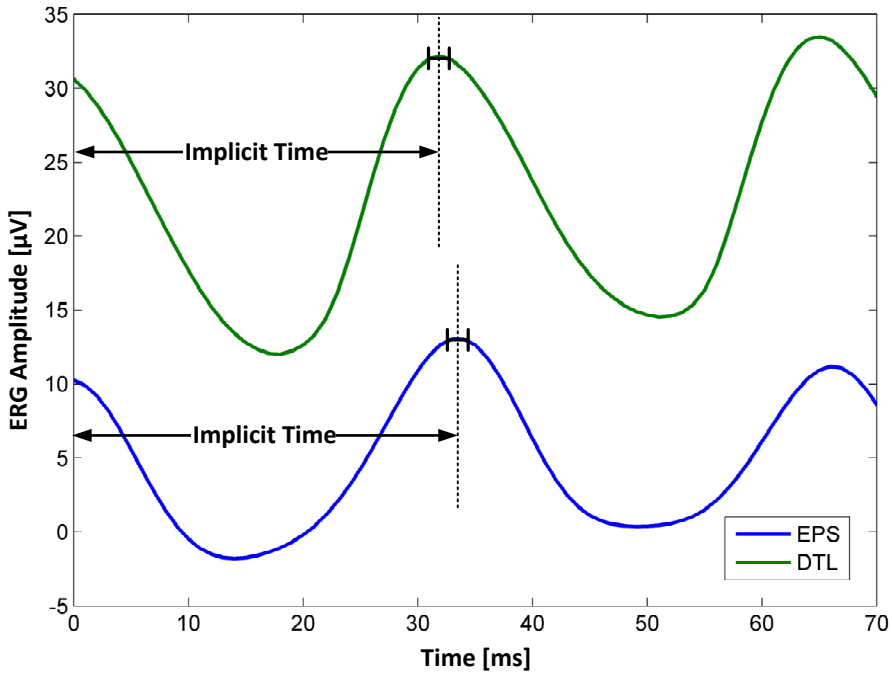

Figure 4.10 Comparison of implicit time measurements from photopic ERG signals resulting from a 30 Hz full-field LED stimulus, measured simultaneously by the EPS and DTL fibre electrodes, signals averaged 10 times over a 70 ms period

Table 4.4 Implicit time measurements from 30 Hz flicker ERG

Electrode Type	Implicit Time (mean ± SD)
EPS	33.1 ± 2.1 ms
DTL	32.2 ± 1.2 ms

Implicit time measurements correlate well between the two different types of recording electrodes. Both results agree with both previously presented data (Section 4.3.2.2) and with previously published data [116, 128, 129].

Fourier analysis was carried out on data from both types of recording electrodes; results are presented in Figure 4.11 for one second worth of data. We can see from the graphs that for both the DTL fibre and the EPS recordings, a clear 30 Hz frequency component is present, as well as the smaller second and third harmonics at 60 Hz and 90 Hz.

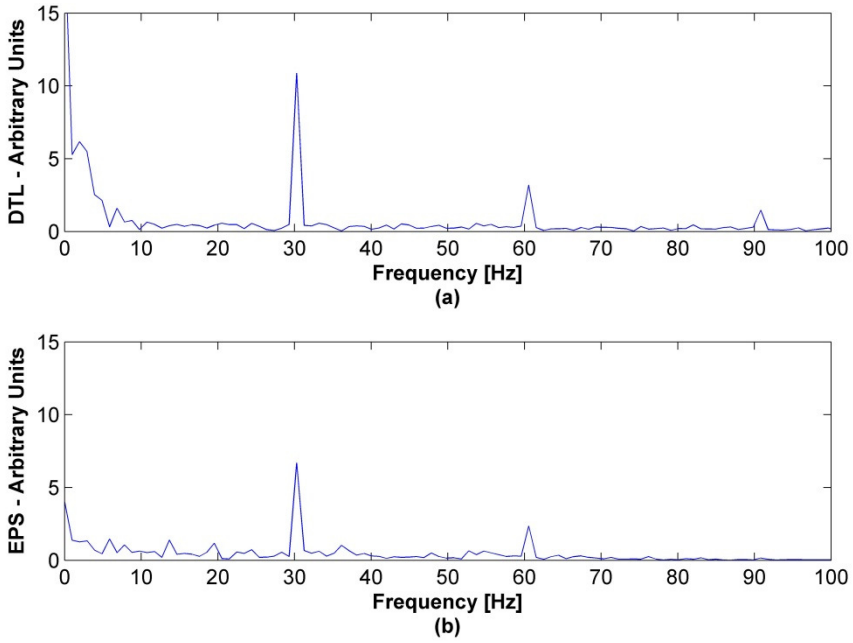

Figure 4.11 Frequency domain measurement of the 30 Hz evoked potential comparison between signals measured with a DTL fibre (a) and the EPS (b)

4.4.2.2 1 Hz Response

Figure 4.12 shows the raw ERG and stimulus triggers acquired during a white 1 Hz full-field stimulation. It is clear that the ERG response follows the trigger with a trough and peak in amplitude as expected. Although the third response at time ~2.1 s is smaller in amplitude than the others, it is still discernible as an evoked response due to the timing of the b-wave peak in amplitude following the stimulus. Figure 4.13 shows the ERGs simultaneously recorded from the EPS and the DTL fibre for the 1 Hz stimulus, but no averaging has been done on the data due to the recording capabilities of the conventional equipment used. Also with such a slow stimulus, it is difficult for the subject to hold the eye open without introducing movement artefacts or blinks into the signal acquisition. Again we can see a slight delay of the b-wave peak recorded by the EPS which can be attributed to the front end characteristics.

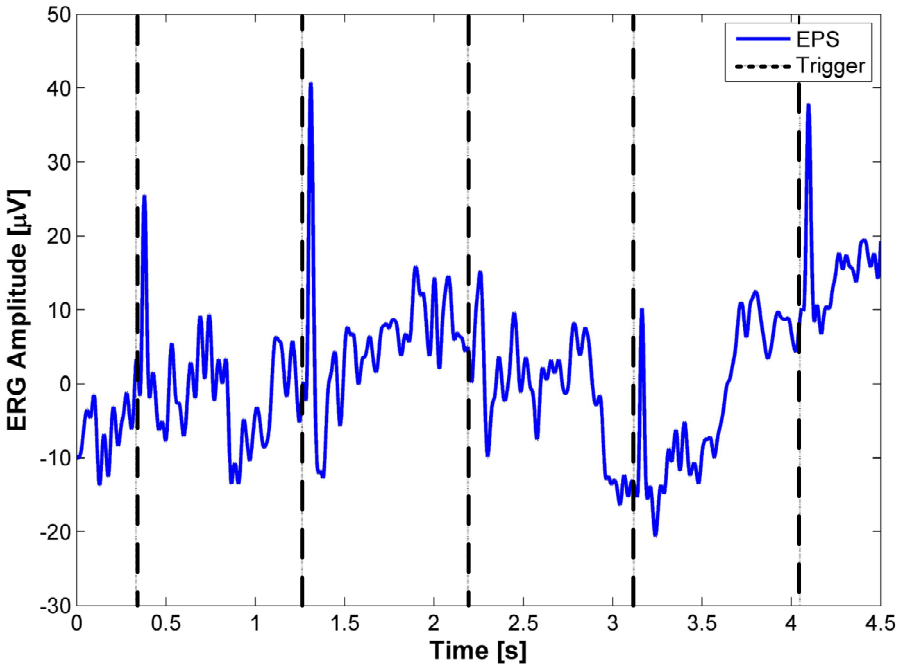

Figure 4.12 EPS measurement of five ERG responses to 1 Hz stimulus over 4.5 seconds

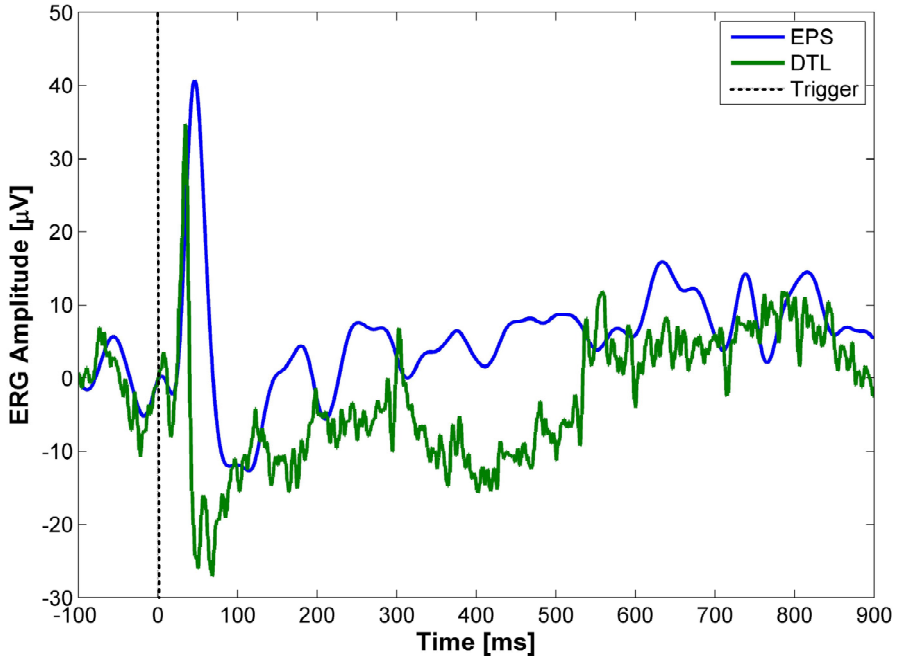

Figure 4.13 Comparison of non-averaged photopic ERG signals resulting from a 1 Hz full-field LED stimulus measured simultaneously by the EPS and DTL fibre electrodes

In Figure 4.14 implicit time measurements have been added to a magnified portion of Figure 4.13. Table 4.5 outlines the implicit time measure in terms of mean and standard deviation.

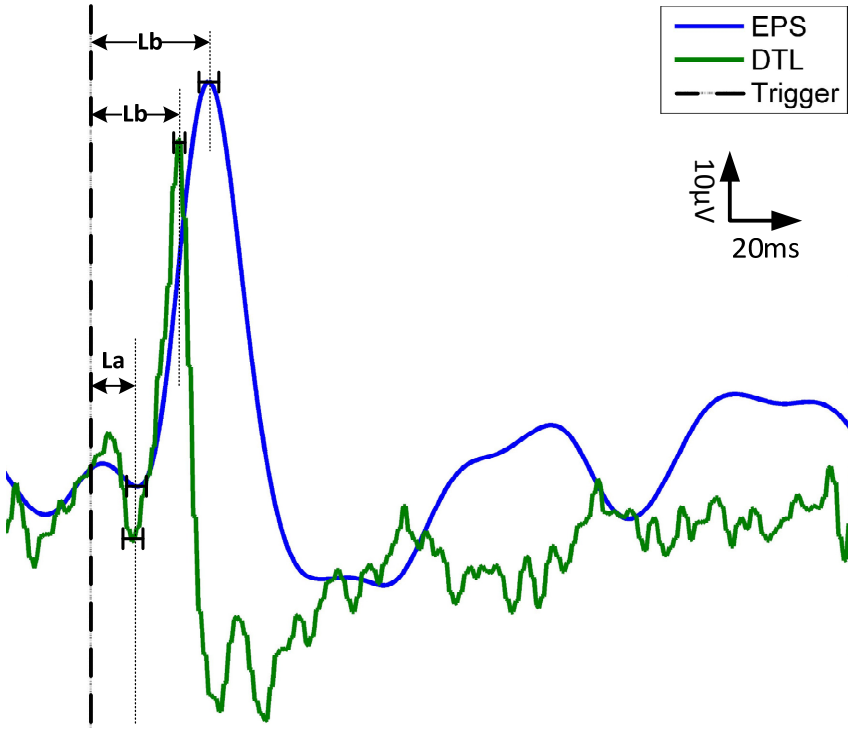

Figure 4.14 Comparison of implicit time measurements from photopic ERG signals resulting from a 1 Hz full-field LED stimulus, measured simultaneously by the EPS and DTL fibre electrodes

Table 4.5 Implicit time measurements from the 1 Hz flash ERG

	Implicit Time mean ± SD	
Electrode Type	L_a (a-wave)	L_b (b-wave)
EPS	17.3 ± 1.3 ms	42 ± 3.2 ms
DTL	16.6 ± 0.5 ms	34.6 ± 0.5 ms

Good results can be seen when comparing the EPS and DTL recordings; the longer b-wave implicit time can again be attributed to the capacitive input characteristics of the EPS.

4.5 Discussion and Future Work

The research presented aimed to investigate the feasibility of using the Electric Potential Sensor for surface recordings of high quality electroretinograms, a visually evoked potential of the retina. ERGs were compared for the same subject using different stimulus colour, frequencies and recording electrodes. ERGs recorded with the EPS were compared to those recorded from some conventional style electrodes, more specifically the invasive DTL fibre and the non-invasive Ag-AgCl skin electrode. Comparable results of implicit time measures were achieved across the stimulus frequency range investigated (1 Hz, 5 Hz and 30 Hz). Throughout investigations a common occurrence was apparent: the EPS introduced a slight smearing effect or time delay in the recording of the ERG signals. This can be attributed to the capacitive input characteristics of the EPS. While the EPS has a 0.1 Hz hardware low frequency cut-off, the conventional electrodes are DC electrodes and will not be affected in this way.

One of the main objectives of this investigation was to determine if the EPS could be a viable replacement for the Ag-AgCl electrodes. As discussed in Section 4.2, these electrodes are not ideal for children; there are time dependant factors when using these electrodes such that skin preparation is required and gel must be applied. The preparation process must be repeated if the electrodes are incorrectly positioned. While the EPS electrode in its physical form provides a unique alternative since no preparation is required, the signal quality at low frequencies is not up to a standard acceptable for clinical diagnosis. From an electronic engineering point of view, this experiment was successful, proving that the EPS can successfully acquire this type of visually evoked potential. However, in terms of acceptance of a new technology into the medical field, improved results would be necessary. In addition to this, statistical verification of the results would be necessary. This would be achieved by observing ERGs across a variety of subjects and determining if they are statistically significant, Appendix E outlines a protocol for testing the results achieved by the EPS as well as a method to benchmark this against conventional technologies.

Possible future work could be to increase the input impedance at the sensor input to achieve an improved low frequency response. Alterations to the shape and size of the sensor housing, electrode and guarding could be investigated. Holding an electrode of 10 mm diameter to ones lower eye lid can cause difficulties achieving a full guard around the active electrode, which in turn degrades the signal levels and increases noise susceptibility. Decreasing the diameter could possibly overcome these issues.

5 Upper Limb Rehabilitation using Surface Electromyography (SEMG) and Real-Time Biofeedback

5.1 Introduction

Electromyography (EMG), the term used to describe the technique for recording and evaluating electrical activity produced by muscles [130], has been around since 1849 [131]. Muscles are made up of many fibres; these fibres carry electrical impulses transferred from the central nervous system. Each individual fibre can be thought of as a conducting strip carrying the impulses. These impulses, called motor unit action potentials (MUAPs), are what cause the muscle to contract. The central nervous system controls the muscle force by adjusting the amplitude and frequency of the MUAPs sent to the muscle fibres. Figure 5.1 shows a schematic of the EMG signal path from the neurological origin to its summation of MUAPs innervating the muscle. In early days, highly invasive techniques were used to detect these action potentials, whereby a needle electrode would be inserted into the muscle fibre. However, the summation of MUAPs causing a muscle to contract can be detected at the skin surface above the origin of the signal. The acquiring and evaluation of these signals from the skin is called surface electromyography (SEMG).

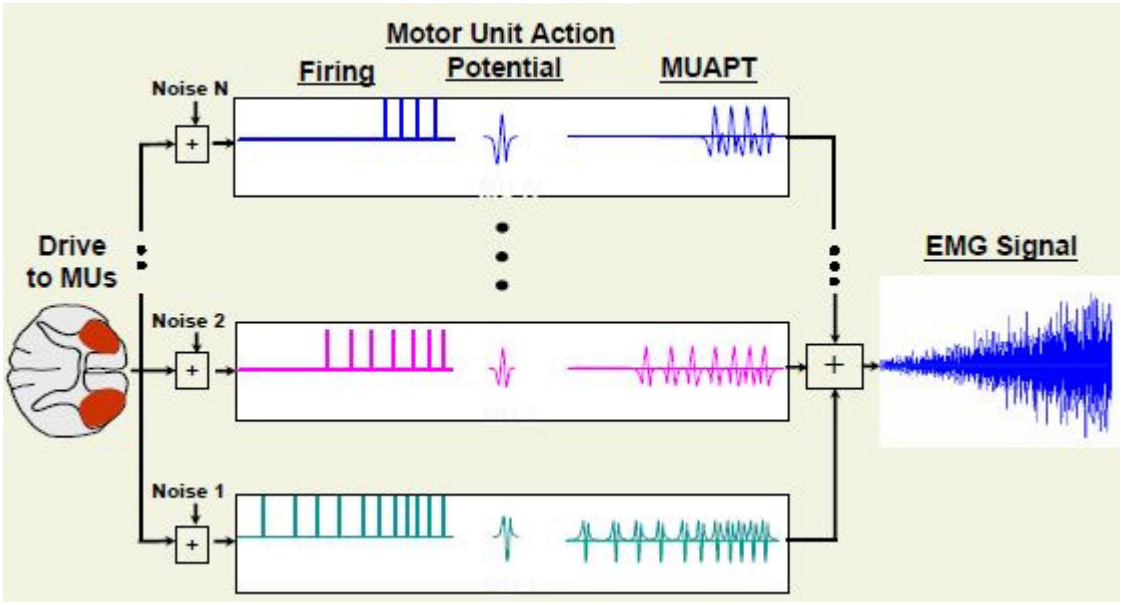

Figure 5.1 Illustration of how the EMG signal results from a summation of Action Potentials originating from the central nervous system, taken with permission from [61]

Two main types of voluntary muscular contractions exist: isometric and isotonic. An isometric contraction occurs when there is no change in muscle length and hence there is no associated movement. An isotonic contraction causes dynamic movement and the muscle length shortens and/or lengthens. The ability to collect information about muscle contractions non-invasively from the skin has attracted considerable interest in the fields of medical research [10, 11, 132], rehabilitation [12-18, 26-29], assistive technologies [25, 133-140] and sport science [16, 141, 142].

5.1.1 SEMG Signal Characteristics

Several attributes of the SEMG signals make them attractive signals for research use in the aforementioned fields. The main power frequency spectrum of SEMG signals typically ranges from 10 Hz to 250 Hz, depending on the type of contractions under investigation, it is generally accepted that amplifiers must provide a bandwidth up to at least 500 Hz [61, 62, 143]. Power spectral density (PSD) functions allow for frequency domain measures to be analysed. Mean, median and peak frequencies can be observed over time and are frequently used in muscle fatigue studies [133, 134, 144-146].

The SEMG potentials detected at the skin depend on several factors, including individuals, sensor placements and time of observation. Time domain analysis of muscle signals can include raw and rectified amplitudes. While these measures can offer valuable information they are not typically used due to their unquantifiable and variable nature. More common place in SEMG time domain analysis are the moving average filter, linear envelope filter and root mean square (RMS) calculations. The preferred recommendation for time domain processing of SEMG signals is the RMS [130, 147, 148]. Time domain analyses are a highly exploitable characteristic of SEMG signals for use in assistive technologies; applications such as wheelchair control [21, 23, 24, 149, 150], prosthesis control [135, 138-140] and assistive robots and robots for rehabilitation [28, 136, 137, 151-162] have all been proven successful in research. Since SEMG amplitudes can vary greatly they may not be useful for group comparisons or following events over time unless a suitable reference value is available. Several normalisation methods employing Maximum Voluntary Isometric Contractions (MVICs), for use as a reference have been described and reviewed, it is generally acceptable to choose the method which best suits the study [163, 164].

The experimental work discussed in this chapter focuses on a system designed for rehabilitation monitoring using normalised RMS SEMG amplitudes to monitor progression through a program of rehabilitation.

5.1.2 Biofeedback and Rehabilitation

Biofeedback is a technique where a person can learn to control some types of bodily responses at will. The technique can aid in developing a self-awareness of the body and help it to become more functional. The biofeedback process provides information usually on a meter, visual display, auditory unit or computer screen, about various bodily functions in order to achieve improved regulation. The aim of a biofeedback system is to provide a user with the correct information to support learning to move towards better control. There is considerable interest in using surface electromyography for quantitative rehabilitation studies [15, 17, 18, 165] as well as employing real-time SEMG signals in assistive [29, 158, 166] and biofeedback systems [68, 69, 167].

The systems presented in the literature [68, 69] propose a similar framework and user interface for ease of interpretation by a subject. In both examples the user is shown normalised SEMG amplitudes, acquired using surface As-AgCl electrodes, as an indication of

muscular force. The system presented aims to support the rehabilitation process [68], however provides no experimental results to support the use of their system. The second system was tested by 10 healthy subjects [69]; the bicep muscle EMG was monitored when the subject was instructed to carry out a specific task. No quantitative results have been published, however a usability report completed by the test subjects showed an 80% approval rate on potential system usability in a rehabilitation environment.

The system proposed in this chapter is similar in framework and interface to those presented [68, 69]; however an opportunity presented itself to test the system on a subject alongside a course of rehabilitation following an injury. The aim of the following experiment was not only to test an EPS biofeedback system on an appropriate subject but also to examine the effects of limb immobilisation following injury. Long periods of inactivity, brought about by hospitalization or broken limbs can influence the body in a variety of ways. The general influence of inactivity due to immobilization on the structure and function of skeletal muscle can cause muscle morphology (atrophy) or a change (decrease) in muscle function. Various models have been chosen to study the effects of limb inactivity on muscle function of healthy subjects, such as bed rest [168] and forearm immobilisation [169-172]. In the bed rest study [168], lower limb muscle activity was monitored. Flexion of the knee was performed prior to and after six weeks of bed rest, a 44% increase in normalised EMG (%MVIC) translating into a reduction in strength was observed at six weeks. Forearm immobilisation using casts have shown a range of reductions in strength, three week immobilisation studies have produced results ranging from a 14.7% [169] to 27% [171] and 29.3% [170] reduction during wrist flexion. In a shorter study with nine days of immobilisation, wrist flexion and extension decreased by 19.9% and 32.5%, respectively [172].

5.2 Method

A 31 year old female subject was presented following severe shoulder trauma. Injury was sustained to the right humerus, including shoulder dislocation and a fracture of the surgical neck with proximal migration of the humeral shaft. Surgery was required for plate fixation on the humerus; the subject was immobilised in a sling for six weeks post-surgery. During the first six weeks, the subject was advised not to actively move the injured arm. Muscle atrophy was visually realised resulting from the length of inactivity of the shoulder muscles. Extensive

rehabilitation was required in order for the subject to regain muscle mass, function and strength.

Once the subject had reached the active rehabilitation stage she agreed to weekly muscle monitoring sessions. Details of the SEMG monitoring system can be found in the following section (5.2.1); further details on the activities carried out during monitoring sessions are outlined in Section 5.2.2.

5.2.1 System

In order to monitor the rehabilitation progress a system was designed such that SEMG signals could be acquired and displayed in real-time on a custom GUI. The SEMG signals were acquired directly from the skin with the use of six Electric Potential Sensors. The sensors, which have been discussed previously in Chapter 1, included internal two stage amplification of x114. The sensors provided a bandwidth from 10 Hz to 3 kHz using a hardware first order bandpass filter. The output signals from the sensors were taken through a control box with an additional ten times amplification and anti-aliasing filtering before being converted from analog to 16-bit digital signals at 5 kSamples per second by a National-Instruments USB-6212 real-time data acquisition card. LabVIEW software was used to acquire, process and record the SEMG signals. Real-time signals were filtered using a 6^{th} order Butterworth filter from 20 Hz to 500 Hz in order to view the main signal components of the SEMG signals. Mains noise was filtered out using a 6^{th} order bandstop filter centred on 50 Hz with a 2 Hz bandwidth.

Single differential measurements were taken, from each of the sensors placed over the active muscles under investigation, with respect to reference sensors. Reference sensors are placed on a part of the body, away from the measurement point, with minimal EMG activity. The process of taking the single differential measurement removes common mode noise from the electrode measurement system. The single differential measurements were fed through an RMS filter with a 500 ms time constant before being displayed in real time to the user. Figure 5.2 shows a block diagram of the full system including both the hardware and software. LabVIEW Program code can be found in Appendix B4.

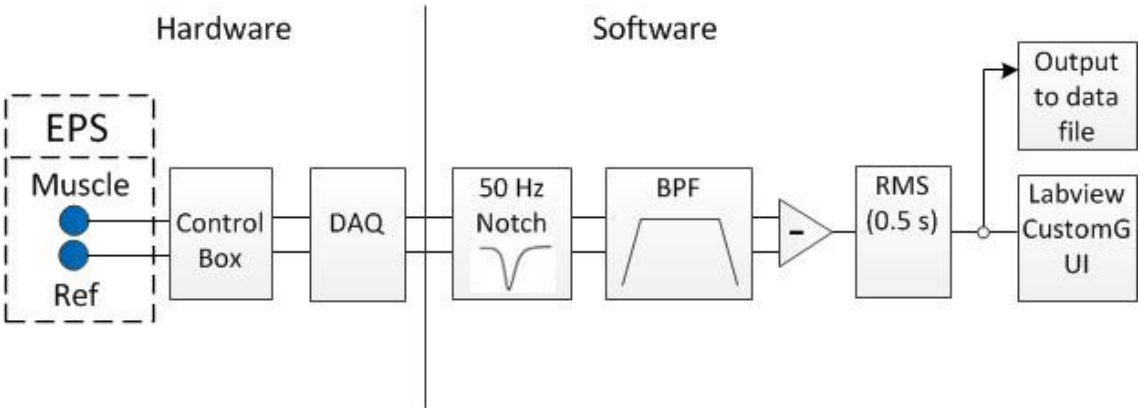

Figure 5.2 Block diagram demonstrating the configuration of sensors, DAQ and the associated software components for acquiring SEMG signals

SEMG signal amplitudes were displayed in an easy to interpret graphical form. Before any monitoring took place, the subject was given a short tutorial on the user interface so that she could easily understand the results. Normalised RMS amplitudes were displayed in real time, as well as a bar graph indicating %MVIC. The front panel display is shown in Figure 5.3.

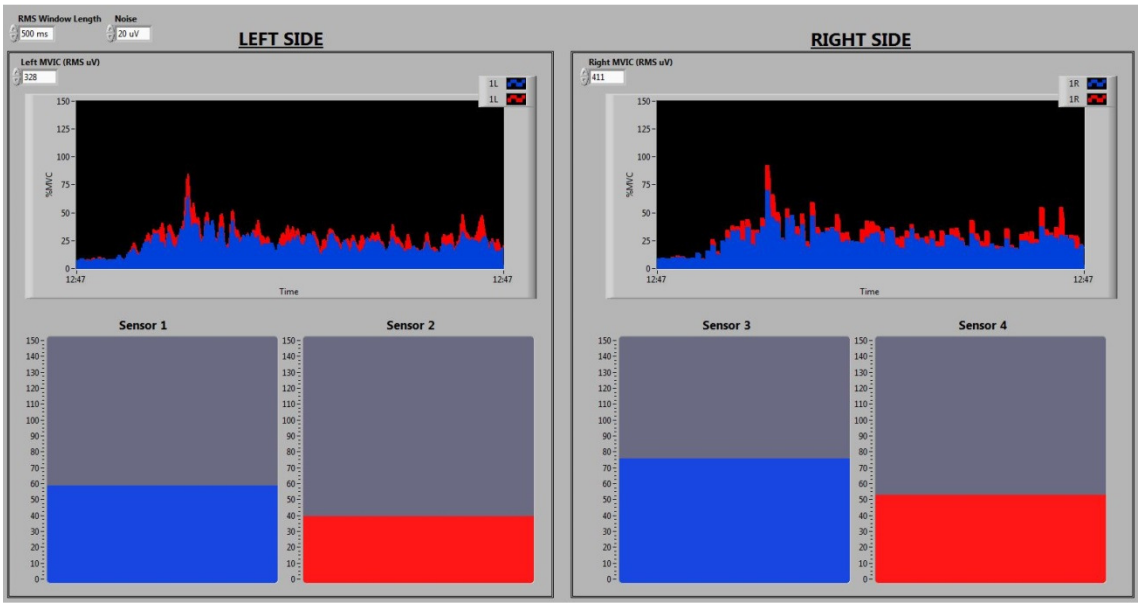

Figure 5.3 Real-time Biofeedback rehabilitation graphical user interface showing muscular activity for the left and right side of the body

5.2.2 Procedure

Rehabilitation exercises were aimed at gaining strength and range of motion during flexion and abduction movements of the shoulder. The normal range of motion of the shoulder can be seen in Figure 5.4. The deltoid muscle was chosen for observation during rehabilitation exercises because of visible signs of atrophy and due to the fact that it is a large close to the surface muscle which is highly innervated during these types of shoulder movements.

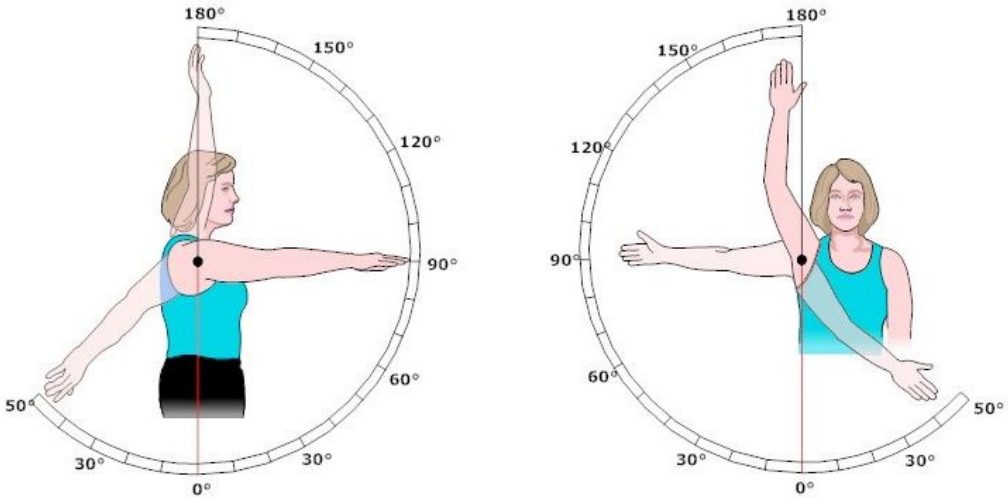

(a) **(b)**

Figure 5.4 Normal shoulder range of motion: (a) Flexion, from 0° to 180° (b) Abduction, from 0° to 180°, taken from [173]

Sensors were attached to the subjects left and right shoulders above anterior and lateral deltoids (Figure 5.5). Electrode locations were chosen using the SENIAM recommendations for sensor locations in the shoulder [143]. Two further reference electrodes were attached to each wrist. Reference sensors were required for both the left and the right side of the body in order to eliminate any ECG contamination that could arise from a cross body differential measurement. No skin preparation was required due to the capacitive nature of the EPS; sensors were attached to the shoulder using surgical tape to secure them in place.

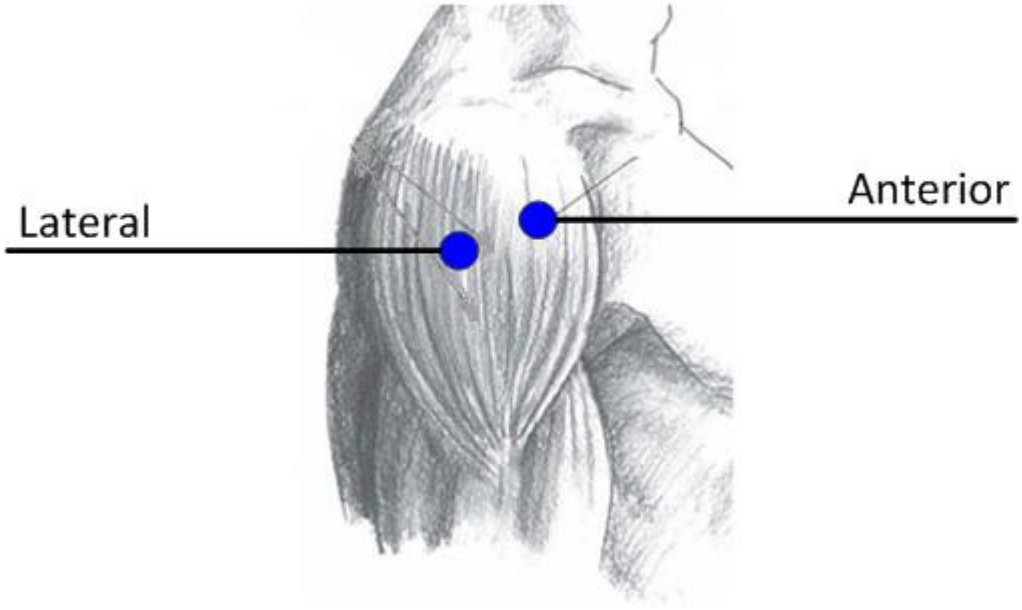

Figure 5.5 EPS electrode placement for acquiring SEMG signals during rehabilitation exercises, taken from [174]

Prior to monitoring and measuring, the subject warmed up with some light stretching and arm pendulum exercises. Once she felt she was adequately warmed up MVIC measurements for the session were recorded. MVICs were collected during each session in order to compare the muscle activities over the course of rehabilitation. To obtain the MVIC for each muscle tested, the subject was directed to perform a series of static resisted isometric contractions. While standing in an upright position the arm was restricted at 0° with resistance applied close to the elbow. For the lateral deltoid MVIC the thumb was pointing out, for the anterior deltoid the palm was neutral. The subject then applied a maximal effort contraction against the restriction for both abduction and flexion movements. The average RMS SEMG amplitude during three five second contractions was used as the MVIC for normalisation. The subject was instructed to rest for two minutes between each MVIC measurement in order to minimise fatigue. Once the MVIC for each muscle was ascertained, it was entered into the program for normalising the SEMG signals before displaying them on screen.

Measurements of system noise were also determined at the start of each recording session, the subject was instructed to stand still in an upright position while completely relaxing her deltoid muscles. Ten seconds of RMS data was averaged and used as the reference system noise for additional normalisation. Noise measurement results were consistently found to be 20 μV RMS.

Two exercises were carried out by the subject during each session: side lateral raise (abduction) and front raise (flexion). Repetitions were completed in a slow and controlled manner with an aim of keeping the MVICs for both arms around the same level as much as possible. The subject was allowed to practice, but advised to keep the number of repetitions minimal including at least a two second rest between movements to avoid fatigue.

5.3 Results

The procedure outlined in Section 5.2.2 was repeated during each monitoring session; sessions were carried out at six, eight, ten, 12 and 24 weeks post-surgery. Surface EMG data was collected for three repetitions of each of the movements. The data recorded using LabVIEW was post processed using MATLAB software. Post processing was used to compute the average of the SEMG amplitudes during three sustained contractions as well as graphically interpreting the results. During the primary stages of rehabilitation the subject was unable to raise her injured arm fully without the shoulder joint lifting in an irregular form. This was taken as an indication that incorrect muscles were being used to lift the arm and the results were discarded from the study. Maximum shoulder deflection, with no visual shoulder deformation, was recorded at each session and was used as a reference for progress. Table 5.1 shows a summary of the maximum deflection angles achieved (highlighted in grey) per session as well as the angles monitored to show the subjects progression.

Table 5.1 Maximum shoulder deflection angles, where no shoulder deformation occurred, during monitoring of rehabilitation exercises

Monitoring Week	**6**	**8**	**10**	**12**	**24**
Maximum shoulder deflection achieved [°]	**30**	30	30	30	30
		60	60	60	60
			90	**90**	**90**

In each of the cases above, a wall mounted measuring tape was used to infer a reference joint angle on the healthy shoulder. Before recording any data, the maximum normal deflection of the injured shoulder was measured at the fingertips visually along the tape. This distance was then used as the reference point; physical markers were used for either side of the body as end of movement points ensuring that both arms moved to the same angle. Calculation of the angle was then carried out using trigonometry and limb measurements. A shoulder to fingertip

measurement was taken as well as a hip to fingertip measurement in order to calculate the physical movement angle.

Figure 5.6 shows the results of the left and right lateral and anterior normalised SEMG amplitudes over time for 30° shoulder abductions. Data points represent the mean over three repetitions of each of the movements; the error bars indicate the associated standard deviations. There is a clear indication that the right injured shoulder required a much greater muscular force, in terms of %MVIC, to reach the desired deflection angle. Over time, the right SEMG tends towards the level of the healthy left SEMG and hence the isotonic contraction generated in the shoulder muscle in order to cause the arm to lift to a 30° deflection angle reduces.

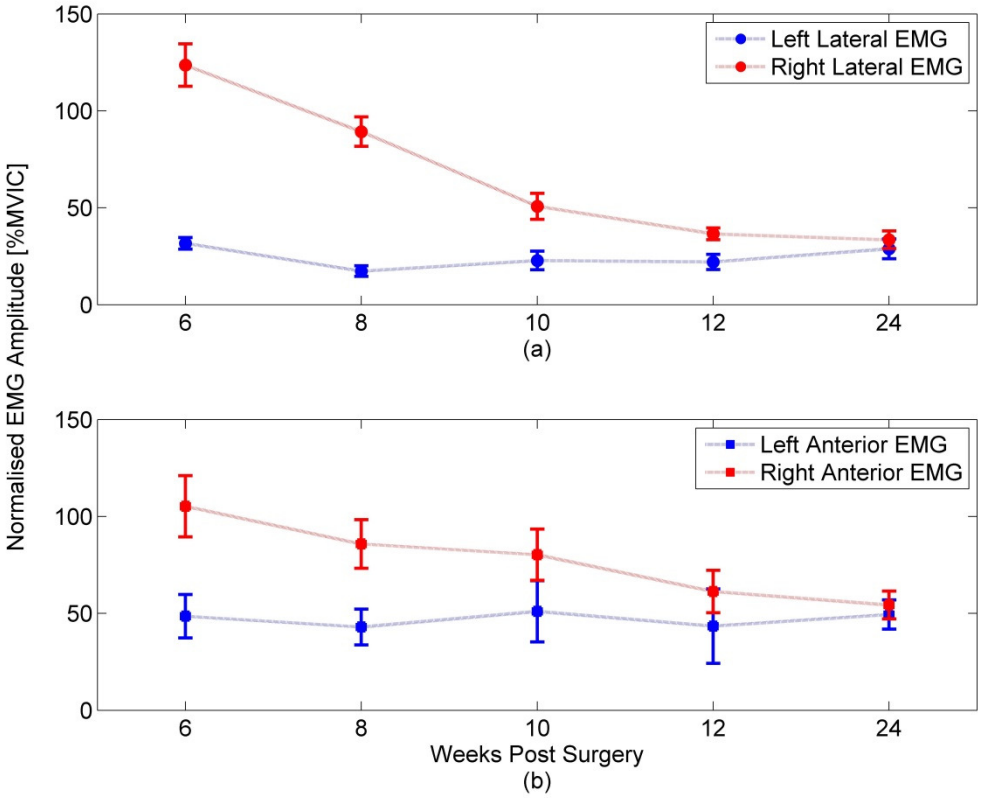

Figure 5.6 Comparison of normalised SEMG signals for right (injured) and left (healthy) shoulder muscles during a 30° abduction of the arms

Similar results can be found in Figure 5.7 for shoulder flexion movements. When comparing the SEMG amplitudes between the electrode locations, the anterior muscle appears to work harder than the lateral during both types of contractions. This is to be expected since the

anterior deltoid is responsible for joint stabilisation and will need to work harder, where the lateral deltoid is responsible for the physical movement.

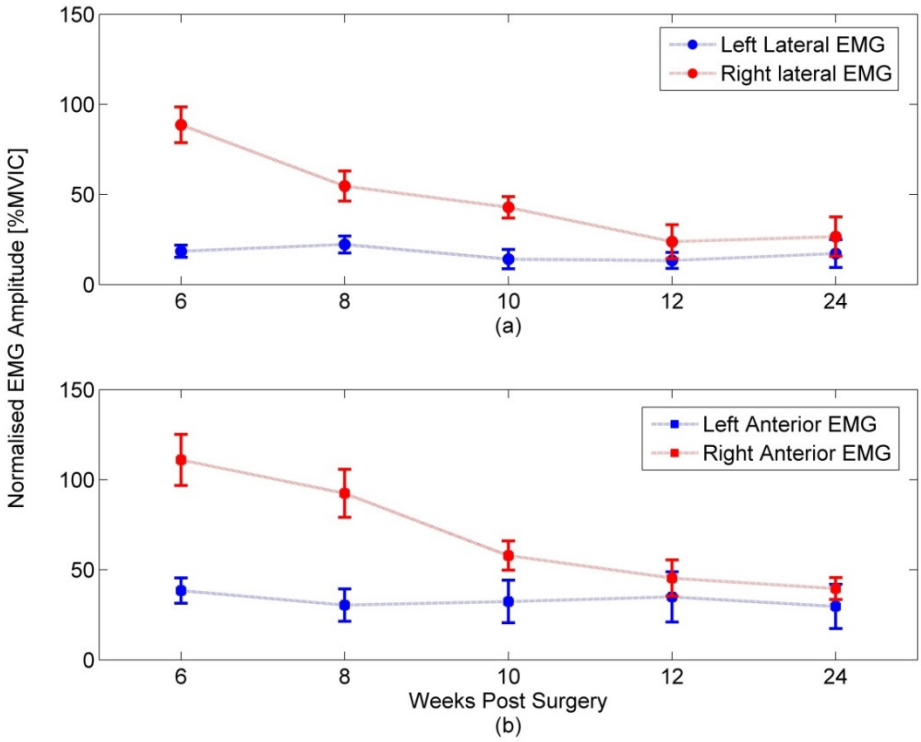

Figure 5.7 Comparison of normalised SEMG signals for right (injured) and left (healthy) shoulder muscles during a 30° flexion of the arms

Results for left and right lateral and anterior normalised SEMG amplitude versus time for 60° and 90° shoulder deflections in abduction and flexion showed similar tendencies (see 0). Figure 5.8 to Figure 5.10 show the results of the differences between left and right lateral and anterior normalised SEMG amplitude versus time for 30°, 60° and 90° shoulder deflections in abduction and flexion. It is clear that the right injured shoulder required a much greater muscular effort, in terms of %MVIC, to reach the desired deflection angle during the early stages of rehabilitation. Over time the right SEMG tends towards the level of the healthy left SEMG level required to generate the isotonic contraction to cause the arm to lift to the 30°, 60° and 90° deflection angles.

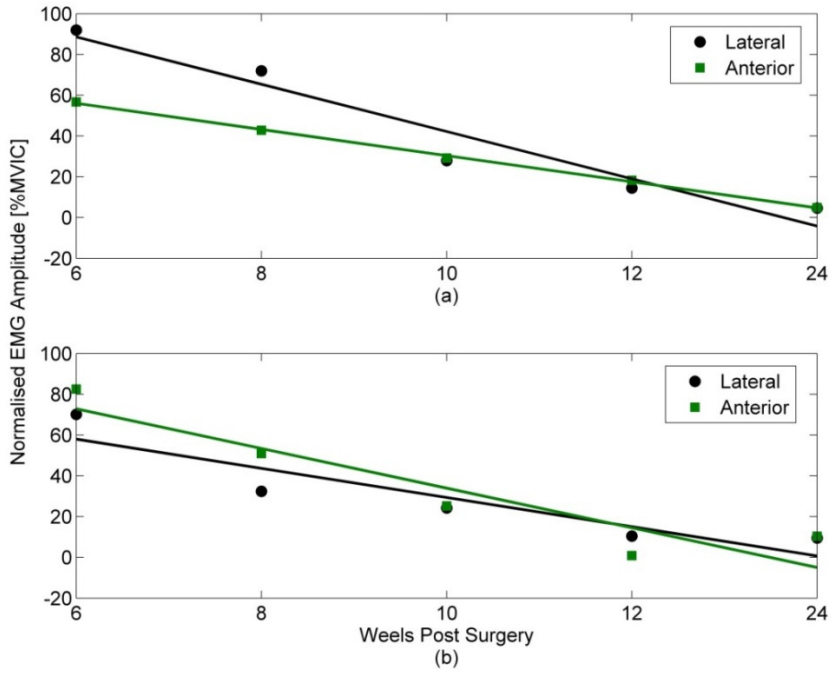

Figure 5.8 Comparison of the difference between the normalised SEMG amplitudes for the right and the left shoulder over the course of rehabilitation for a 30° abduction (a) and a 30° flexion (b)

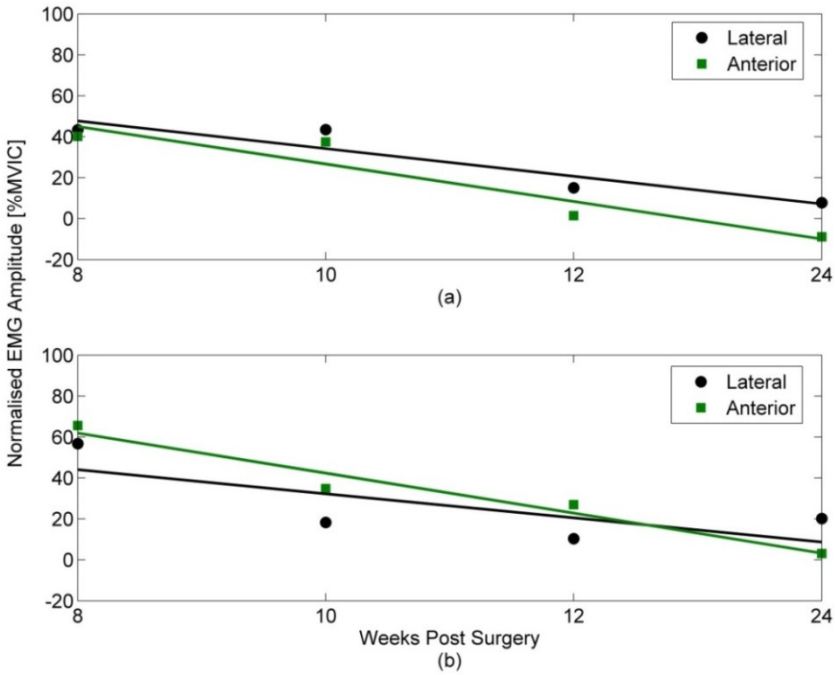

Figure 5.9 Comparison of the difference between the normalised SEMG amplitudes for the right and the left shoulder over the course of rehabilitation for a 60° abduction (a) and a 60° flexion (b)

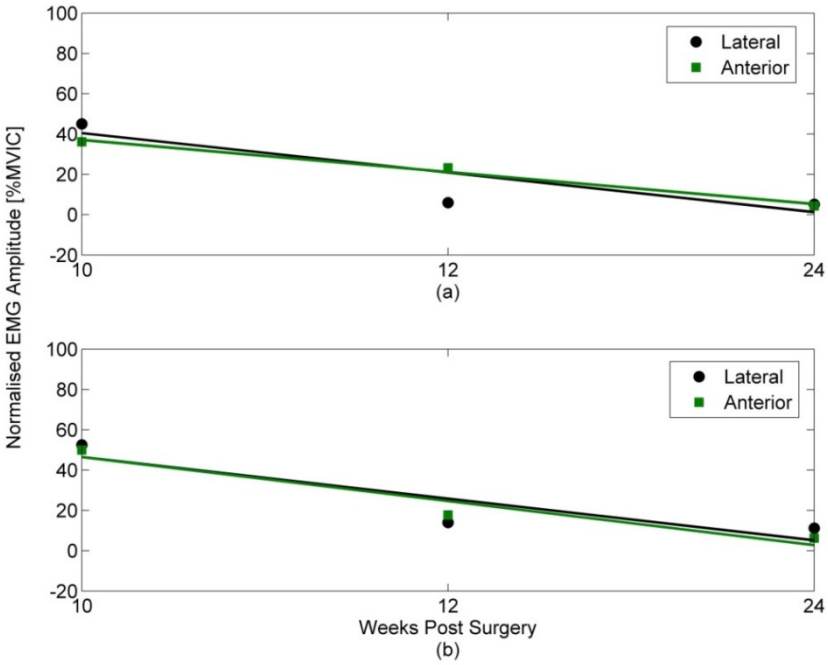

Figure 5.10 Comparison of the difference between the normalised SEMG amplitudes for the right and the left shoulder over the course of rehabilitation for a 90° abduction (a) and a 90° flexion (b)

5.4 Discussion

This chapter aimed to investigate the feasibility of using the Electric Potential Sensor in a real-time biofeedback rehabilitation program. During the monitoring we were evaluating the use of the EPS and the legitimacy of using biofeedback in the rehabilitation process. In the opinion of the user she felt it was useful to see, when performing rehabilitation exercises, the intensity levels of the muscles being used during exercises and to quantify progression. She commented that the sensors were comfortable to wear throughout the monitoring process. Attaching the EPS was not an invasive procedure and repositioning when necessary was achieved quickly and painlessly.

Further off-line results showed that there was a marked increase in isotonic contraction intensity for each of the desired shoulder deflection angles. A certain increase in SEMG activity seems logical in light of the decrease in muscle mass due to the atrophied muscle having to produce a larger innervation to reach the desired joint angle. This effect can be supported by results seen in the literature [168-172]. The differences in results can easily be attributed to

the fact these immobilisation studies were carried on healthy subject, for smaller immobilisation time durations.

During the initial monitoring session the results indicated a clear loss of muscle function and hence an increased need for deltoid muscle contraction in order to cause arm movements at the injured shoulder, compared with that of the healthy shoulder. The right shoulder SEMG tended towards the same level as the left shoulder SEMG over the course of rehabilitation. An increase of 99.04% and 58.19% in MVIC during shoulder abduction was displayed in the injured shoulder at the first monitoring session. These differences decreased to just 8.96% and 7.18% MVIC by the final monitoring session at 24 weeks. The amplitudes are far closer in intensity, which we would assume is correct as the subject underwent six weeks of rehabilitation then went back on to normal everyday activities.

6 SEMG Recordings of the Bicep Muscle During Fixed Trajectory Movements

6.1 Introduction

Surface electromyography has been used widely as an information source regarding human movement intentions for myoelectric control of prosthesis [135, 138-140, 175, 176] and assistive robots for rehabilitation [13, 26-29, 136, 158, 162, 166, 167, 175] or mobility [21-23, 149, 151, 155, 177]. Conventional research aims to produce control structures based on mapping muscle activity to human joint torque estimation [178]. However the performance of this type of control is influenced by several factors that can limit performance. These factors include a wide range of muscle types, ranges in muscle properties such as fibre lengths and densities as well limb positions used during said control algorithms [179, 180].

In the previous chapter a study was carried out where muscle movements were monitored over the course of rehabilitation. However, during the study, various factors were ignored. External constraints such as the timing of limb movements, limb acceleration and the load being moved by the limb were not included in the study. In depth human movement studies include controllability of many of these factors. Similar experiments are carried out while changing the static set of variables during discrete movements of a single joint in order to properly verify any kinematic myoelectric relationships that may arise [70-75]. An experiment was designed to incorporate such external constraints, aiming to investigate the relationship between limb dynamics and SEMG signals acquired using the EPS, and thus identify a relationship between joint torque and SEMG amplitudes. An apparatus was employed that ensured a similar trajectory would be followed each time the limb under investigation was moved. The apparatus also included the ability to monitor real-time changes in joint angle which allowed for off line calculations of limb dynamics.

The experimental work of this chapter relies on a single healthy male subject, 32 years old with no prior arm injuries. Bicep SEMGs were recorded for both sides of the body, alongside the physical movement information.

6.2 Method

The apparatus used for this experiment allowed that, while seated, the upper arm be fixed in position while the lower portion of the arm could be moved by applying force to a handle. The axis of rotation was aligned with the elbow joint, with the arm abducted to the front at 90°. The mechanical set up of the joint movement apparatus allowed for a simplification of the applied torque realisation through an optimisation of the moments of inertia of the device. In order to quantify the dynamics of the limb under observation certain measurements were required. A rotary encoder was fixed at the axis of rotation so that angular displacement of the joint could be measured. From this information measures of angular velocity (ω) and angular acceleration (α) could be derived from joint displacement measurements (θ), as follows:

$$\omega = \frac{\partial \theta}{\partial t} \tag{6.1}$$

$$\alpha = \frac{\partial \omega}{\partial t} = \frac{\partial^2 \theta}{\partial t^2} \tag{6.2}$$

Calculations of torque were derived based on the apparatus applying a constant static torque by means of a mass suspended from the axis of rotation, as shown below in Figure 6.1, and, also in Figure 6.2, where *m* is the mass to be moved and *r* is the radius of the rotating cog from which the mass is hung.

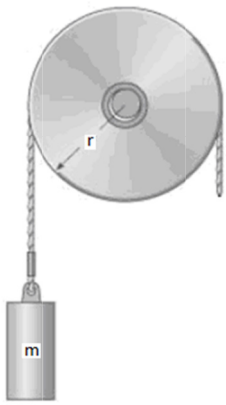

Figure 6.1 Experimental model of the arm manipuladum apparatus

Based on Newton's second law of motion, $F = ma$; if a torque is applied to a system in equilibrium, an angular acceleration will result. This is generally proportional to the second moment of inertia of the whole system. However in the simplified system, as long as the mass used is substantial enough to require a large torque to accelerate it, the effects of the smaller, less significant moments of inertia of the apparatus can be neglected, giving an overall torque for the system of:

$$T = mgr + m\alpha r \tag{6.3}$$

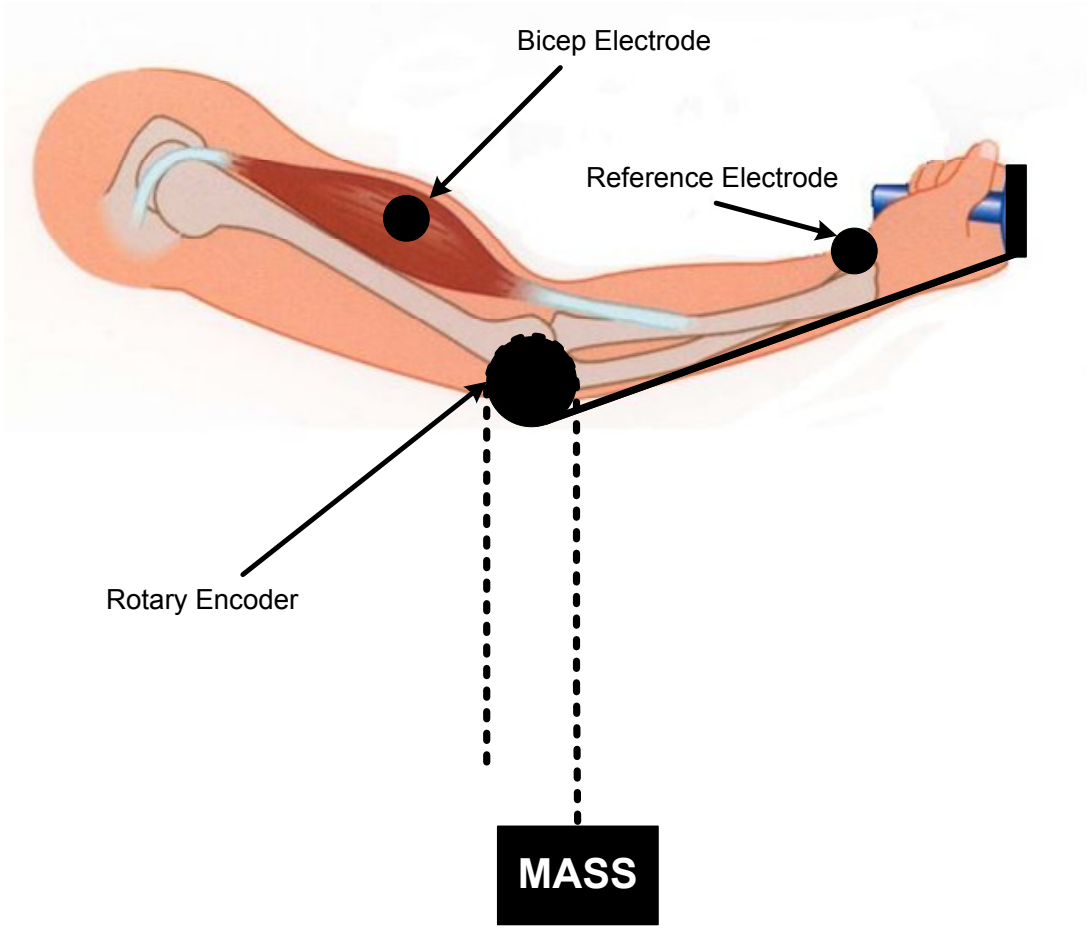

Figure 6.2 Configuration of the apparatus used to measure real-time physical joint deflection angles, including EPS placement locations used to measure real-time SEMG signals from the bicep, based on image taken from [181]

SEMG signals were acquired directly from the skin using the sensors and software configuration that was outlined in Section 5.2.1 and Figure 5.2. An EPS sensor was placed on the belly of the bicep with an additional reference sensor attached to the wrist (Figure 6.2). Angular displacement measured at the joint by the rotary encoder was by the same system used for the SEMG signals. The subject was seated in front of a computer monitor that displayed real-time data from the rotary encoder, showing measurements of the physical joint angle (Figure 6.3). A large LED indicator was also on screen that would light once the subject had reached the target angle under test. The subject was instructed to perform 10 elbow flexion movements in his own time, aiming to accurately reach the target each time. Results were recorded for both left and right biceps while completing movements to target angles of 18°, 36°, 54°, 72° and 90°. The mass used for all target angles, 3.75 kg, remained constant throughout the experiment. All recordings were taken during one recording session where the electrodes remained on the subject for the duration of the experiment.

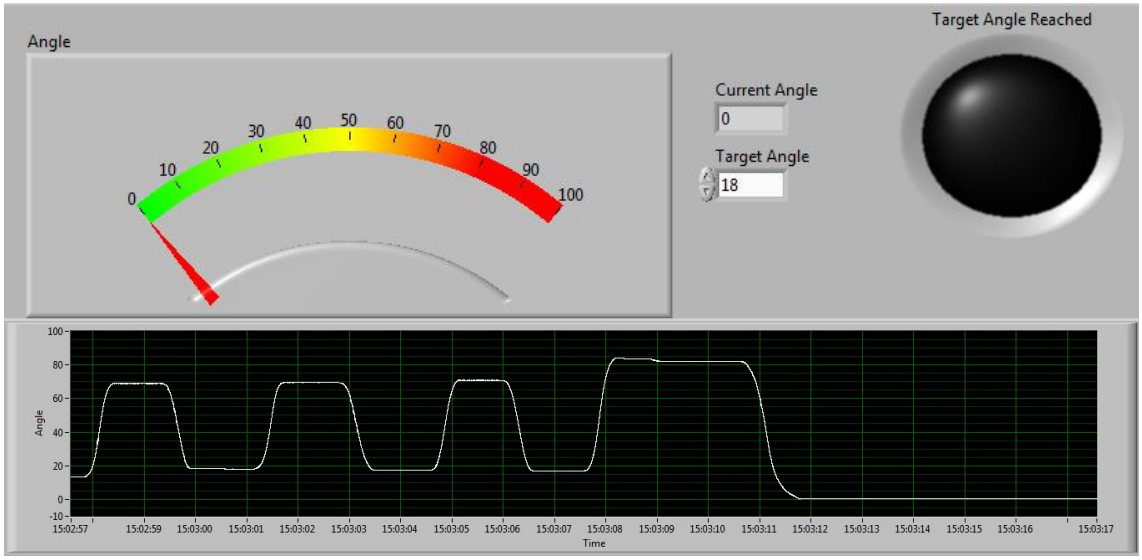

Figure 6.3 Graphical user interface showing real-time joint movement measurements, displayed to the subject during the limb dynamics experiment

6.3 Results

The SEMG results presented here were RMS filtered with a 500 ms window, MVIC normalised and noise corrected. SEMG data was recorded by LabVIEW; all post processing was completed using MATLAB. The MVIC normalisation amplitude was acquired in a similar manner to that outlined in Section 5.2.2. For this experiment the subject made brief MVICs with the apparatus

locked at 90°. Three, five-second isometric contractions in flexion were recorded. The average RMS SEMG during sustained contractions was used as the MVIC. Between each contraction the subject had two minutes rest to minimise fatigue. Measurements of system noise were taken while the subject was seated and at rest. He was instructed to relax for a single 10 second recording. Noise levels were determined off line by averaging the RMS amplitude over the 10 second recording. For both arms the noise was measured at 20 µV RMS. This noise represents noise from the full sensing system as well as any residual muscle noise presented from the subject at rest.

Figure 6.4 shows the three stages of SEMG signal processing with a normalised 18° joint target angle recording for reference. The SEMG data is displayed in blue and the data from the rotary encoder is displayed in red. Data from the rotary encoder depicting physical joint movement has been normalised to an arbitrary scale for reference. Figure 6.4(a) shows the rectified SEMG signal from the bicep of the right arm with the physical movement signal.

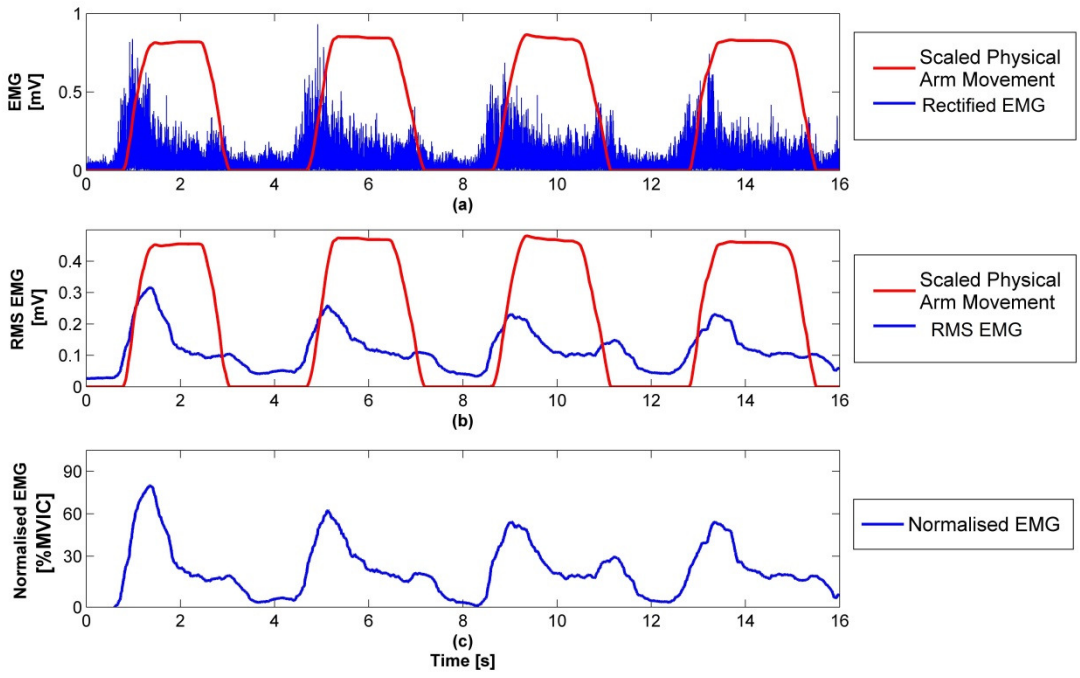

Figure 6.4 Right arm data: (a) Rectified SEMG and normalised physical limb movement, to 18° target (b) RMS SEMG with a 500 ms window and normalised limb movement (c) Normalised SEMG as %MVIC

Figure 6.4 (b) shows the rectified SEMG signal after RMS filtering. The RMS interpretation of the SEMG signal accurately represents the SEMG signal. A slight lead in SEMG activity can be seen compared to the physical movement, and this is due to the electro-mechanical attributes of limbs and muscle function [63]. The RMS signal normalised to the MVIC and noise corrected is shown in Figure 6.4 (c).

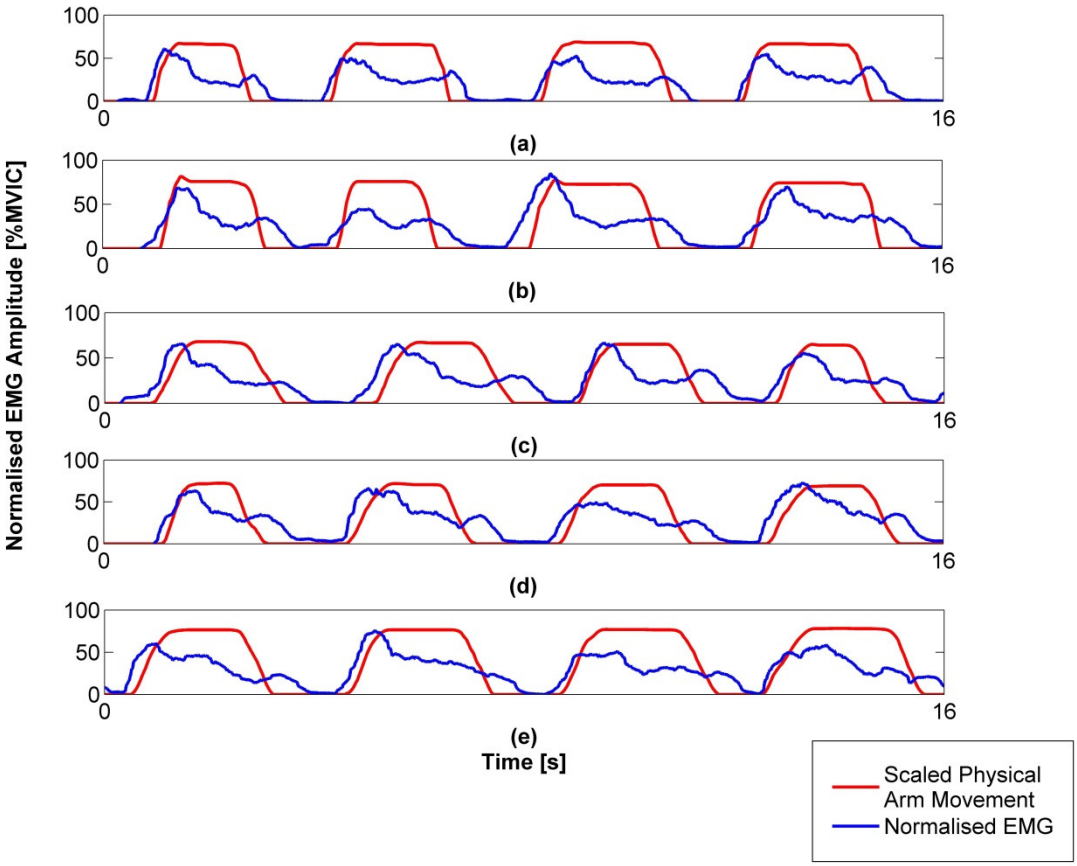

Figure 6.5 Right bicep normalised SEMG amplitudes (blue) and normalised physical limb movements (red) to target angles of (a) 18° (b) 36° (c) 54° (d) 72° and (e) 90°

Figure 6.5 shows normalised SEMG amplitudes (blue) along with scaled physical limb movements (red) for five different target angles. Again data from the rotary encoder depicting physical joint movement has been normalised to an arbitrary scale for reference.

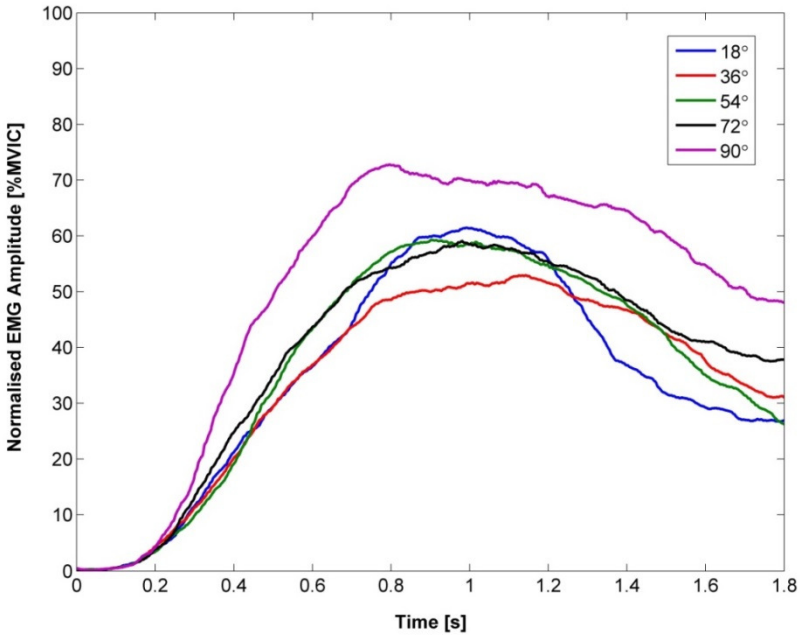

Figure 6.6 Right bicep: Averaged normalised RMS SEMGs for x10 lower arm movements to different target angle

In Figure 6.6, above, normalised right bicep SEMG signals averaged over the 10 repetitions for each target angle, are displayed. Averages have been calculated from the muscle activation onset; this is taken as the first sustained contraction over the noise baseline [63, 182]. Similar results were achieved for left arm movements; these can be seen in 0.

Figure 6.7 shows a comparison between normalised SEMG amplitudes for each of the joint target angles for each arm. There is a slightly linear correlation between normalised SEMG amplitude for the isotonic contractions and the corresponding joint target angle. There is also a notable difference between the sensitivities of the left arm (blue) and right arm (red). However large error bars, representing the standard deviations for each target angle trial, are present on the graph. The deviations, which range from 5.23 % MVIC to 12.73 % MVIC, along with the variation in sensitivities between arms, render the linear relationship untenable.

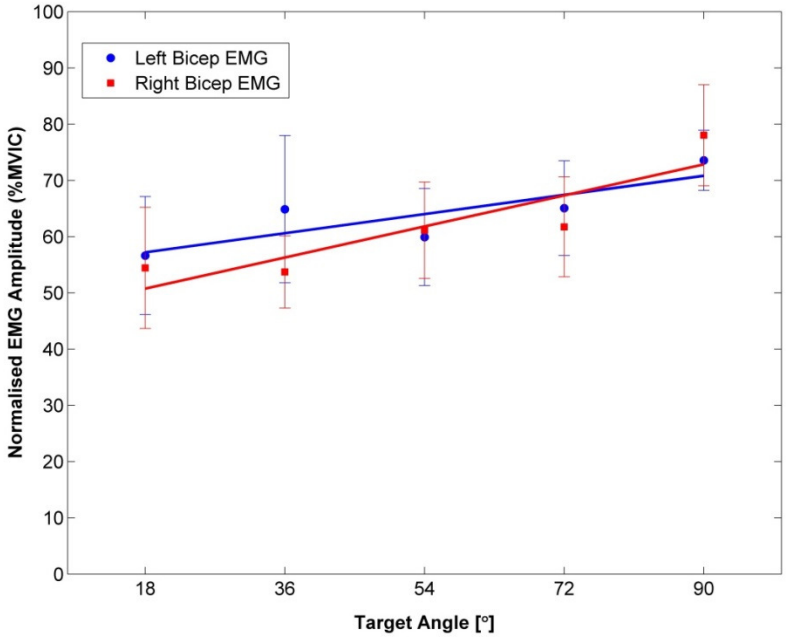

Figure 6.7 Normalised left and right bicep SEMG versus limb target angle

Figure 6.8(a) shows data, from the rotary encoder, for the physical limb movements to the visual targets of 18°, 36°, 54°, 72° and 90°. Figure 6.8 (b), (c) and (d) are calculations of angular velocity, angular acceleration and torque for each of the target angles using equations (6.1) to (6.3). From the calculations of the torque produced by the limb, we can correlate limb target angle with peak joint torque. This provides a linear relationship, which is expected as the calculations are based on linearly changing values of angular velocity and acceleration, (see Figure 6.9). A relationship between peak joint torque and normalised SEMG has been investigated in Figure 6.10.

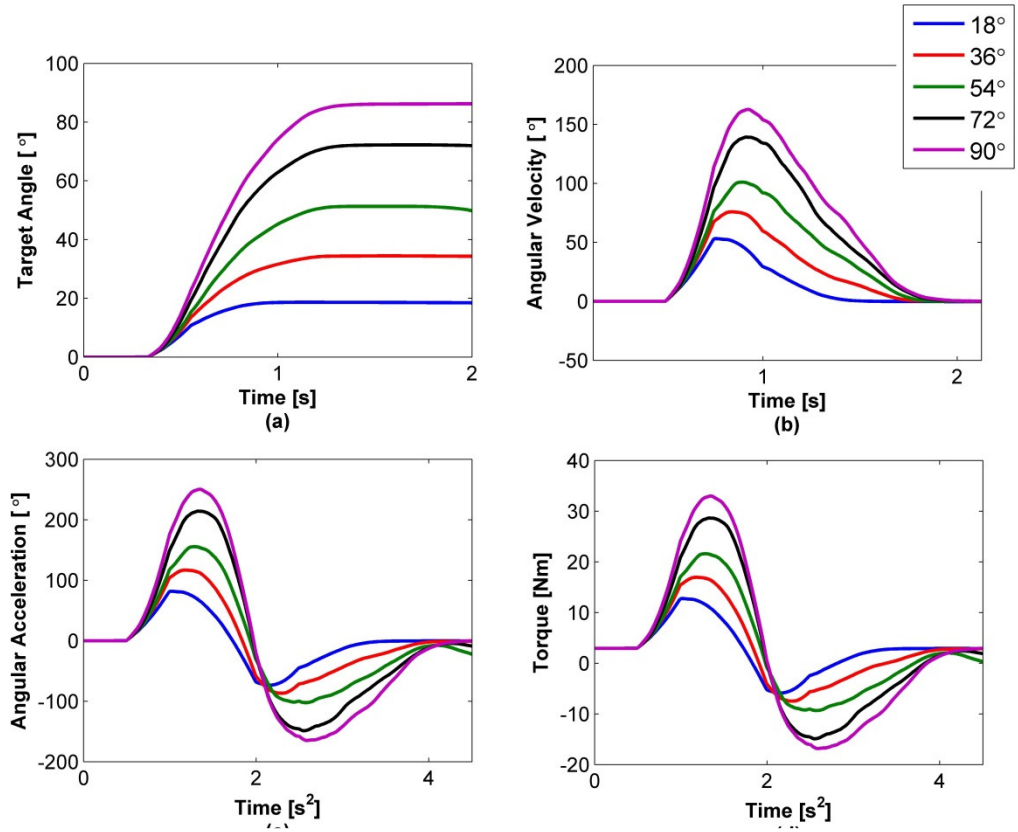

Figure 6.8 Right arm limb dynamics for fixed movement trajectory, x10 averages: (a) limb trajectory data (b) angular velocity (c) angular acceleration (d) joint torque

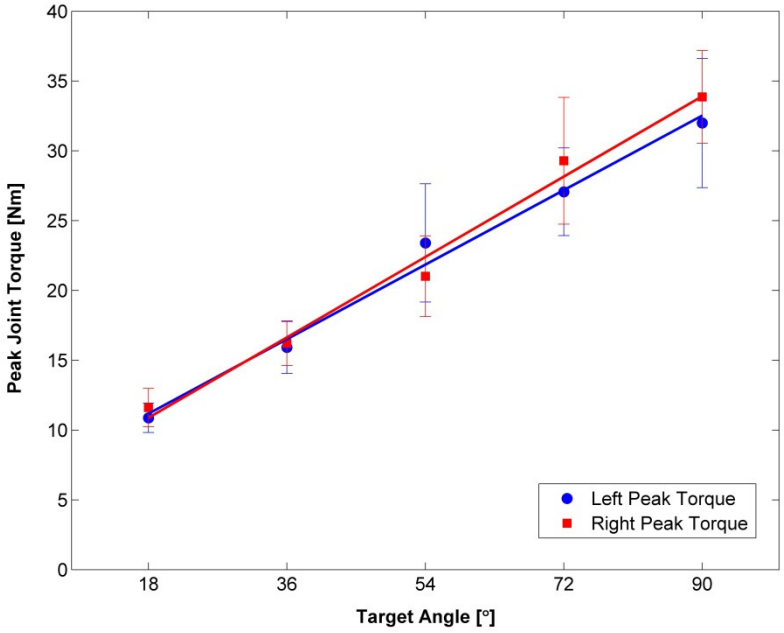

Figure 6.9 Peak joint torque developed during fixed trajectory movement versus limb target angle

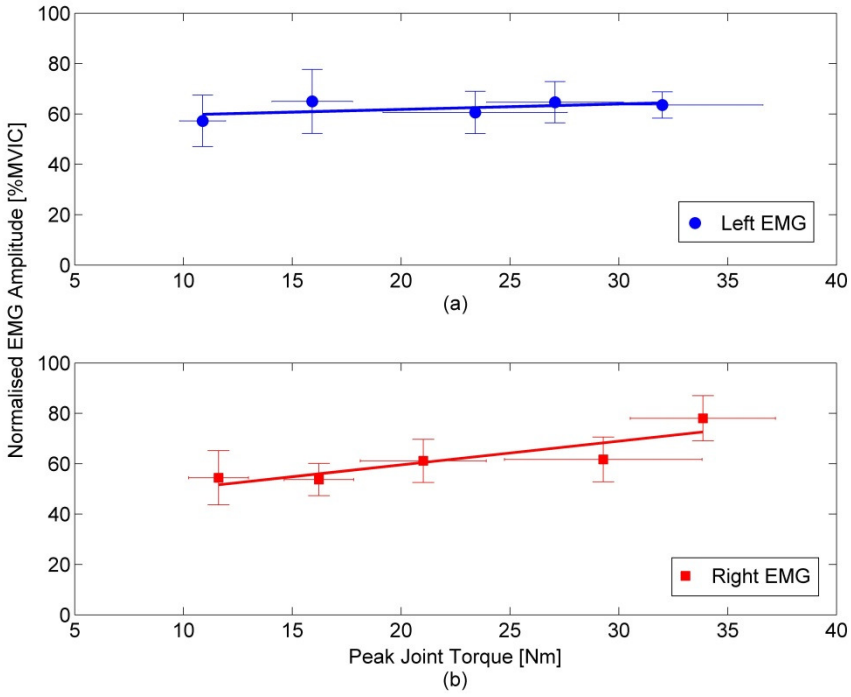

Figure 6.10 Normalised SEMG amplitude versus peak joint torque developed during fixed trajectory movement: (a) Left arm (b) Right arm

The relationship shown in Figure 6.10 is difficult to summarise when comparing results from the left and right sides as the torques produced on either side of the body were not identical. There is a slightly linear relationship evident between the torque and SEMG signals, this being more evident for the right arm studies. However, there is also evidence of non-linearity due to the significant variability in the trials. Successful studies of both of these relationships have been published; there are those who support and have successfully applied control algorithms based on a linear relationship [175, 180] and those who have used more complex non-linear control structures [136, 183-185].

6.4 Discussion and Future Work

The analysis covered in this chapter offers both encouraging and cautionary results on the use of SEMG magnitude as an indicator of muscle force. SEMG magnitudes show a linear relationship with increasing target distance as did the joint torque output; however the significant variability in the SEMG amplitudes leads to speculation that this correlation may not be consistent under all conditions. Deviations in normalised SEMG amplitudes per target ranged from 5.23 %MVIC to 12.73 %MVIC. The corresponding peak joint torques deviated from the linear best fit model ranging from 5.13 Nm to 22.44 Nm. If we were to hypothesise that a linear relationship existed, in order to infer a joint torque relative to a SEMG amplitude, the slope would be far smaller than the statistical deviations.

The results presented here have not been directly compared to any published work due to the wide variations in processing techniques. Further experiments are recommended, which include direct comparison to conventional technologies such as Ag-AgCl electrode recordings. Signal processing and SEMG normalisation protocols would need to be identical such that a direct comparison could be made through the application of benchmarking statistical analysis to better quantify the capabilities of the EPS as an SEMG sensor. Proposed statistical analysis methods are outlined in Appendix E.2. Supplementary to these experiments, further investigations would be needed to correlate the SEMG signals with the physical attributes of limb dynamics. Experiments would need to include a more diverse set of variables such as, more experimental subjects and monitored muscles, varying weights and timing parameters. To clarify relations between joint torque and SEMG amplitude, experimental designs where joint torque could be controlled would be optimal. In addition to

7 Conclusions

The most desirable outcome when developing new applications relating to healthcare and assistive technologies is an improvement in quality of life. This quality of life can be established in several different ways, be it personal comfort during electrophysiological signal monitoring for health diagnostics, to cost and ease of use for assistive products for use in the home. Ease of use has metrics such as hardware application and configurations as well as software learning times. Sensors must be robust and reliable, with the capability to deliver high quality, low noise signal resolutions. A range of applications based on the versatile Electric Potential Sensor (EPS), configured in both contact and remote mode, have been presented. The aim of this research was to verify that employing the EPS for healthcare and assistive technologies (AT) can deliver the fidelity of electrophysiological signals required, along with the benefit of improved quality of life due to its ease of use and non-invasive properties.

The first application discussed was a non-contact sensing system used to predict the position of a hand within a sensing area. The system benefited from detecting perturbations in the ambient electric field caused by a grounded target, the hand, within the sensing field. The method employed meant that there was no requirement for an induced electric field, and hence the hardware associated with the system maintained simplicity. A robust two sensor system, reliant on minimal signal processing, for one dimensional sensing over 300 mm was presented. The one dimensional sensing plane allows for detection of grounded objects passing through the electric field between the sensors, hence the system could be applied to larger sensing areas, such as a room or hall. This type of sensing has many potential applications for full human movement detection, such as room occupancy detection and smart lighting systems. A more complex system was developed such that two dimensional sensing was achieved; this system required a more complex control algorithm but remained solely reliant on the perturbations to the ambient field caused by the hand, thus the system maintained simplicity. The real-time two dimensional hand tracking system was interfaced with a PC, and simple predictive text program, such that a user could control a mouse cursor to type solely using the movement of the hand in the space above the sensing area. While this system proved easy to learn through user testing, tests were only carried on healthy individuals who commented that a conventional mouse was easier to use. The system would

be suitable for those that have difficulty using conventional PC mice; further testing on this demographic would be highly beneficial.

The EPS was also used to acquire electrophysiological signals from the surface of the body, more specifically, signals originating from the eyes and the muscles. Two different versions of the EPS were designed to suit the amplitude and bandwidth demands of the two types of signals. The sensors designed to acquire signals originating from the eyes provided a bandwidth from 0.1 Hz to 86 Hz. The sensors for acquiring muscle signals provided a bandwidth from 10 Hz to 3 kHz. Both sensors provided x114 gain which proved adequate amplification for the low signal levels which range from micro to millivolts. The low amplitudes of these electrophysiological signals require that the sensors have a low noise profile. Noise measurements showed that the integrated noise voltages over the sensor bandwidth for the eye sensors was 154 nV, and for the muscle sensors was 2.34 µV.

A three sensor eye tracking system, based on electrooculgraphy (EOG) was presented in chapter three. The three sensor configuration eliminated the need for additional facial electrodes as is found in typical EOG systems. Horizontal and vertical gaze positions were determined by measuring displacement voltages presented by the rotation of the eyes. The sensors were mounted on an easy to apply headband, several users were tested on their ability to put on the sensing device individually with little instruction. Results for horizontal and vertical resolutions, <1° and 2° respectively, were comparable with conventional sensing techniques used in similar research. It was found that depending on the subjects and the sensor placements, sensitivities varied but maintained linear relationships in the range of ±40°. To create a viable application based on EOG signals a calibration routine is required to normalise signal amplitudes for any user such that they could be used as inputs for control algorithms. A full application based on the EOG headband was not discussed; however future projects could include various control systems such as eye typing, vehicle control and video gaming. It would also be beneficial to miniaturise the sensors in order to mount them on a pair of glasses; this would make them easier to put on, more comfortable to wear and much more aesthetically pleasing.

Chapter four presented a comparison between the EPS and conventional eye health monitoring equipment used in Ophthalmologic clinics for diagnostics. The EPS was employed

to record electroretinograms (ERGs) for direct comparison to typical sensing electrodes. The EPS was proven capable of recording these signals to a similar standard to the Ag-AgCl surface electrodes. Comparable results were achieved. For example, ERG signals were acquired for 1 Hz and 5 Hz full-field flash stimuli, implicit time measurements (La and Lb) were found to be: 17.3 ± 1.3 ms and 42 ± 3.2 ms for the 1 Hz stimulus and 25 ± 2.2 ms and 44.7 ± 3.6 ms for the 5 Hz stimulus. Further measurements were made for implicit time, on signals acquired during two separate 30 Hz flicker ERG stimuli experiments, the results of which were 32.9 ± 2.7 ms and 33.1 ± 2.1 ms. The benefit of using the EPS being that no conductive gels or skin abrasion was necessary. The placement of electrodes for this type of sensing is crucial, direct contact with the lower eye lid is absolutely necessary in order to acquire ERGs. In this sense the EPS has a downfall for this type of sensing, as the sensor housing is large compared with conventional electrodes. Improvements to the sensor design could be made to ensure a more comfortable experience for the subject. As these experiments were only carried out on a single subject, it would be crucial to carry out further experimental trials on a range of subjects in order to verify the accessibility of successful infiltration into this sensing market.

Chapters five and six were focused on the use of surface electromyograms for monitoring muscle movements. Chapter five specifically focused on a real-time biofeedback rehabilitation monitoring application. A unique opportunity was presented where an injured subject was available for SEMG monitoring throughout the course of rehabilitation. Access to this subject for experimental work allowed for valuable feedback to be gained on both the use of the EPS and the biofeedback system. Bi-weekly monitoring of rehabilitation exercises was carried out; during each monitoring session the electric potential sensors were applied to the subjects injured and healthy shoulders. Due to the extent of the injuries sustained the subject required assistance applying the sensors, but felt the EPS was easy to apply and comfortable during the monitoring sessions. The subject also noted that the real-time biofeedback system was easy to understand and provided helpful visual progression indicators of muscle improvements, which when carrying out a lengthy rehabilitation program with slow progression helped to keep up moral. Improvements to the sensor design would be beneficial so that a user could apply them individually; this could lead into the development of home rehabilitation systems and telehealth monitoring applications.

Chapter six aimed to study and analyse the correlation, if any, between bicep SEMG signals and limb dynamics of the lower arm. The potential of this relationship lies in a use for complex

control algorithms for various systems such as mobility aids, robotic limbs and prosthetics. In studies of this type there are various decisions to be made regarding the sensor placements, and external constraints such as the limb load, positioning and movement trajectory as well as the associated signal processing that must be involved when extracting information from raw SEMG signals. Results presented somewhat supported a linear relation between joint torque and normalised RMS SEMG amplitude. Due to the small amount of experimental trials and dynamic constraints, this relationship was found to be tenuous at best; the inconclusive results are consistent with findings in the literature. Experimental work presented provides an initial glimpse into the vast subject of limb dynamics. Further investigations including a variety of subjects, limb loads and positions is absolutely necessary to better develop any control algorithms that may be transferred to an AT application based on this type of monitoring.

This thesis has presented a wide variety of applications of the Electric Potential Sensor for healthcare and assistive technologies. Several advantages and disadvantages have been highlighted and it has been shown that these sensors have significant potential for future applications, configured both as contact or non-contact sensors. These applications could include, but are not limited to, occupancy monitoring, eye controlled applications for communication and mobility, as well as home rehabilitation and physiological monitoring suites.

References

[1] R. Beech and D. Roberts, "Assistive technology and older people," *SCIE website–briefing paper,* vol. 28, 2008.

[2] *Historic and Projected Mortality Data (1981 to 2062) from the UK Life Tables, 2012-Based*. Office for National Statistics licensed under the Open Government Licence v.2.0. (Last retrieved: 05/02/2014).

[3] R. Cracknell, "The ageing population," *Key issues for the new parliament,* p. 44, 2010.

[4] J. Borg*, et al.*, "The right to assistive technology: for whom, for what, and by whom?," *Disability & Society,* vol. 26, pp. 151-167, 03/01 2011, DOI: 10.1080/09687599.2011.543862.

[5] M. Chan*, et al.*, "A review of smart homes—Present state and future challenges," *Computer Methods and Programs in Biomedicine,* vol. 91, pp. 55-81, 2008, DOI: 10.1016/j.cmpb.2008.02.001.

[6] A. Arcelus*, et al.*, "Integration of Smart Home Technologies in a Health Monitoring System for the Elderly," in *Advanced Information Networking and Applications Workshops, 2007, AINAW '07. 21st International Conference on*, 2007, pp. 820-825, DOI: 10.1109/ainaw.2007.209.

[7] S. Banerjee*, et al.*, "Telesurveillance of elderly patients by use of passive infra-red sensors in a'smart'room," *Journal of telemedicine and telecare,* vol. 9, pp. 23-29, 2003, DOI: 10.1258/135763303321159657.

[8] C. N. Scanaill*, et al.*, "A review of approaches to mobility telemonitoring of the elderly in their living environment," *Annals of Biomedical Engineering,* vol. 34, pp. 547-563, 2006, DOI: 10.1007/s10439-005-9068-2.

[9] A. Sixsmith and N. Johnson, "A smart sensor to detect the falls of the elderly," *Pervasive Computing, IEEE,* vol. 3, pp. 42-47, 2004.

[10] A. Malone*, et al.*, "Electromyographic characteristics of gait impairment in cervical spondylotic myelopathy," *European Spine Journal,* vol. 22, pp. 2538-2544, 2013, DOI: 10.1007/s00586-013-2928-9.

[11] D. E. Krebs, "Isokinetic, Electrophysiologic, and Clinical Function Relationships Following Tourniquet-aided Knee Arthrotomy," *Physical Therapy,* vol. 69, pp. 803-815, October 1 1989.

[12] A. Yee Mon and A. Al-Jumaily, "Shoulder rehabilitation with biofeedback simulation," in *Mechatronics and Automation (ICMA), 2012 International Conference on*, 2012, pp. 974-979, DOI: 10.1109/icma.2012.6283382.

[13] M. Sha*, et al.*, "EMG Biofeedback Based VR System for Hand Rotation and Grasping Rehabilitation," in *Information Visualisation (IV), 2010 14th International Conference*, 2010, pp. 479-484, DOI: 10.1109/iv.2010.73.

[14] H. Townsend*, et al.*, "Electromyographic analysis of the glenohumeral muscles during a baseball rehabilitation program," *The American Journal of Sports Medicine,* vol. 19, pp. 264-272, 1991.

[15] R. A. Hintermeister*, et al.*, "Electromyographic activity and applied load during shoulder rehabilitation exercises using elastic resistance," *The American Journal of Sports Medicine,* vol. 26, pp. 210-220, 1998, DOI: 0363-5465/98/2626.

[16] R. F. Escamilla*, et al.*, "Electromyographic analysis of traditional and nontraditional abdominal exercises: implications for rehabilitation and training," *Phys Ther,* vol. 86, pp. 656-71, May 2006, DOI: 10.2165/00007256-200939080-00004.

[17] M. M. Reinold*, et al.*, "Electromyographic analysis of the supraspinatus and deltoid muscles during 3 common rehabilitation exercises," *Journal of athletic training,* vol. 42, pp. 464-469, 2007.

[18] R. F. Escamilla*, et al.*, "Shoulder muscle activity and function in common shoulder rehabilitation exercises," *Sports medicine,* vol. 39, pp. 663-685, 2009.

[19] R. Barea*, et al.*, "System for assisted mobility using eye movements based on electrooculography," *Neural Systems and Rehabilitation Engineering, IEEE Transactions on,* vol. 10, pp. 209-218, December 2002, DOI: 10.1109/TNSRE.2002.806829.

[20] R. Barea*, et al.*, "Electro-Oculographic Guidance of a Wheelchair Using Eye Movements Codification," *The International Journal of Robotics Research,* vol. 22, pp. 641-652, July 2003, DOI: 10.1177/02783649030227012.

[21] J.-S. Han*, et al.*, "Human-machine interface for wheelchair control with EMG and its evaluation," vol. 2, pp. 1602 - 1605 Vol.2, 17-21 2003, DOI: 10.1109/IEMBS.2003.1279672.

[22] I. Moon*, et al.*, "Intelligent robotic wheelchair with EMG-, gesture-, and voice-based interfaces," vol. 4, pp. 3453 - 3458 vol.3, 27-31 2003, ISBN: 0-7803-7860-1.

[23] N. Kim-Tien and N. Truong-Thinh, "Using Electrooculogram and Electromyogram for powered wheelchair," in *Robotics and Biomimetics (ROBIO), 2011 IEEE International Conference on*, 2011, pp. 1585 -1590, DOI: 10.1109/ROBIO.2011.6181515.

[24] Y. Zhang*, et al.*, "Design of a surface EMG based human-machine interface for an intelligent wheelchair," in *Electronic Measurement & Instruments (ICEMI), 2011 10th International Conference on*, 2011, pp. 132-136, DOI: 10.1109/icemi.2011.6037871.

[25] A. Silva*, et al.*, "Virtual electric wheelchair controlled by electromyographic signals," in *Biosignals and Biorobotics Conference (BRC), 2013 ISSNIP*, 2013, pp. 1-5, ISBN: 978-1-4673-3024-4.

[26] L. Dipietro*, et al.*, "Customized interactive robotic treatment for stroke: EMG-triggered therapy," *Neural Systems and Rehabilitation Engineering, IEEE Transactions on,* vol. 13, pp. 325 -334, September 2005, DOI: 10.1109/TNSRE.2005.850423.

[27] M. Johnson*, et al.*, "Potential of a suite of robot/computer-assisted motivating systems for personalized, home-based, stroke rehabilitation," *Journal of NeuroEngineering and Rehabilitation,* vol. 4, p. 6, 2007.

[28] S. Rong*, et al.*, "Assistive Control System Using Continuous Myoelectric Signal in Robot-Aided Arm Training for Patients After Stroke," *Neural Systems and Rehabilitation Engineering, IEEE Transactions on,* vol. 16, pp. 371-379, 2008, DOI: 10.1109/tnsre.2008.926707.

[29] S. Parasuraman and A. W. Oyong, "An EMG-driven musculoskeletal model for robot assisted stroke rehabilitation system using sliding mode control," in *Mechatronics and its Applications (ISMA), 2010 7th International Symposium on*, 2010, pp. 1-6, ISBN: 978-1-4244-6665-8.

[30] J. J. Tecce*, et al.*, "Eye movement control of computer functions," *International Journal of Psychophysiology,* vol. 29, pp. 319 - 325, August 1998, DOI: 10.1016/S0167-8760(98)00020-8.

[31] P. Majaranta and K. J. Räihä, "Twenty years of eye typing: systems and design issues," in *Proceedings of the 2002 symposium on Eye tracking research & applications*, USA, 2002, pp. 15-22, DOI: 10.1145/507072.507076.

[32] R. J. Jacob and K. S. Karn, "Eye tracking in human-computer interaction and usability research: Ready to deliver the promises," *Mind,* vol. 2, p. 4, 2003.

[33] M. Yan*, et al.*, "Development of mouse cursor control system using electrooculogram signals and its applications in revised hasegawa dementia scale task," in *World Automation Congress (WAC), 2012*, 2012, pp. 1-6, ISBN: 978-1-4673-4497-5.

[34] P. Ridden. (April 2011) Tobii releases eye-controlled mouse system. *Gizmag*. Available: http://www.gizmag.com/tobii-pceye-eye-control-mouse-release/18328/ (Last retrieved: 03/02/2014).

[35] E. Spinelli and M. Haberman, "Insulating electrodes: a review on biopotential front ends for dielectric skin–electrode interfaces," *Physiological measurement,* vol. 31, p. S183, 2010.

[36] Y. M. Chi*, et al.*, "Dry-contact and noncontact biopotential electrodes: methodological review," *Biomedical Engineering, IEEE Reviews in,* vol. 3, pp. 106-119, 2010.

[37] A. Clippingdale*, et al.*, "Ultra-high impedance voltage probes and non-contact electrocardiography," *Sensors: Technology, systems and applications, KTV Grattan (Ed.),* pp. 469-472, 1991.

[38] A. Searle and L. Kirkup, "A direct comparison of wet, dry and insulating bioelectric recording electrodes," *Physiological measurement,* vol. 21, p. 271, 2000.

[39] P. Richardson, "The insulated electrode: A pasteless electrocardiographic technique," in *20th Annual conference on engineering in medicine and biology*, 1967.

[40] N. J. McDonald*, et al.*, "The invisible electrode–zero prep time, ultra low capacitive sensing," in *Proceedings of the 11th International Conference on Human-Computer Interaction*, 2005.

[41] M. Oehler*, et al.*, "A multichannel portable ECG system with capacitive sensors," *Physiological measurement,* vol. 29, p. 783, 2008.

[42] B. Hyun Jae*, et al.*, "Conductive Polymer Foam Surface Improves the Performance of a Capacitive EEG Electrode," *Biomedical Engineering, IEEE Transactions on,* vol. 59, pp. 3422-3431, 2012, 10.1109/tbme.2012.2215032.

[43] H. Prance, "Sensor developments for electrophysiological monitoring in healthcare," *Applied Biomedical Engineering, Applied Biomedical Engineering. InTech. ISBN,* pp. 978-953, 2011.

[44] R. J. Prance*, et al.*, "An ultra-low-noise electrical-potential probe for human-body scanning," *Measurement Science and Technology,* vol. 11, pp. 291-297, 2000.

[45] A. J. Clippingdale*, et al.*, "Ultrahigh impedance capacitively coupled heart imaging array," *Review of Scientific Instruments,* vol. 65, pp. 269-270, 1994.

[46] N. Steinhausen*, et al.*, "Human Computer Interface based on Eye Movement (EOG) Signals," presented at the Proceedings of AAATE 2011, Maastricht, Netherlands, 2011, DOI: 10.3233/978-1-60750-814-4-790.

[47] H. Prance*, et al.*, "High spatial resolution, dry-electrode surface EMG acquisition system," in *Proceedings of AAATE 2009*, 2009, pp. pp 109-113.

[48] C. J. Harland*, et al.*, "Remote monitoring of biodynamic activity using electric potential sensors," *Journal of Physics: Conference Series,* vol. 142, 2008, DOI:10.1088/1742-6596/142/1/012042.

[49] R. J. Prance*, et al.*, "Remote detection of human electrophysiological signals using electric potential sensors," *Applied Physics Letters,* vol. 93, p. 033906, 2008.

[50] C. J. Harland*, et al.*, "High resolution ambulatory electrocardiographic monitoring using wrist-mounted electric potential sensors," *Measurement Science and Technology,* vol. 14, pp. 923-928, 2003.

[51] C. J. Harland*, et al.*, "Applications of electric potential (displacement current) sensors in human body electrophysiology," in *3rd World Congress on industrial process tomography Banff Canada*, 2003.

[52] C. J. Harland*, et al.*, "Remote detection of human electroencephalograms using ultrahigh input impedance electric potential sensors," *Applied Physics Letters,* vol. 81, pp. 3284-3286, 2002, DOI: 10.1063/1.1516861.

[53] H. Prance, *et al.*, "Position and movement sensing at metre standoff distances using ambient electric field," *Measurement Science and Technology,* vol. 23, 2012, DOI: 10.1088/0957-0233/23/11/115101.

[54] S. Beardsmore-Rust, *et al.*, "Passive tracking of targets using electric field sensors," in *SPIE Defense, Security, and Sensing*, 2010, DOI: 10.1117/12.849642.

[55] S. Beardsmore-Rust, *et al.*, "Detecting electric field disturbances for passive through-wall movement and proximity sensing," *Smart Biomedical and Physiological Sensor Technology VI,* vol. 7313, 2009, DOI:10.1117/12.817919.

[56] R. J. Prance, *et al.*, "Non-contact VLSI imaging using a scanning electric potential microscope," *Measurement Science and Technology,* vol. 9, p. 1229, 1998.

[57] *Plessey Semiconductors*. Available URL: http://www.plesseysemiconductors.com/ (Last retrieved: 18/02/2014).

[58] P. Watson, "High resolution electric field imaging using ultra-low capacitance probes," PhD, Engineering, University of Sussex, Brighton, 2011.

[59] L. R. Young and D. Sheena, "Eye-movement measurement techniques," *American Psychologist,* vol. 30, pp. 315-330, 1975, DOI: 10.1037/0003-066X.30.3.315.

[60] International Society for Clinical Electrophysiology of Vision (ISCEV). Available URL: www.iscev.org (Last retrieved: 03/03/2014).

[61] C. J. D. Luca. (2008). *Practicum on the Use of Surface EMG Signals in Movement Sciences (v1.5). ISBN: 978-0-9798644-0-7* (Last retrieved: 25-01-2014).

[62] P. Konrad, "The abc of emg," *A practical introduction to kinesiological electromyography,* vol. 1, 2005.

[63] J. R. Cram and E. Criswell, *Cram's Introduction to Surface Electromyography*: Jones & Bartlett Learning, 2011.

[64] H. W. Ott, *Noise reduction techniques in electronic systems*: Wiley New York, 1988.

[65] R. Dongseok, *et al.*, "T-less : A novel touchless human-machine interface based on infrared proximity sensing," in *Intelligent Robots and Systems (IROS), 2010 IEEE/RSJ International Conference on*, 2010, pp. 5220-5225, DOI: 10.1109/iros.2010.5649433.

[66] J. Suarez and R. R. Murphy, "Hand gesture recognition with depth images: A review," in *RO-MAN, 2012 IEEE*, 2012, pp. 411-417, ISBN: 978-1-4673-4606-1/12.

[67] H. Kolb, *et al.* (2011). *WEBVISION: The Organization of the Retina and Visual System* -. Available URL: http://webvision.med.utah.edu/ (Last retrieved: 03/03/2014).

[68] G. Sheng, *et al.*, "The Design of a Rehabilitation Training System with EMG Feedback," in *Biomedical Engineering and Biotechnology (iCBEB), 2012 International Conference on*, 2012, pp. 917-920, DOI: 10.1109/iCBEB.2012.410.

[69] A. N. Silva, *et al.*, "A virtual electro myographic biofeedback environment for motor rehabilitation therapies," in *Biosignals and Biorobotics Conference (BRC), 2013 ISSNIP*, 2013, pp. 1-4, DOI: 10.1109/brc.2013.6487541.

[70] Corcos, *et al.*, "Organizing principles for single-joint movements. IV. Implications for isometric contractions," *Journal of Neurophysiology,* vol. 64, p. 10, 1990.

[71] Corcos, *et al.*, "Organizing Principles for Single-Joint Movements II. A Speed-Sensitive Strategy," *Journal of Neurophysiology,* vol. 62, p. 11, 1989.

[72] Gottlieb, "Muscle Activation Patterns During Two Types of Voluntary Single-Joint Movement," *The American Physiological Society,* p. 9, 1998.

[73] Gottlieb, *et al.*, "Organizing principles for single joint movements. III. Speed-insensitive strategy as a default," *Journal of Neurophysiology,* vol. 63, p. 12, 1990.

[74] G. Gottlieb, *et al.*, "Organizing principles for single-joint movements. I. A speed-insensitive strategy," *Journal of Neurophysiology,* vol. 62, 1989.

[75] G. L. Gottlieb, *et al.*, "Relations between joint torque, motion, and electromyographic patterns at the human elbow," *Experimental Brain Research,* vol. 103, pp. 164-167, 1995, DOI: 10.1007/BF00241973.

[76] V. Garg and N. K. Bansal, "Smart occupancy sensors to reduce energy consumption," *Energy and Buildings,* vol. 32, pp. 81-87, 2000, DOI: 10.1016/S0378-7788(99)00040-7.

[77] D. Ebling and G. Thomas, "Review of life signs monitoring in custody cells: The cell occupancy monitoring system, COSATT," *Home Office Scientific Developement Branch, Horsham UK,* 2008.

[78] S. S. Rautaray and A. Agrawal, "Interaction with virtual game through hand gesture recognition," presented at the Multimedia, Signal Processing and Communication Technologies (IMPACT), 2011 International Conference on, 2011, DOI:10.1109/mspct.2011.6150485.

[79] S. M. A. Hussain and A. B. M. H. Rashid, "User independent hand gesture recognition by accelerated DTW," presented at the Informatics, Electronics & Vision (ICIEV), 2012 International Conference on, 2012, DOI:10.1109/iciev.2012.6317364.

[80] M. A. S. Ponraj and M. E. N. Daniel, "A Wireless Gesture Controlled Human Computer Interface," *International Journal of Engineering Technology and Computer Applications,* vol. 2, 2012.

[81] C. Jingyuan*, et al.*, "On body capacitive sensing for a simple touchless user interface," presented at the Medical Devices and Biosensors, 2008. ISSS-MDBS 2008. 5th International Summer School and Symposium on, 2008, DOI: 10.1109/issmdbs.2008.4575031.

[82] K. Tsukada and M. Yasumura, "Ubi-finger: Gesture input device for mobile use," in *Proceedings of APCHI*, 2002, pp. 388-400.

[83] F. Bevilacqua*, et al.*, "Wireless sensor interface and gesture-follower for music pedagogy," in *Proceedings of the 7th international conference on New interfaces for musical expression*, 2007, pp. 124-129, DOI: 10.1145/1279740.1279762.

[84] L. Garner, "For that different sound, Music a la Theremin," *Popular Electronics,* vol. 27, pp. 29-33,102, 1967.

[85] T. G. Zimmerman*, et al.*, "Applying electric field sensing to human-computer interfaces," presented at the Proceedings of the SIGCHI Conference on Human Factors in Computing Systems, Denver, Colorado, USA, 1995, DOI: 10.1145/223904.223940.

[86] T. G. Zimmerman, "Personal Area Networks: Near-field intrabody communication," *IBM Systems Journal,* vol. 35, pp. 609-617, 1996, DOI: 10.1147/sj.353.0609.

[87] National Instruments Corp. (UK) Ltd. 21 Kingfisher Court, Hambridge Road, Newbury, Berkshire, UK. Available URL: http://uk.ni.com/.

[88] Dynamic Keyboard. CanAssist, University of Victoria, 3800 Finnerty Rd., Victoria, BC, Canada, V8P 5C2. Available URL: http://www.canassist.ca/.

[89] A. Duchowski, *Eye Tracking Methodology: Theory and Practice*: Springer London, 2007.

[90] C. J. Erkelens, "Coordination of smooth pursuit and saccades," *Vision Research,* vol. 46, pp. 163 - 170, January 2006, DOI: 10.1016/j.visres.2005.06.027.

[91] R. J. Jacob, "What you look at is what you get: eye movement-based interaction techniques," presented at the Proceedings of the SIGCHI Conference on Human Factors in Computing Systems, Seattle, Washington, USA, 1990, DOI: 10.1145/97243.97246.

[92] C. H. Morimoto and M. R. M. Mimica, "Eye gaze tracking techniques for interactive applications," *Computer Vision and Image Understanding,* vol. 98, pp. 4 - 24, April 2005, DOI: 10.1016/j.cviu.2004.07.010.

[93] M. Reale*, et al.*, "Pointing with the eyes: Gaze estimation using a static/active camera system and 3D iris disk model," in *Multimedia and Expo (ICME), 2010 IEEE International Conference on*, 2010, pp. 280-285, DOI: 10.1109/icme.2010.5583014.

[94] D. Beymer and M. Flickner, "Eye gaze tracking using an active stereo head," in *Computer Vision and Pattern Recognition, 2003. Proceedings. 2003 IEEE Computer Society Conference on*, 2003, pp. 451-458, DOI: 10.1109/cvpr.2003.1211502.

[95] H. Yu*, et al.*, "A Study on the Features of Eye Movement Based on Different Types of Poetry Reading," in *Intelligent System Design and Engineering Applications (ISDEA), 2013 Third International Conference on*, 2013, pp. 195-199, DOI: 10.1109/isdea.2012.52.

[96] U. Engelke*, et al.*, "Comparative Study of Fixation Density Maps," *Image Processing, IEEE Transactions on,* vol. 22, pp. 1121-1133, 2013, DOI: 10.1109/tip.2012.2227767.

[97] H. Manabe and M. Fukumoto, "Full-time wearable headphone-type gaze detector," in *CHI '06 Extended Abstracts on Human Factors in Computing Systems*, New York, NY, USA, 2006, pp. 1073-1078, DOI: 10.1145/1125451.1125655.

[98] R. Barea*, et al.*, "Wheelchair Guidance Strategies Using EOG," *Journal of Intelligent and Robotic Systems,* vol. 34, pp. 279-299, July 2002, DOI: 10.1023/A:1016359503796.

[99] V. Häkkinen*, et al.*, "The effect of small differences in electrode position on EOG signals: application to vigilance studies," *Electroencephalography and Clinical Neurophysiology,* pp. 294-300, April 1993, DOI: 10.1016/0013-4694(93)90111-8.

[100] A. B. Usakli*, et al.*, "On the use of electrooculogram for efficient human computer interfaces," *Computational Intelligence and Neuroscience,* January 2010, DOI: 10.1155/2010/135629.

[101] K. Yamagishi*, et al.*, "Development of EOG-Based Communication System Controlled by Eight-Directional Eye Movements," in *Engineering in Medicine and Biology Society, 2006. EMBS '06. 28th Annual International Conference of the IEEE*, 2006, pp. 2574 - 2577, DOI: 10.1109/IEMBS.2006.259914.

[102] S. Vijayprasath*, et al.*, "Experimental explorations on EOG signal processing for realtime applications in labview," in *Advanced Communication Control and Computing Technologies (ICACCCT), 2012 IEEE International Conference on*, 2012, pp. 67 -70, DOI: 10.1109/ICACCCT.2012.6320743.

[103] MATLAB 2009a, 2012a and 2012b, The MathWorks Inc. Natick, Massachusetts, USA. Available URL: http://www.mathworks.co.uk/.

[104] C. Evinger*, et al.*, "Eyelid movements. Mechanisms and normal data," *Investigative Ophthalmology & Visual Science,* vol. 32, pp. 387-400, 1st February, 1991.

[105] Dr. Alison Binns and Dr. Tom Margin - School of Optometry and Vision Sciences. Available URL: http://www.cardiff.ac.uk/optom/index.html (Last retrieved: 12/03/2013).

[106] R. Challis and R. Kitney, "Biomedical signal processing (in four parts)," *Medical and Biological Engineering and Computing,* vol. 28, pp. 509-524, 1990, DOI: 10.1007/BF02446290.

[107] L. Sörnmo and P. Laguna, "Chapter 4 - Evoked Potentials," in *Bioelectrical Signal Processing in Cardiac and Neurological Applications*, ed Burlington: Academic Press, 2005, pp. 181-336.

[108] G. W. Weinstein*, et al.*, "Visually evoked potentials and electroretinography in neurologic evaluation," *Neurologic clinics,* vol. 9, p. 225, 1991.

[109] A. Kriss*, et al.*, "The electroretinogram in infants and young children," *Journal of Clinical Neurophysiology,* vol. 9, pp. 373-393, 1992.

[110] I. Audo*, et al.*, "The negative ERG: clinical phenotypes and disease mechanisms of inner retinal dysfunction," *Survey of ophthalmology,* vol. 53, p. 16, 2008, DOI: 10.1016/j.survophthal.2007.10.010.

[111] A. Halliday*, et al.*, "Visual evoked response in diagnosis of multiple sclerosis," *British Medical Journal,* vol. 4, p. 661, 1973.

[112] P. Walsh*, et al.*, "The clinical role of evoked potentials," *Journal of Neurology, Neurosurgery & Psychiatry,* vol. 76, pp. ii16-ii22, June 1 2005, DOI: 10.1136/jnnp.2005.068130.

[113] M. Breton*, et al.*, "Analysis of ERG a-wave amplification and kinetics in terms of the G-protein cascade of phototransduction," *Investigative Ophthalmology & Visual Science,* vol. 35, pp. 295-309, 1994.

[114] K. Bradshaw*, et al.*, "Comparison of ERGs recorded with skin and corneal-contact electrodes in normal children and adults," *Documenta Ophthalmologica,* vol. 109, pp. 43-55, 2004, DOI: 10.1038/eye.1993.36.

[115] S. G. Coupland and M. Janaky, "ERG electrode in pediatric patients: Comparison of DTL fiber, PVA-gel, and non-corneal skin electrodes," *Documenta Ophthalmologica,* vol. 71, pp. 427-433, 1989., DOI: 10.1007/BF00152771.

[116] J. Larsson and S. Andréasson, "Photopic 30 Hz flicker ERG as a predictor for rubeosis in central retinal vein occlusion," *British Journal of Ophthalmology,* vol. 85, pp. 683-685, 2001, DOI: 10.1136/bjo.85.6.683

[117] A. Halliday*, et al.*, "Delayed visual evoked response in optic neuritis," *The Lancet,* vol. 299, pp. 982-985, 1972, DOI: http://dx.doi.org/10.1016/S0140-6736(72)91155-5.

[118] A. M. Binns and T. H. Margrain, "Evaluating retinal function in age-related maculopathy with the ERG photostress test," *Investigative Ophthalmology & Visual Science,* vol. 48, pp. 2806-2813, 2007.

[119] M. Marmor*, et al.*, "ISCEV Standard for full-field clinical electroretinography (2008 update)," *Documenta Ophthalmologica,* vol. 118, pp. 69-77, 2009, DOI 10.1007/s10633-008-9155-4.

[120] L. Esakowitz*, et al.*, "A comparison of flash electroretinograms recorded from Burian Allen, JET, C-glide, gold foil, DTL and skin electrodes," *Eye,* vol. 7, pp. 169-171, 1993.

[121] A. Kriss, "Skin ERGs: their effectiveness in paediatric visual assessment, confounding factors, and comparison with ERGs recorded using various types of corneal electrode," *International Journal of Psychophysiology,* vol. 16, pp. 137-146, 1994., DOI: http://dx.doi.org/10.1016/0167-8760(89)90040-8.

[122] unimed electrode supplies Ltd. Available URL: http://www.unimed-electrodes.co.uk/ (Last retrieved: 03/02/2014).

[123] *Mini Ganzfeld Stimulators, LKC Technologies, Inc.* [Brochure]. Available URL: http://www.lkc.com/products/Mini-Ganzfeld/ (Last retrieved: 05/07/2013).

[124] *CMGS-1 Color Min-Ganzfeld System, LKC Technologies Inc* [User's Manual (v2.3)]. Available URL: http://www.lkc.com/products/Mini-Ganzfeld/ (Last retrieved: 05/07/2013).

[125] Oxford Instruments. Available URL: http://www.oxford-instruments.com/?src=tn (Last retrieved: 20/04/2013).

[126] D. C. Hood*, et al.*, "A comparison of the components of the multifocal and full-field ERGs," *Visual neuroscience,* vol. 14, pp. 533-544, 1997, DOI: http://dx.doi.org/10.1017/S0952523800012190.

[127] D. McCulloch*, et al.*, "Comparisons of contact lens, foil, fiber and skin electrodes for patterns electroretinograms," *Documenta Ophthalmologica,* vol. 94, pp. 327-340, 1997, DOI: 10.1007/BF02580858.

[128] J. Larsson*, et al.*, "The 30-Hz flicker cone ERG for monitoring the early course of central retinal vein occlusion," *Acta Ophthalmologica Scandinavica,* vol. 78, pp. 187-190, 2000, DOI: 10.1034/j.1600-0420.2000.078002187.

[129] M.-M. Parvaresh*, et al.*, "Normal Values of Standard Full Field Electroretinography in an Iranian Population," *Journal of Ophthalmic & Vision Research,* vol. 4, pp. 97-101, 2009.

[130] J. V. Basmajian, *Muscles Alive: Their Functions Revealed by Electromyography*: Academic Medicine 37(8), 1962.

[131] C. Luca. (2006). *Electromyography. Encyclopedia of Medical Devices and Instrumentation* (Last retrieved: Last retrieved: 03/02/2014).

[132] C. Menon*, et al.*, "A preliminary investigation assessing the viability of classifying hand postures in seniors," *BioMedical Engineering OnLine 2011,* vol. 10, 2011, DOI: 10.1186/1475-925X-10-79.

[133] Y. Zhang*, et al.*, "An improved incremental online training algorithm for reducing the influence of muscle fatigue in sEMG based HMI," in *Robotics and Biomimetics (ROBIO), 2012 IEEE International Conference on*, 2012, pp. 683-688, DOI: 10.1109/robio.2012.6491046.

[134] T. D. Lalitharatne*, et al.*, "A study on effects of muscle fatigue on EMG-based control for human upper-limb power-assist," in *Information and Automation for Sustainability (ICIAfS), 2012 IEEE 6th International Conference on*, 2012, pp. 124-128, DOI: 10.1109/iciafs.2012.6419892.

[135] M. Gauthaam and S. S. Kumar, "EMG controlled bionic arm," in *Innovations in Emerging Technology (NCOIET), 2011 National Conference on*, 2011, pp. 111-114, DOI: 10.1109/ncoiet.2011.5738813.

[136] K. Kiguchi and Y. Hayashi, "An EMG-Based Control for an Upper-Limb Power-Assist Exoskeleton Robot," *Systems, Man, and Cybernetics, Part B: Cybernetics, IEEE Transactions on,* vol. 42, pp. 1064-1071, 2012, DOI: 10.1109/tsmcb.2012.2185843.

[137] T. Lenzi*, et al.*, "Intention-Based EMG Control for Powered Exoskeletons," *Biomedical Engineering, IEEE Transactions on,* vol. 59, pp. 2180-2190, 2012, DOI: 10.1109/tbme.2012.2198821.

[138] A. Akhtar*, et al.*, "Prediction of distal arm joint angles from EMG and shoulder orientation for prosthesis control," in *Engineering in Medicine and Biology Society (EMBC), 2012 Annual International Conference of the IEEE*, 2012, pp. 4160-4163, DOI: 10.1109/embc.2012.6346883.

[139] G. Matrone*, et al.*, "Two-channel real-time EMG control of a dexterous hand prosthesis," in *Neural Engineering (NER), 2011 5th International IEEE/EMBS Conference on*, 2011, pp. 554-557, DOI: 10.1109/ner.2011.5910608.

[140] E. Ambrosini*, et al.*, "An EMG-controlled neuroprosthesis for daily upper limb support: A preliminary study," in *Engineering in Medicine and Biology Society,EMBC, 2011 Annual International Conference of the IEEE*, 2011, pp. 4259-4262, DOI: 10.1109/iembs.2011.6091057.

[141] R. C. So*, et al.*, "Application of surface electromyography in assessing muscle recruitment patterns in a six-minute continuous rowing effort," *J Strength Cond Res,* vol. 21, pp. 724-30, Aug 2007, DOI: 10.1519/r-19985.1.

[142] N. Masso*, et al.*, "Surface electromyography applications in the sport," *Apunts Med Esport,* vol. 45, pp. 121-130, 2010.

[143] *SENIAM: Surface ElectrMyoGraphy for the Non-Invasive Assessment of Muscles* [Sensor Locations Guide: Recommendations for sensor loactions on individual muscles]. Available URL: http://seniam.org/shoulder_location.htm (Last retrieved: 31/01/2014).

[144] Jankovic*, et al.*, "An EMG system for studying motor control strategies and fatigue," in *Neural Network Applications in Electrical Engineering (NEUREL), 2010 10th Symposium on*, 2010, pp. 15-18, DOI: 10.1109/neurel.2010.5644044.

[145] K. Ollivier*, et al.*, "Repeatability of surface EMG parameters at various isometric contraction levels and during fatigue using bipolar and Laplacian electrode configurations," *Journal of Electromyography and Kinesiology,* vol. 15, pp. 466 - 473, 2005, DOI: http://dx.doi.org/10.1016/j.jelekin.2005.01.004.

[146] A. Eberstein and B. Beattie, "Simultaneous measurement of muscle conduction velocity and emg power spectrum changes during fatigue," *Muscle & Nerve,* vol. 8, pp. 768-773, 1985, DOI: 10.1002/mus.880080905.

[147] C. J. De Luca, "The use of surface electromyography in biomechanics," *Journal of applied biomechanics,* vol. 13, pp. 135-163, 1997.

[148] C. J. De Luca and M. Knaflitz, *Surface Electromyography: What's New?*: CLUT Ed., 1992.

[149] A. Ferreira*, et al.*, "Human-machine interfaces based on EMG and EEG applied to robotic systems," *Journal of NeuroEngineering and Rehabilitation,* vol. 5, p. 10, 2008, DOI: 10.1088/1742-6596/90/1/012094.

[150] I. Moon*, et al.*, "Intelligent robotic wheelchair with EMG-, gesture-, and voice-based interfaces," in *Intelligent Robots and Systems, 2003.(IROS 2003). Proceedings. 2003 IEEE/RSJ International Conference on*, 2003, pp. 3453-3458, DOI: 10.1109/IROS.2003.1249690.

[151] R. Gopura*, et al.*, "Recent Trends in EMG-Based Control Methods for Assistive Robots," 2013, DOI: http://dx.doi.org/10.5772/56174.

[152] K. Shima*, et al.*, "EMG-based control for a feeding support robot using a probabilistic neural network," in *Biomedical Robotics and Biomechatronics (BioRob), 2012 4th IEEE RAS & EMBS International Conference on*, 2012, pp. 1788-1793, DOI: 10.1109/BioRob.2012.6290876.

[153] S. K. Choudhary*, et al.*, "Development of Cost Effective EMG Controlled Three Fingered Robotic Hand," in *Computer and Communication Technology (ICCCT), 2012 Third International Conference on*, 2012, pp. 104-109, DOI: 10.1109/iccct.2012.29.

[154] T. M. Lubecki*, et al.*, "Development of intuitive human-machine interface based on Electromyography for assistive robot (KAAD)," in *System Integration (SII), 2011 IEEE/SICE International Symposium on*, 2011, pp. 908-913, DOI: 10.1109/sii.2011.6147570.

[155] Z. Chi*, et al.*, "Power assistance for human elbow motion support using minimal EMG signals with admittance control," in *Mechatronics and Automation (ICMA), 2011 International Conference on*, 2011, pp. 276-281, DOI: 10.1109/icma.2011.5985670.

[156] P. K. Artemiadis and K. J. Kyriakopoulos, "An EMG-Based Robot Control Scheme Robust to Time-Varying EMG Signal Features," *Information Technology in Biomedicine, IEEE Transactions on,* vol. 14, pp. 582-588, 2010, DOI: 10.1109/titb.2010.2040832.

[157] P. K. Artemiadis and K. J. Kyriakopoulos, "EMG-Based Control of a Robot Arm Using Low-Dimensional Embeddings," *Robotics, IEEE Transactions on,* vol. 26, pp. 393-398, 2010, DOI: 10.1109/tro.2009.2039378.

[158] P. Wang*, et al.*, "Rehabilitation control strategies for a gait robot via EMG evaluation," presented at the IEEE International Conference on Rehabilitation Robotics, 2009. (ICORR 2009). , Kyoto, 2009, DOI: 10.1109/ICORR.2009.5209554.

[159] P. K. Artemiadis and K. J. Kyriakopoulos, "Teleoperation of a robot manipulator using EMG signals and a position tracker," pp. 1003 - 1008, August 2005, DOI: 10.1109/IROS.2005.1545509.

[160] M. DiCicco*, et al.*, "Comparison of control strategies for an EMG controlled orthotic exoskeleton for the hand," in *Robotics and Automation, 2004. Proceedings. ICRA '04. 2004 IEEE International Conference on*, 2004, pp. 1622 - 1627, DOI: 10.1109/ROBOT.2004.1308056.

[161] L. Lucas*, et al.*, "An EMG-controlled hand exoskeleton for natural pinching," *Journal of Robotics and Mechatronics,* vol. 16, pp. 482-488, 2004.

[162] O. Fukuda*, et al.*, "EMG-based human-robot interface for rehabilitation aid," in *Robotics and Automation, 1998. Proceedings. 1998 IEEE International Conference on*, 1998, pp. 3492-3497 vol.4, DOI: 10.1109/robot.1998.680978.

[163] A. S. Sousa and J. M. R. Tavares, "Surface electromyographic amplitude normalization methods: A review," *Electromyography: New Developments, Procedures and Applications,* 2012, DOI: http://hdl.handle.net/10216/64430.

[164] M. Halaki and K. Ginn. (2012). *Normalization of EMG Signals: To Normalize or Not to Normalize and What to Normalize to?* - Computational Intelligence in Electromyography Analysis - A Perspective on Current Applications and Future Challenges. (Last retrieved: 03/01/2014) Available URL: http://www.intechopen.com/books/export/citation/EndNote/computational-intelligence-in-electromyography-analysis-a-perspective-on-current-applications-and-future-challenges/normalization-of-emg-signals-to-normalize-or-not-to-normalize-and-what-to-normalize-to-.

[165] M. M. Reinold, *et al.*, "Electromyographic analysis of the rotator cuff and deltoid musculature during common shoulder external rotation exercises," *Journal of Orthopaedic and Sports Physical Therapy,* vol. 34, pp. 385-394, 2004.

[166] D. Duong Minh, *et al.*, "EMG-moment model of human arm for rehabilitation robot system," in *Control, Automation, Robotics and Vision, 2008. ICARCV 2008. 10th International Conference on*, 2008, pp. 190-195, DOI: 10.1109/icarcv.2008.4795515.

[167] G. M. Lyons, *et al.*, "A computer game-based EMG biofeedback system for muscle rehabilitation," in *Engineering in Medicine and Biology Society, 2003. Proceedings of the 25th Annual International Conference of the IEEE*, 2003, pp. 1625-1628 Vol.2, DOI: 10.1109/iembs.2003.1279682.

[168] H. Berg, *et al.*, "Lower limb skeletal muscle function after 6 wk of bed rest," *Journal of Applied Physiology,* vol. 82, pp. 182-188, 1997.

[169] J. P. Farthing, *et al.*, "Strength training the free limb attenuates strength loss during unilateral immobilization," *Journal of Applied Physiology,* vol. 106, pp. 830-836, 2009, DOI: 10.1152/japplphysiol.91331.2008.

[170] M. Matsumura, *et al.*, "Low-volume muscular endurance and strength training during 3-week forearm immobilization was effective in preventing functional deterioration," *Dynamic Medicine,* vol. 7, p. 1, 2008.

[171] B. C. Clark, *et al.*, "Neuromuscular plasticity during and following 3 wk of human forearm cast immobilization," *Journal of Applied Physiology,* vol. 105, pp. 868-878, 2008.

[172] M. P. Miles, *et al.*, "Muscle function at the wrist following 9 d of immobilization and suspension," *Medicine and science in sports and exercise,* vol. 26, p. 615, 1994.

[173] *SmartDraw Examples* [Images: 'Range of Motion of Shoulder' and 'Range of Motion of Elbow and Shoulder']. Available URL: http://www.smartdraw.com/examples/healthcare/health--fitness/#/examples/Healthcare/Health--Fitness (Last retrieved: 31/01/2014).

[174] *Quantum Neuromonitoring* [Image: Deltoid]. Available URL: http://quantumneuromonitoring.com/illustrations/recording-sites.php (Last retrieved: 31/01/2014).

[175] H. Bouwsema, *et al.*, "Learning to Control Opening and Closing a Myoelectric Hand," *Archives of Physical Medicine and Rehabilitation,* vol. 91, pp. 1442 - 1446, 2010.

[176] C. E. Stepp, *et al.*, "Vibrotactile feedback aids EMG control of object manipulation," in *Engineering in Medicine and Biology Society,EMBC, 2011 Annual International Conference of the IEEE*, 2011, pp. 1061-1064, 10.1109/iembs.2011.6090247.

[177] C. Casellato, *et al.*, "EMG-based visual-haptic biofeedback: a tool to improve motor control in children with primary dystonia," *Neural Systems and Rehabilitation Engineering, IEEE Transactions on,* vol. PP, pp. 1-1, 2012, 10.1109/tnsre.2012.2222445.

[178] T. Noda, *et al.*, "An electromyogram based force control coordinated in assistive interaction," in *Robotics and Automation (ICRA), 2013 IEEE International Conference on*, 2013, pp. 2657-2662, DOI: 10.1109/icra.2013.6630942.

[179] N. Jiang, *et al.*, "Effect of arm position on the prediction of kinematics from EMG in amputees," *Medical & biological engineering & computing,* pp. 1-9, 2013, DOI: 10.1007/978-1-4471-4802-9_92.

[180] J. Son, *et al.*, "An EMG-based muscle force monitoring system," *Journal of Mechanical Science and Technology,* vol. 24, pp. 2099-2105, 2010/10/01 2010, DOI: 10.1007/s12206-010-0616-9.

[181] *sportEX dynamic 2010; 23 (Jan): 10-13* [Image: Typed of muscle contractions]. Available URL: http://www.omnilexica.com/?q=muscle+contraction (Last retrieved: 31/01/2014).

[182] G. Kamen and D. A. Gabriel, *Essentials of electromyography*: Human Kinetics Publishers, 2010.

[183] C. Fleischer, *et al.*, "Predicting the intended motion with EMG signals for an exoskeleton orthosis controller," in *Intelligent Robots and Systems, 2005. (IROS 2005). 2005 IEEE/RSJ International Conference on*, 2005, pp. 2029-2034, DOI: 10.1109/iros.2005.1545504.

[184] K. Kiguchi, *et al.*, "Neuro-fuzzy control of a robotic exoskeleton with EMG signals," *Fuzzy Systems, IEEE Transactions on,* vol. 12, pp. 481-490, 2004, 10.1109/tfuzz.2004.832525.

[185] K. Kiguchi, *et al.*, "An exoskeletal robot for human elbow motion support-sensor fusion, adaptation, and control," *Systems, Man, and Cybernetics, Part B: Cybernetics, IEEE Transactions on,* vol. 31, pp. 353-361, 2001, DOI: 10.1109/3477.931520.

[186] M. R. Spiegel, *Schaum's outline of theory and problems of statistics*: McGraw-Hill, 1988.

[187] J. Issa, "Performance and power analysis for high performance computation benchmarks," *Central European Journal of Computer Science,* vol. 3, pp. 1-16, 2013/03/01 2013, 10.2478/s13537-013-0101-5.

[188] J. D. Slater, *et al.*, "Quality assessment of electroencephalography obtained from a “dry electrode” system," *Journal of Neuroscience Methods,* vol. 208, pp. 134-137, 2012, http://dx.doi.org/10.1016/j.jneumeth.2012.05.011.

[189] R. S. Nickerson, "Binary-classification reaction time: A review of some studies of human information-processing capabilities," *Psychonomic Monograph Supplements,* vol. 4, pp. 275-318, 1972.

[190] J. Devore, *Probability and Statistics for Engineering and the Sciences*: Cengage Learning, 2011.

[191] A. Bulling, *et al.*, "Eye Movement Analysis for Activity Recognition Using Electrooculography," *Pattern Analysis and Machine Intelligence, IEEE Transactions on,* vol. 33, pp. 741-753, 2011, 10.1109/tpami.2010.86.

Appendices

Appendix A. EPIC Movement Sensor Data Sheet

plessey

PS25405B
EPIC Ultra High Impedance Movement Sensor
Advance Datasheet

Data Sheet 291951 issue 2

FEATURES

- Ultra high effective input resistance, typically 20GΩ.
- Effective input capacitance as low as 15pF.
- Upper 3dB point typically 20kHz.
- Operates with bipolar power supply from ±2.4V to ±5.5V.
- Sensors supplied in a custom package with exposed pins for surface mount assembly.

APPLICATIONS

- Proximity switching of lighting and similar electric circuits
- Remote control of TVs and other domestic appliances
- Presence detection for security / alarm systems
- Room occupancy detection for rescue services
- Simple gesture recognition to control children's toys
- Controller-less computer gaming systems

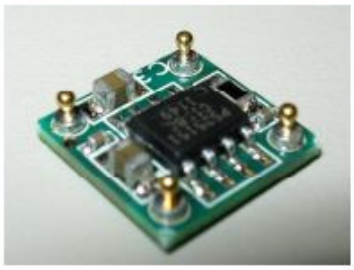

Fig. 1 The PS25405B Sensor

Ordering Information

PS25405B
Custom package

-25°C to +75°C

Plessey Semiconductors Electric Potential Integrated Circuit (EPIC) product line targets a range of applications.

The PS25405B is an ultra high impedance non-contact solid state electric potential sensor. It can be used to detect field disturbance due to the movement of a near-by object. This functionality can be employed in a range of applications including security motion sensors and non-contact electric switches for lighting, door opening, toys etc

The device uses active feedback techniques to both lower the effective input capacitance of the sensing element (Cin) and boost the input resistance (Rin). These techniques are used to realise a sensor with a frequency response suitable for remote sensing applications.

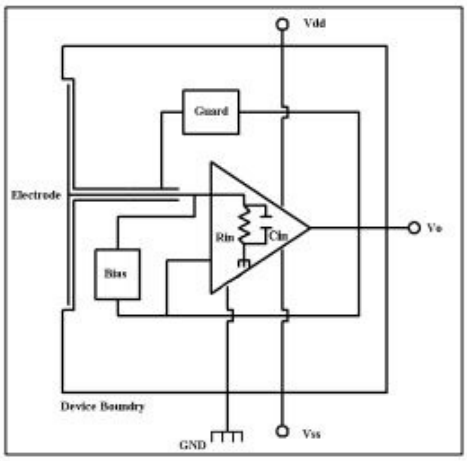

Fig. 2 Internal circuit of EPIC Movement Sensor

Plessey Semiconductors Ltd.
Design & Technology Centre, Delta 500, Delta Business Park, Great Western Way, Swindon, UK SN5 7XE
Tel: +44 1793 518000 Fax: +44 1793 518030 Web: www.plesseysemi.com

ELECTRICAL CHARACTERISTICS

T_{amb} = -25°C to +75°C, Vdd/Vss ±2.4V to ±5.5V. The electrical characteristics are guaranteed by either production test or by design and characterisation. They apply within the specified ambient temperature and supply voltage unless otherwise stated.

Characteristics	Value			Units	Conditions
	Min.	Typ.	Max.		
Supply voltage	±2.4		±5.5	V	Bipolar supply, Gnd=0V
Supply current	1.5	2.5	3.5	mA	
Effective input resistance		20		GΩ	
Effective input capacitance		15		pF	As measured at the sensor electrode
Voltage Gain (Av)		10			When measured with 250pF coupling capacitance
Lower -3dB point		30		Hz	Set by internal DC signal rejection network – coupling capacitor 250pF
Upper -3dB point		20.0		kHz	
Noise		tbd			

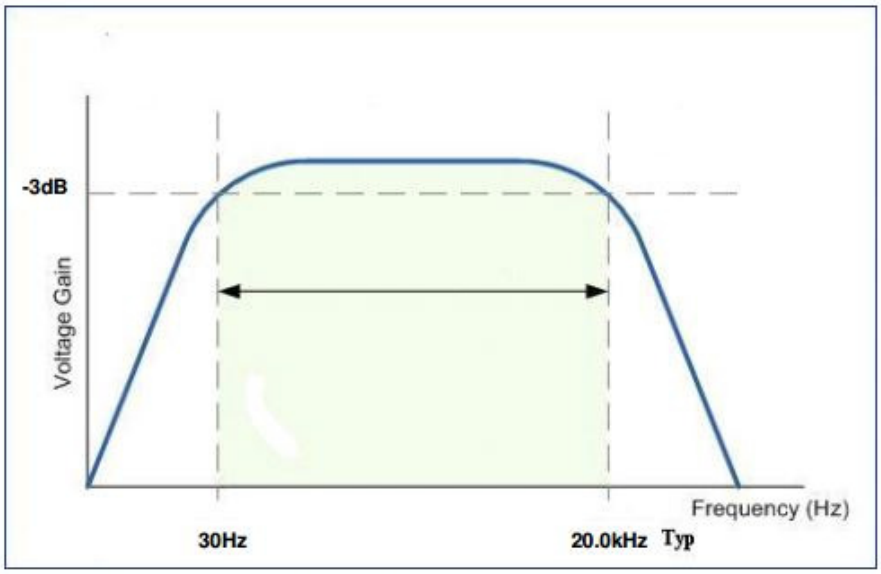

Fig. 3 Typical Bode Plot for PS25405B Sensor with Coupling through 250pF Capacitor

Plessey Semiconductors Ltd.
Design & Technology Centre, Delta 500, Delta Business Park, Great Western Way, Swindon, UK SN5 7XE
Tel: +44 1793 518000 Fax: +44 1793 518030 Web: www.plesseysemi.com

PIN ASSIGNMENT

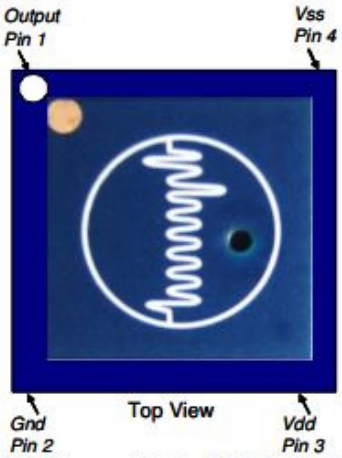

Fig. 4 Pin Assignment for the PS25405B – Top View

MECHANICAL DIMENSIONS

The package diagram is shown below. It is recommended that a solder pad 1.6mm diameter be defined for the mounting of the sensor pins.

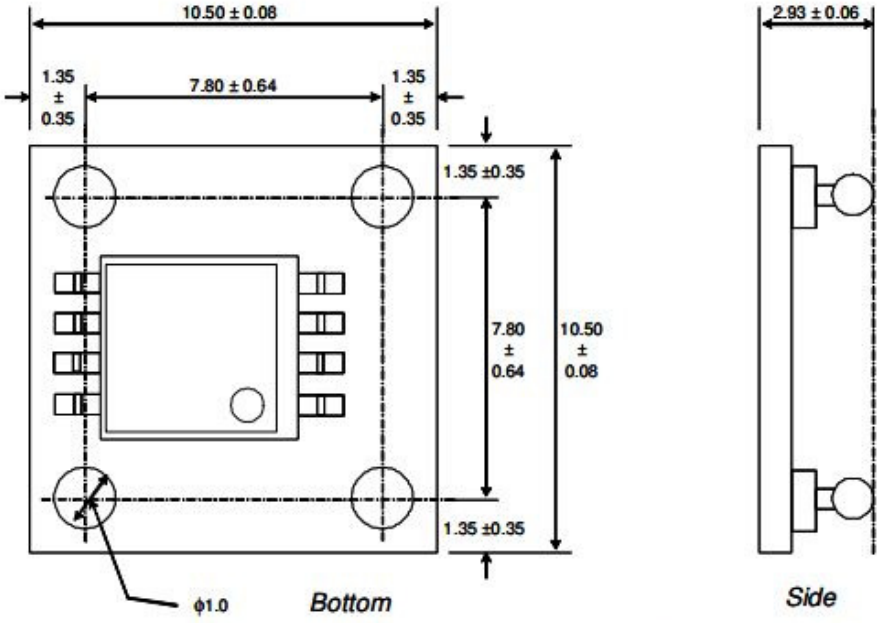

Fig. 5 Mechanical Drawing (all dimensions are nominal and in mm)

Plessey Semiconductors Ltd.
Design & Technology Centre, Delta 500, Delta Business Park, Great Western Way, Swindon, UK SN5 7XE
Tel: +44 1793 518000 Fax: +44 1793 518030 Web: www.plesseysemi.com

ELECTROSTATIC DISCHARGE (ESD) PROTECTION

The PS25405B is manufactured using a high performance analog CMOS process. As for all CMOS components, it is essential that conventional ESD protection protocols be applied for the handling of this device.

PATENTS

This component and many of the associated applications are covered by the following international patents:

602 32 911.6-08 (DE)	EP2174416
AU2007228660	GB1118970.1
CA2646411	JP2009-500908
CN200780026584.8	JP4391823
EP1451595 (CH)	TW097126903
EP1451595 (ES)	TW1308066
EP1451595 (FR)	US12/293872
EP1451595 (IE)	US12/374359
EP1451595 (IT)	US12/669615
EP1451595 (NL)	US13/020890
EP2002273	US13/163988
EP2047284	US7885700

Plessey Semiconductors Ltd.
Design & Technology Centre, Delta 500, Delta Business Park, Great Western Way, Swindon, UK SN5 7XE
Tel: +44 1793 518000 Fax: +44 1793 518030 Web: www.plesseysemi.com

Appendix B. LabVIEW Virtual-Instrument (VI) Program Code

Appendix B1. Position Sensing VIs

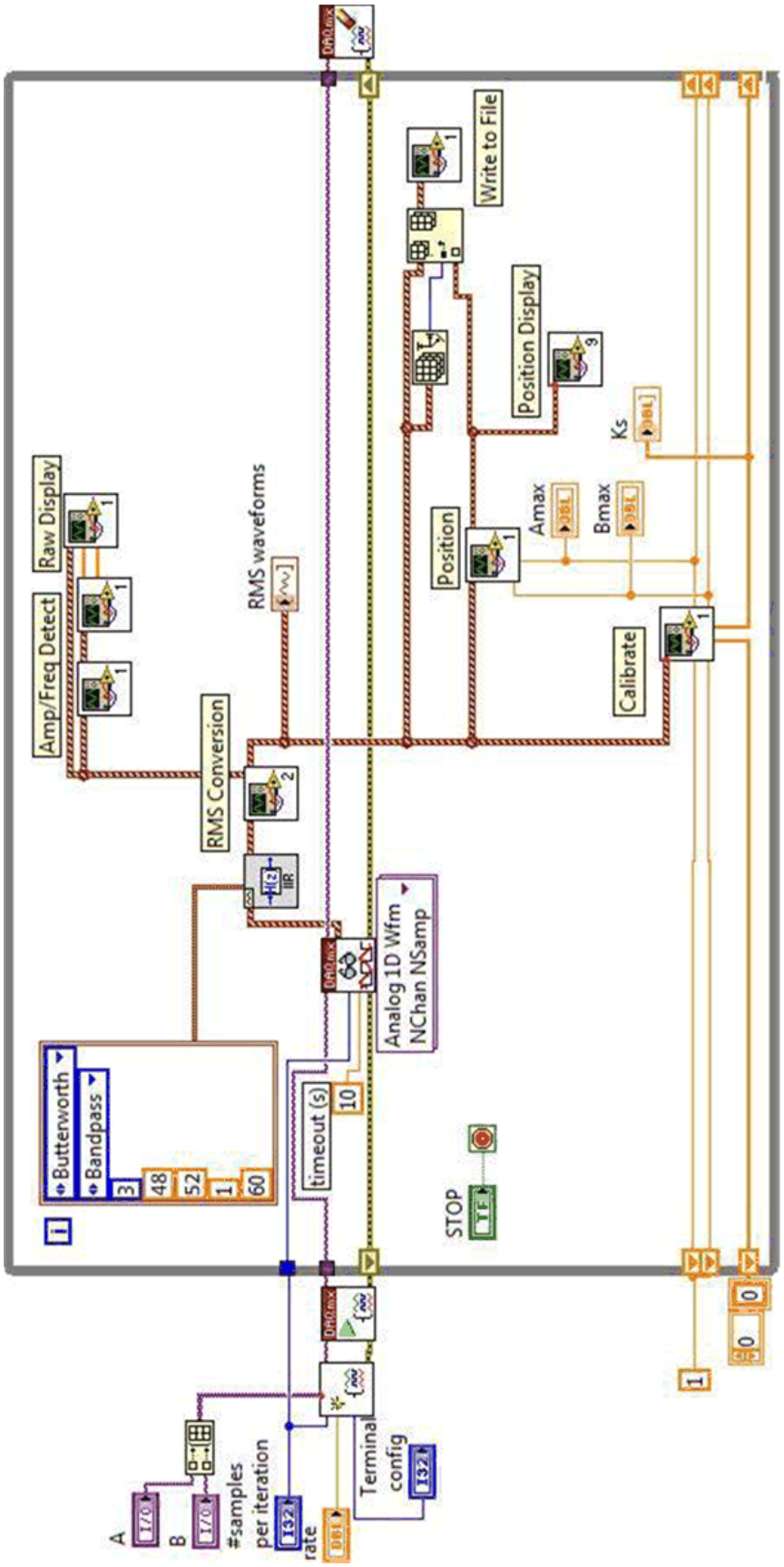

Figure B1.1 Main LabVIEW code for one dimensional position sensing

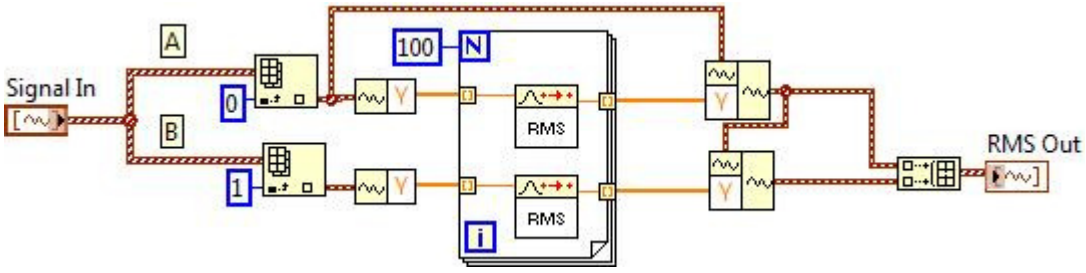

Figure B1.2 LabVIEW program code for calculating sensor RMS voltage used for inferring hand position on a one dimensional plane

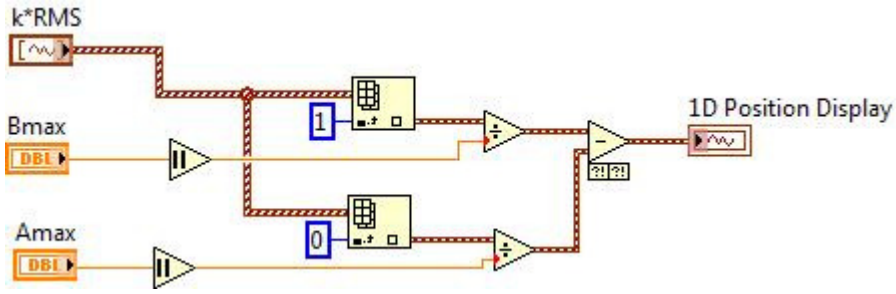

Figure B1.3 LabVIEW program code for normalised hand position determination on a one dimensional plane

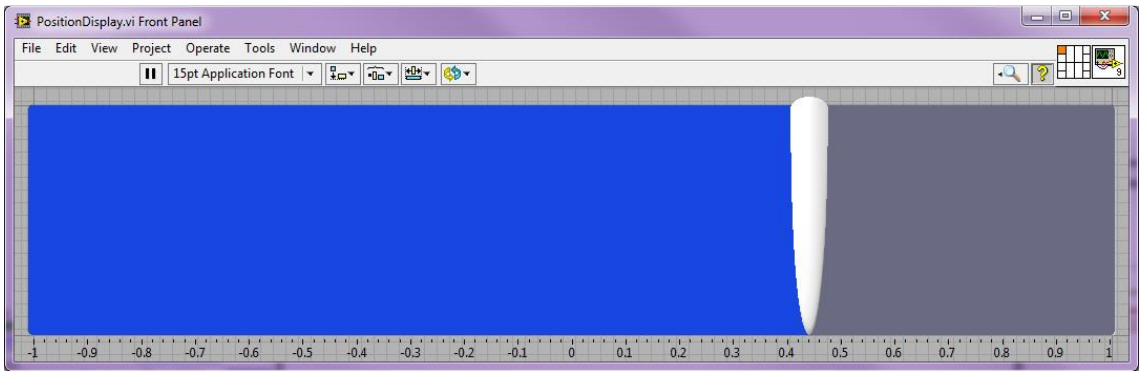

Figure B1.4 Graph showing inferred hand position on one dimensional plane

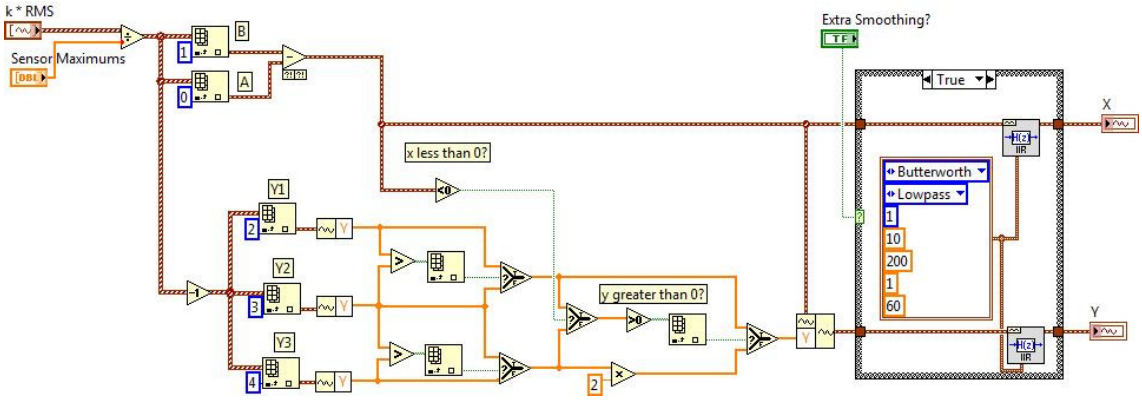

Figure B1.5 LabVIEW program code for normalised hand position determination on a two dimensional plane

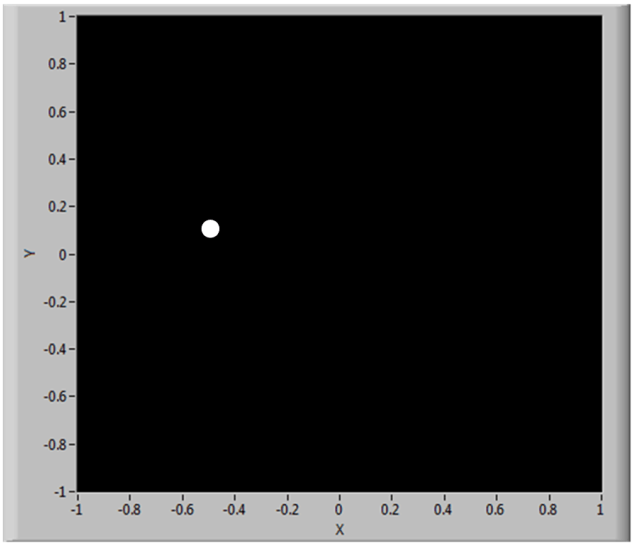

Figure B1.6 Graphical display of inferred hand position on two dimensional plane

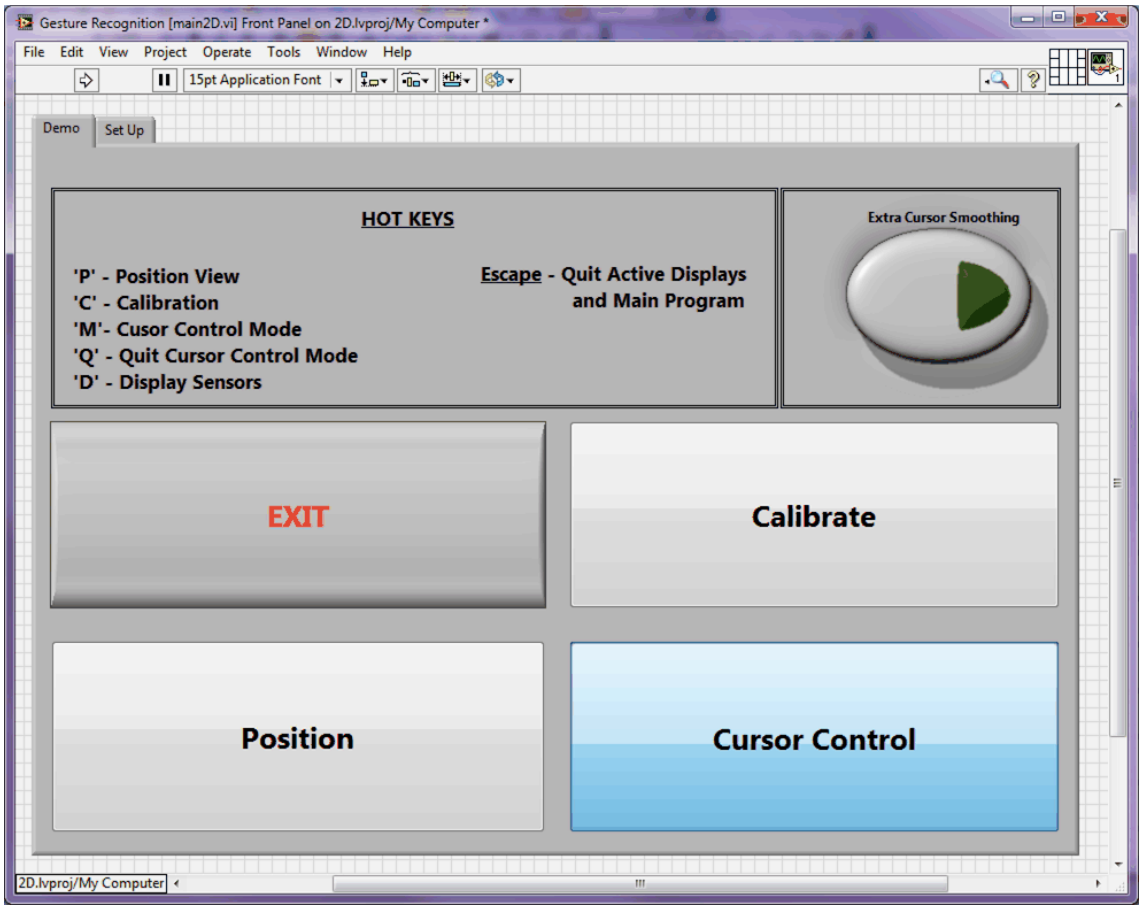

Figure B1.7 Hand position sensing program front panel user interface

Appendix B2. Eye tracking VIs

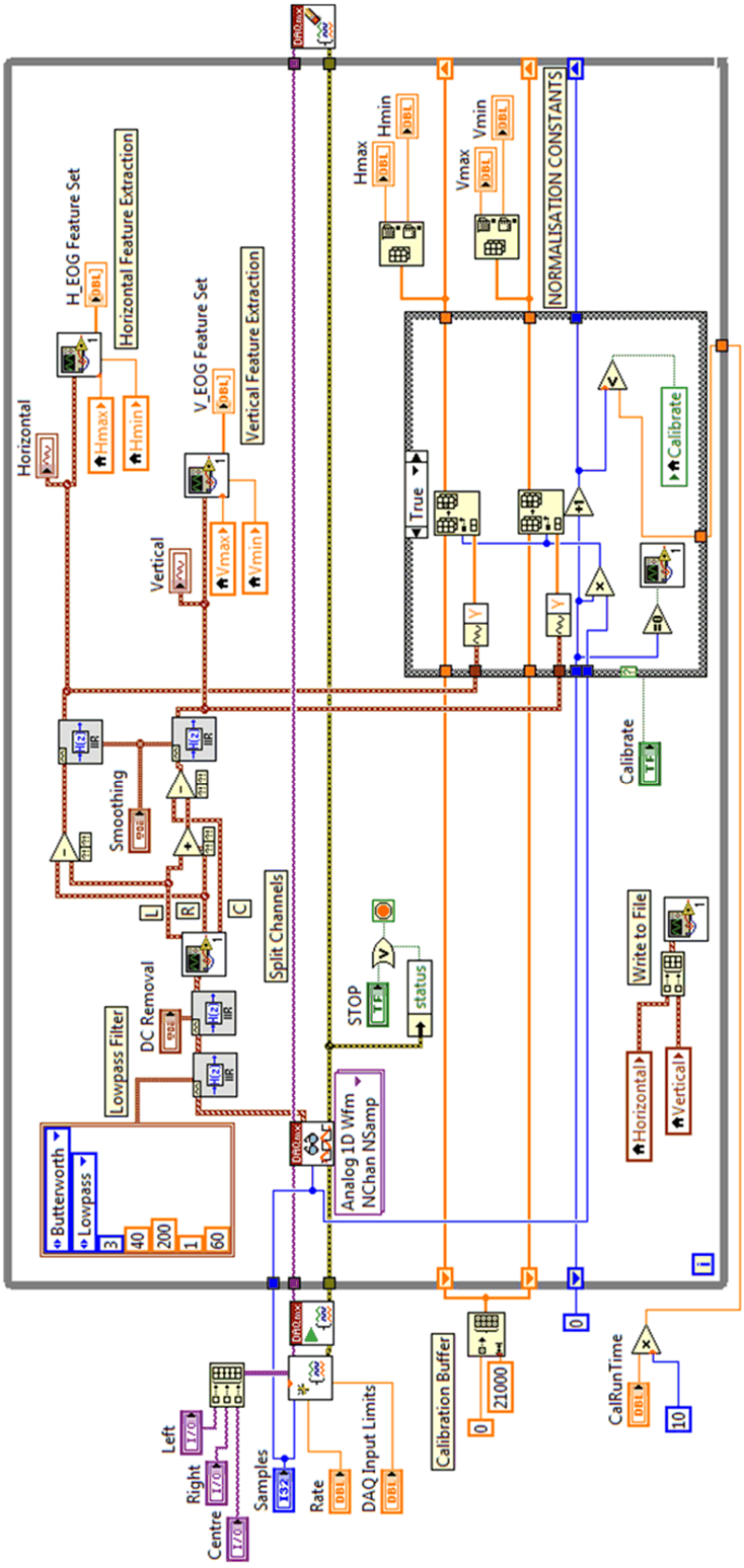

Figure B2.1 Main LabVIEW program code for acquiring and recording EOG signals

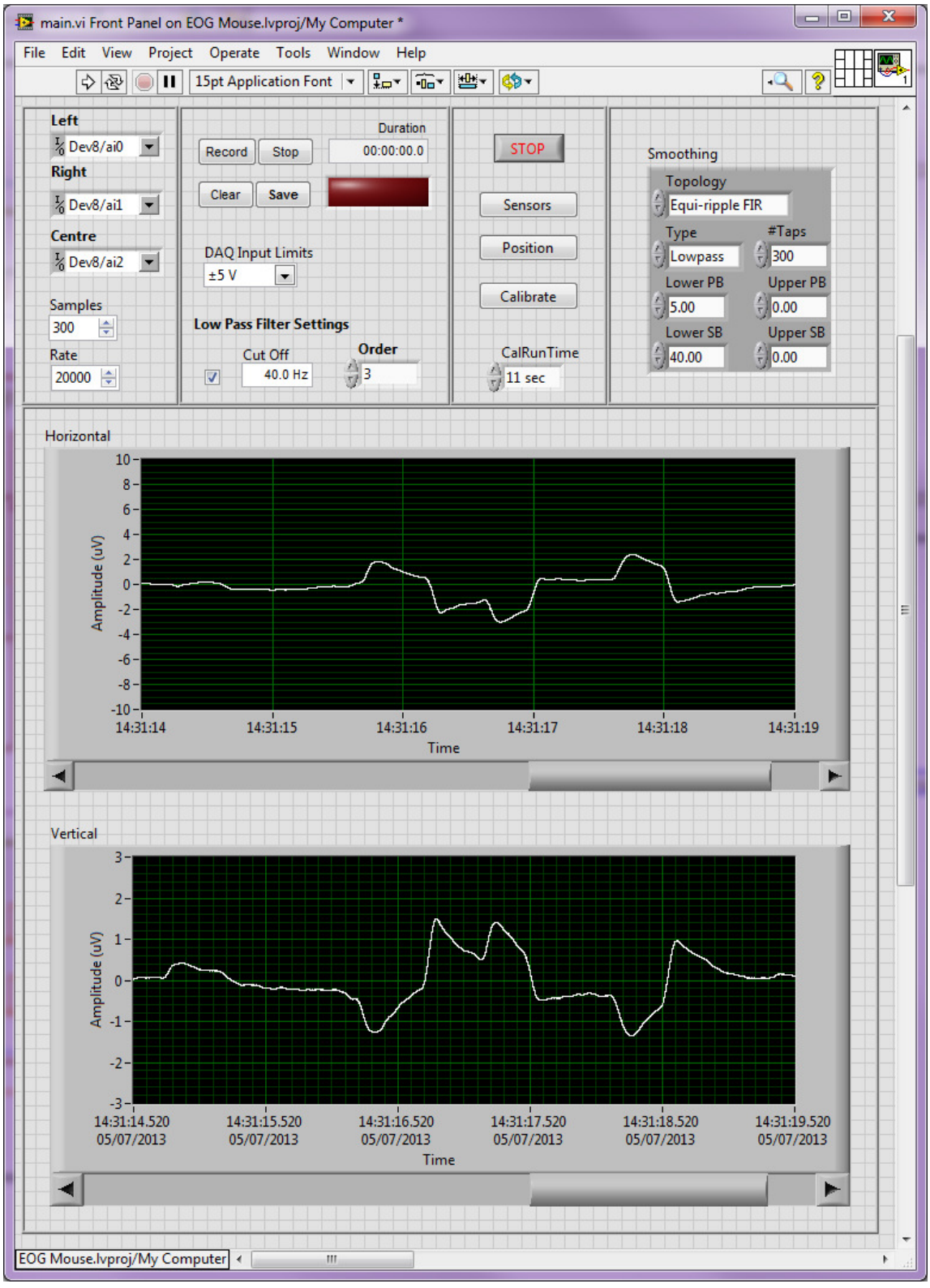

Figure B2.2 LabVIEW front panel display used during EOG eye-tracking program experiments

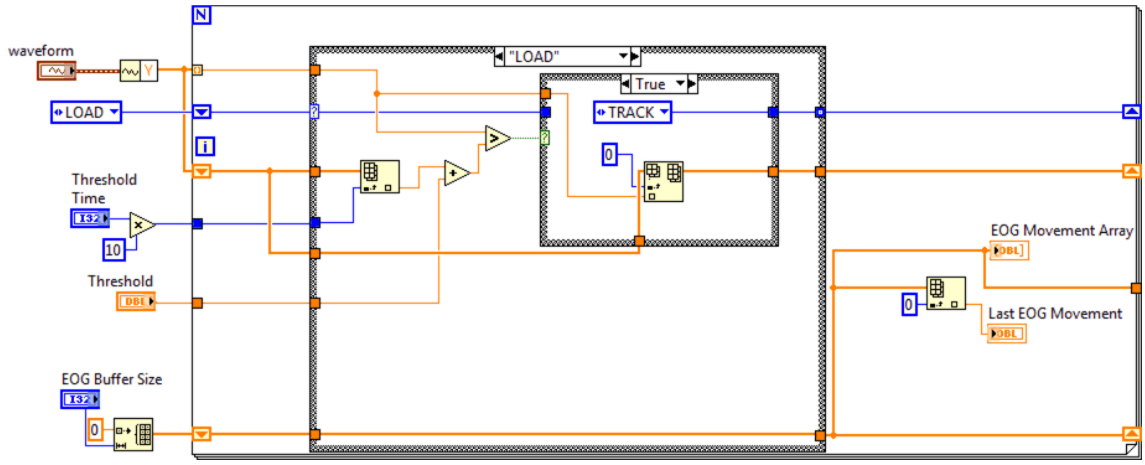

Figure B2.3 Eye-tracking LabVIEW sub-VI -"LOAD": Continuously loads real-time EOG signals until change in amplitude occurs signifying an eye movement.

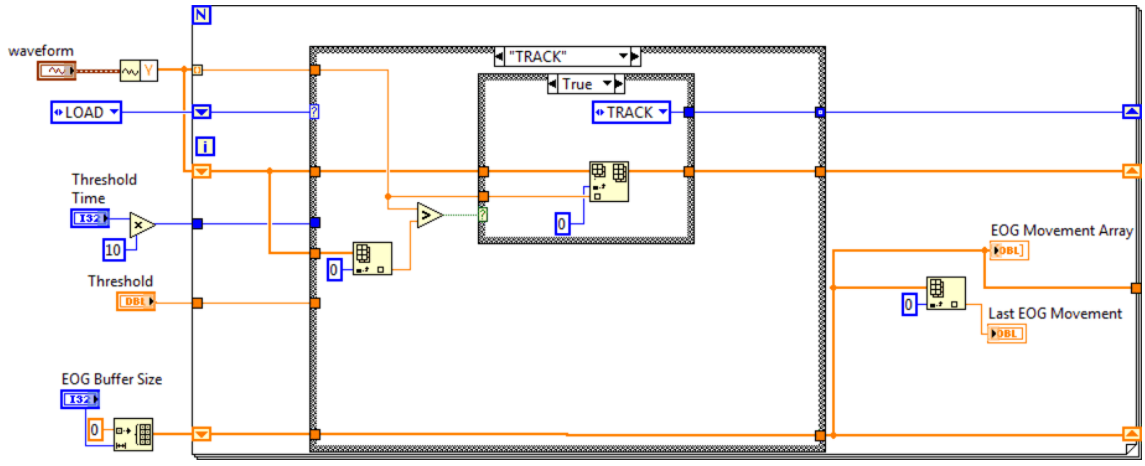

Figure B2.4 Eye-tracking LabVIEW sub-VI - "TRACK": Changes in EOG amplitudes are loaded into a buffer in order to determine the magnitude of the eye movement.

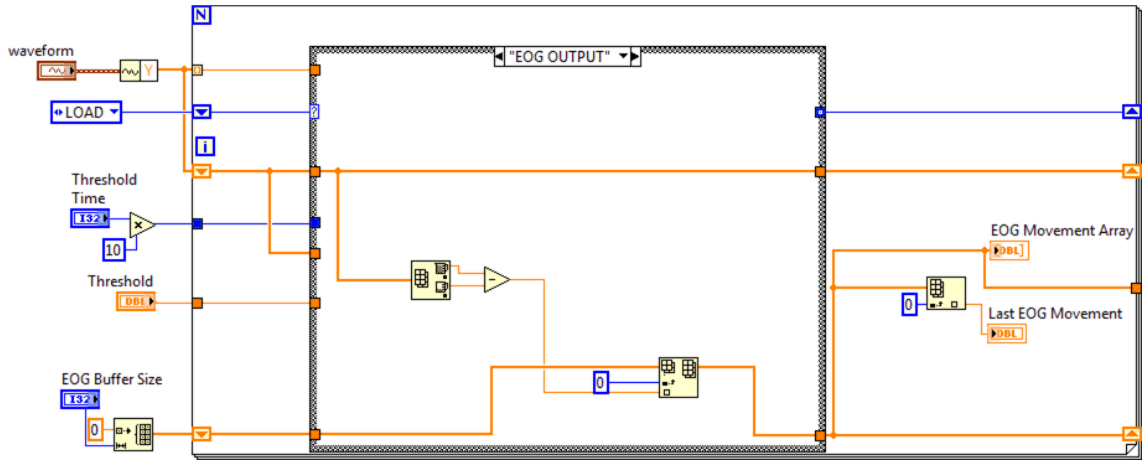

Figure B2.5 Eye-tracking LabVIEW sub-VI - "EOG OUTPUT":Outputs the magnitude of the amplitude change that occurred during an eye movement once the eye movement is complete.

Appendix B3. Recording ERGs VIs

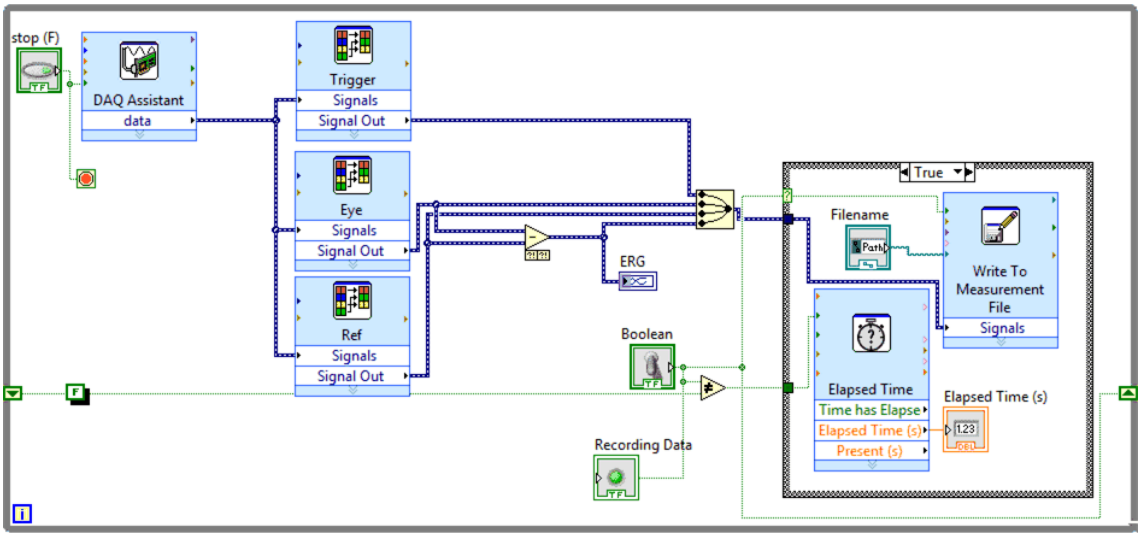

Figure B3.1 Main LabVIEW program code for acquiring and recording the electroretinogram (ERG)

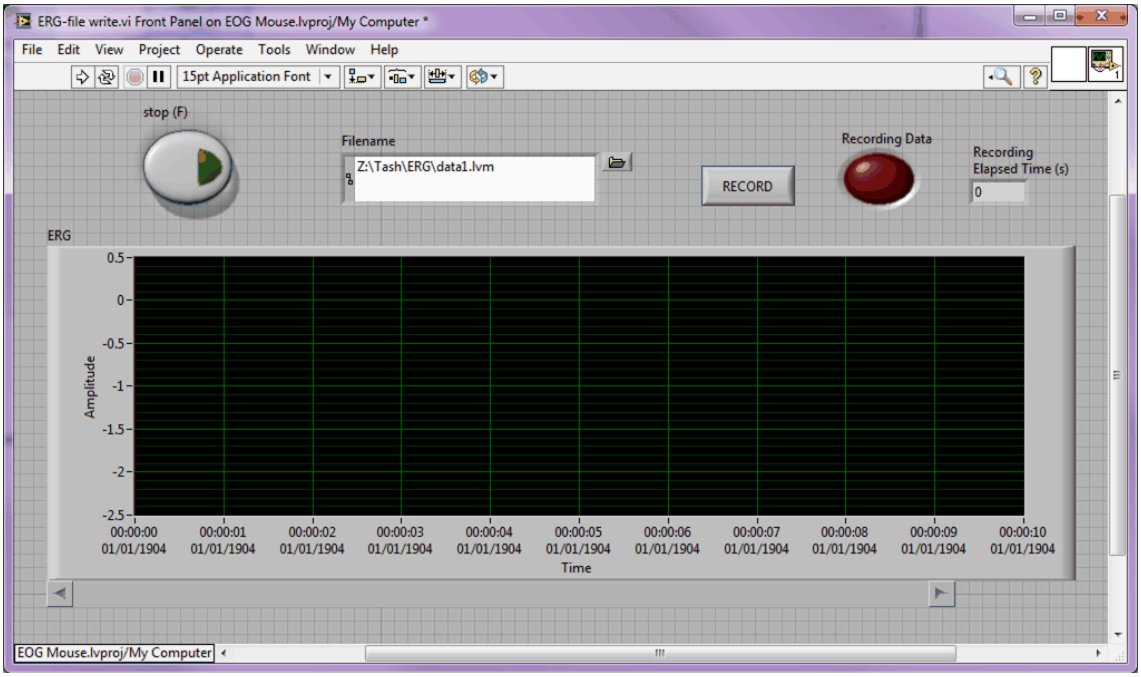

Figure B3.2 LabVIEW front panel display for electroretinogram (ERG) experiments

Appendix B4. SEMG monitoring VI

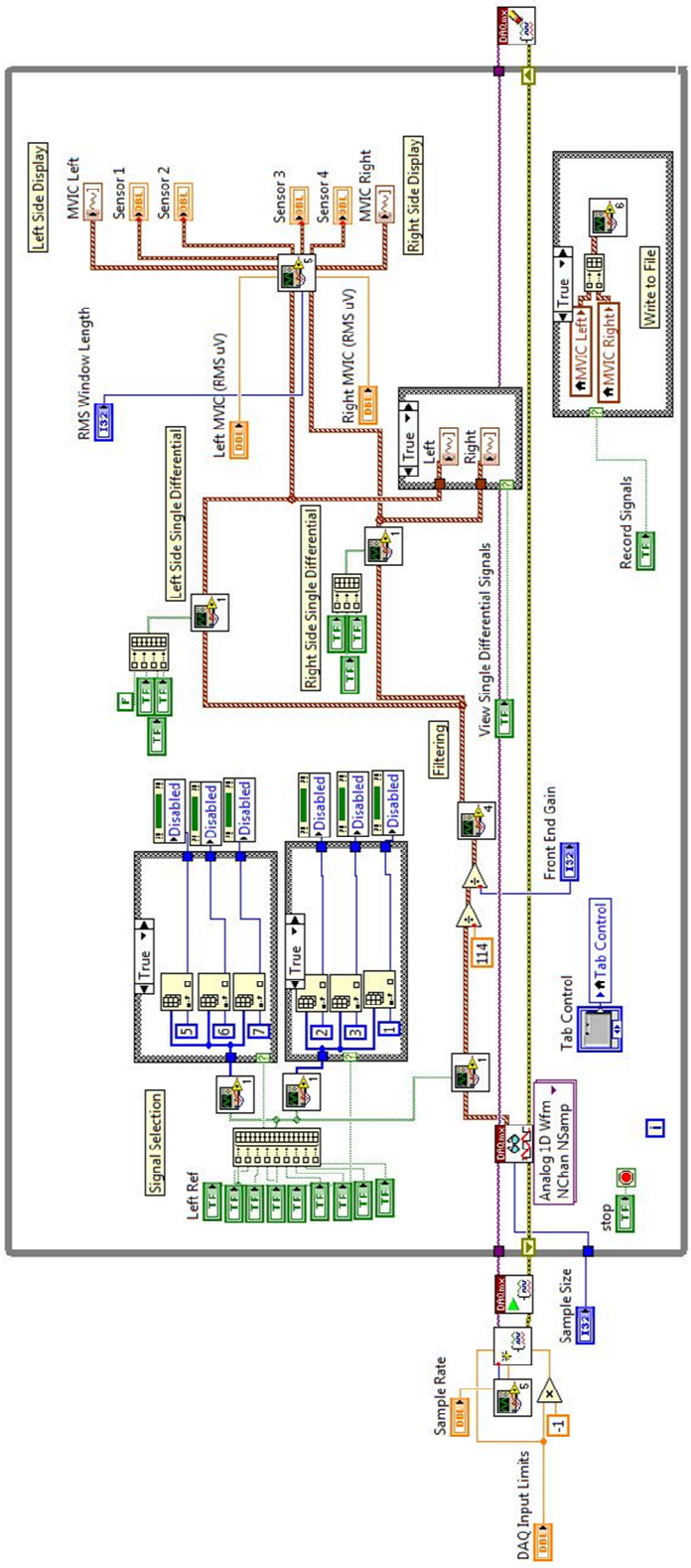

Figure B4.1 Main LabVIEW program code for acquiring and recording SEMG signals

Appendix C. Matlab Code

```
function [ergout] = erg5(data,trig, no_avgs)
ergout =[];
m =1;
trig_index = [];

for i = 1:10000 %check first few triggers, 0.5 sec of data
        if trig(i) > (0.5*max(trig))
            trig_index(m) = i;
            m=m+1;
        end
end
k= trig_index(1); %start point for averaging, first trigger
blocksize = (trig_index(2)-trig_index(1)); %one cycle average, 200ms
i=1;

while i < no_avgs
         ergout(i,:) = data(k:k+blocksize); % create array of ERGs
         k = k + blocksize;
         i = i+1;
end

ergout = sum(ergout)/size(ergout,1); %average ERGs
t = (-0.02:1/20000:((length(ergout)-1)/20000)-0.02).*1e-3; %create time array

figure
hold on
plot(t,ergout); %uV
xlim([-20 180])
```

Figure C.1 Signal averaging and graphing MATLAB program code used for the 5 Hz stimulus ERG

```
function [ergout] = erg30(data,trig, no_avgs)
ergout =[];
m =1;
trig_index = [];

for i = 1:10000 %check first few triggers, 0.5 sec of data
        if trig(i) > (0.5*max(trig))
            trig_index(m) = i;
            m=m+1;
        end
end
k= trig_index(1); %start point for averaging, first trigger
blocksize = (trig_index(4)-trig_index(1)); %three cycle average, 90ms
i=1;

while i < no_avgs
         ergout(i,:) = data(k:k+blocksize); % create array of ERGs
         k = k + blocksize;
         i = i+1;
end

ergout = sum(ergout)/size(ergout,1); %averag ERGs
t = (0:1/20000:((length(ergout)-1)/20000)).*1e-3; %create time array in ms

figure
hold on
plot(t,ergout); %uV
xlim([-20 180])

return
```

Figure C.2 Signal averaging and graphing MATLAB program code used for the 30 Hz stimulus ERG

```
function tashfft(data,fs)
% function takes, data set to be fft'd and the corresponding sample
% frequency

L = length(data);
NFFT = 2^nextpow2(L);
Y = fft(data,NFFT)/L;
y = 2*abs(Y(1:NFFT/2+1));
f = fs/2*linspace(0,1,NFFT/2+1); %frequency vector

figure
hold on
title('EPS FFT');
xlabel('Frequency [Hz]');
ylabel('Amplitude');
plot(f,y); %plot fft amplitude vs. frequency
xlim([0 100])
hold off
```

Figure C.3 Fast Fourier Transform calculation and graphing MATLAB program code user during ERG signal processing

Appendix D. Additional Surface Electromyography Results

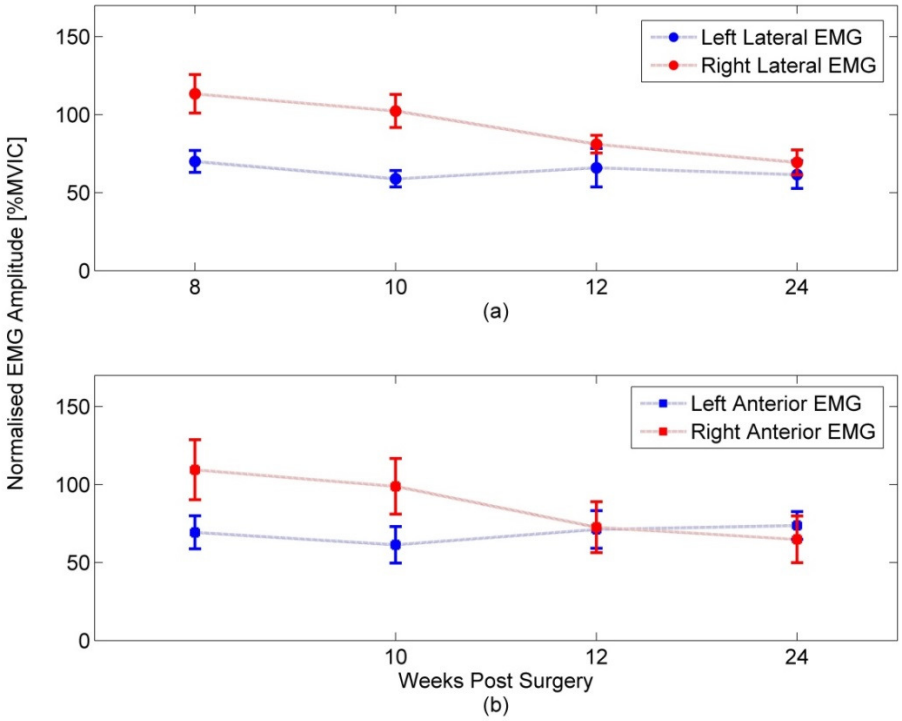

Figure D.1 Comparison of normalised SEMG signals for right (injured) and left (healthy) shoulder muscles during a 60° abduction of the arms

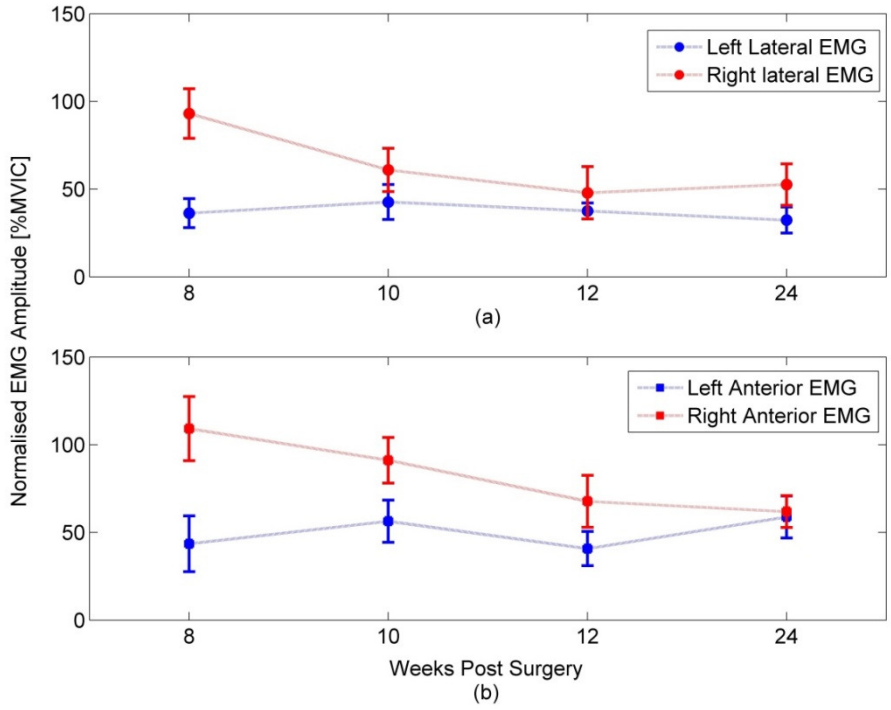

Figure D.2 Comparison of normalised SEMG signals for right (injured) and left (healthy) shoulder muscles during a 60° flexion of the arms

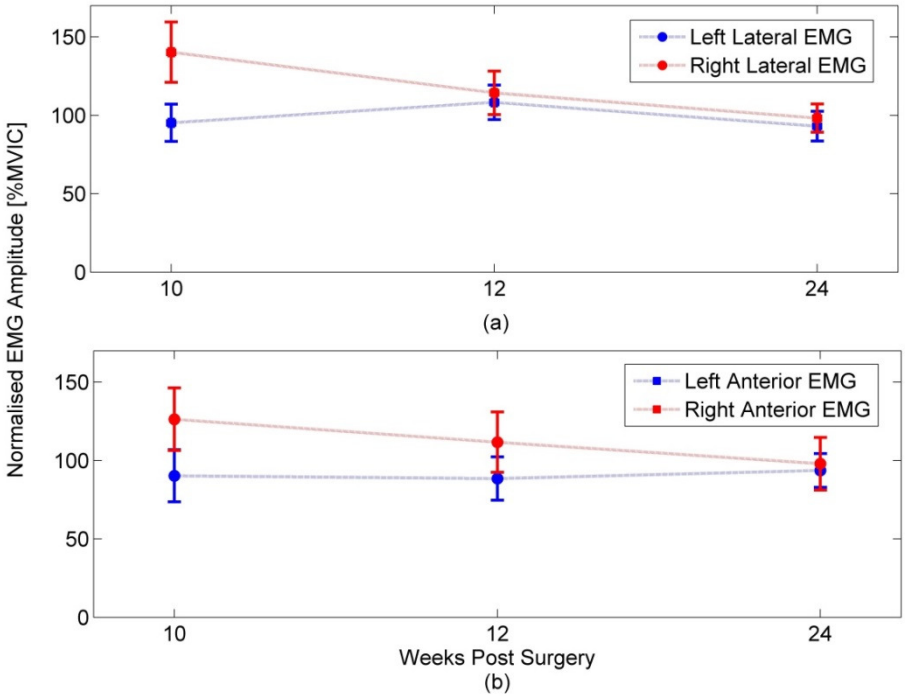

Figure D.3 Comparison of normalised SEMG signals for right (injured) and left (healthy) shoulder muscles during a 90° abduction of the arms

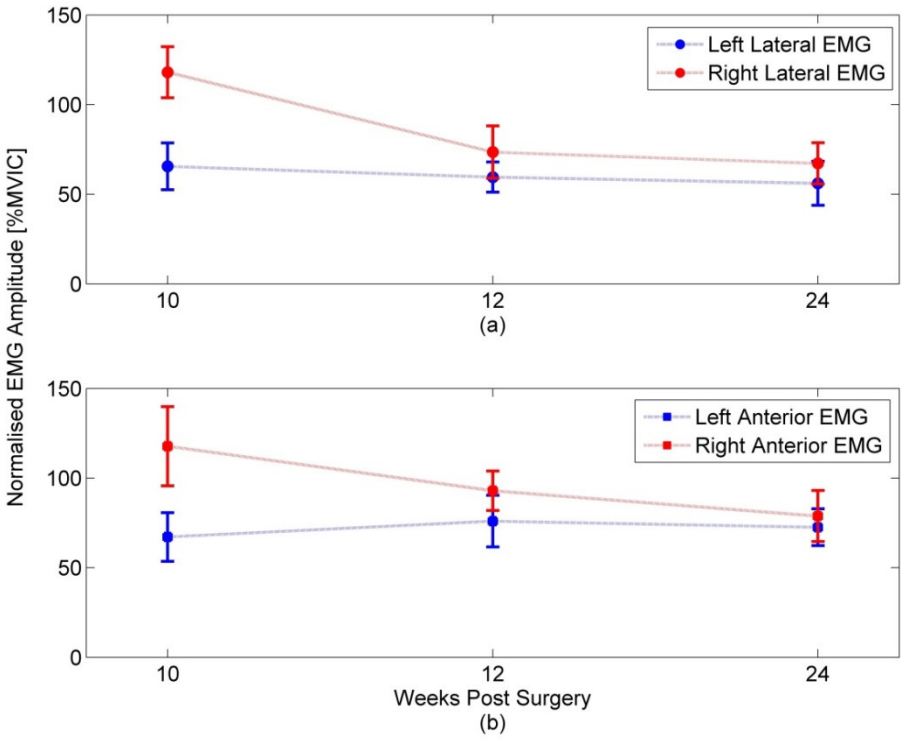

Figure D.4 Comparison of normalised SEMG signals for right (injured) and left (healthy) shoulder muscles during a 90° flexion of the arms

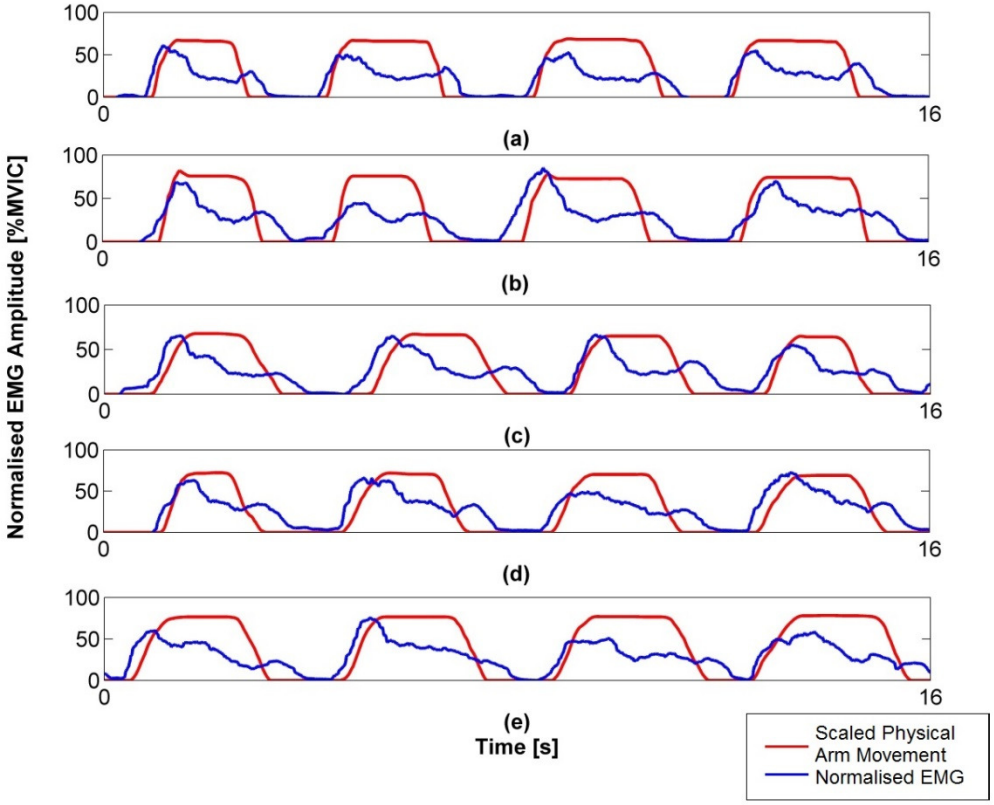

Figure D.5 Left bicep normalised SEMG Amplitudes and physical limb movement to target angles of (a) 18° (b) 36° (c) 54° (d) 72° and (e) 90°

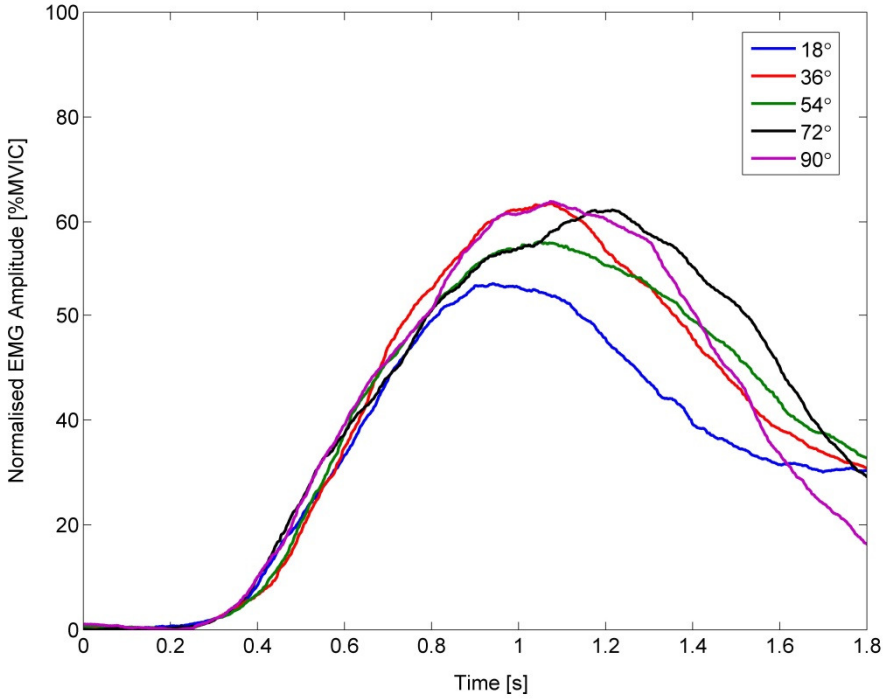

Figure D.6 Right bicep: Averaged RMS EMGs for x10 lower arm movements to each target angle

Appendix E. System Performance Characterisation

Throughout this thesis a variety of sensor systems based on the EPS have been investigated, experimental results have been discussed and in some cases directly compared to industry standard sensing systems. The data observed was presented as descriptive statistics, meaning the metrics used only described the results for the specific set of experiments. These experiments provide preliminary results for which data was modelled. However, this in itself does not provide statistical evidence that the results are true and accurate, and hence further experimental trials would be required in order to interpret the results as significant. This appendix presents methodologies which could be followed for further work on all the discussed sensor systems in order to validate their significance, as well as enable benchmarking against industry standard technologies.

1 Statistical Hypothesis Testing

Statistical hypothesis testing is presented here as a method to validate experimental results achieved by the EPS. Table E.1 below outline the chapters that this method could be applied to and specifies the measurements and metrics that would be used for results verification.

Table E.1 Table outlining the chapters, specific repeated measurements and metrics that would be used to validate the EPS results using a statistical hypothesis test

Chapter	Specific Repeated Measurement	Metric
Three – Electrooculography	Eye-movement series	Gaze position estimation accuracy
Four – Electroretinography	1 Hz, 5 Hz, and 30 Hz ERG measurements	Implicit time measurements (L_a and L_b)

In each experiment results were expressed in terms of means and standard deviations. All of these calculations were based on the assumption that we had a normal distribution of data and the results were true and accurate for the number of experimental data sets that were analysed. In order to validate the system model or hypothesis, and accept that these experimental means are true, a hypothesis test on a larger sample size (number of people) must be carried out. The results can then be tested against the developed hypothesis which is reliant on the initial experimental outcomes [186]. This can be done by the following steps for hypothesis verification:

Step One: Formulate out null and alternative hypothesis (H_0 and H_a) in statistical terms.

H_0: experimental mean is true ($\mu_0 = \mu$)

H_a: experimental mean is false ($\mu_0 \neq \mu$)

Step Two: Set the level of significance, α, which is the probability that we might reject the model results. Alpha is typically set to 0.05, corresponding to a confidence level of 95%.

Step Three: Determine the sample size N, given the model standard deviation from experimental data (σ), required to accurately test the hypothesis:

$$N = \frac{\rho(1-\rho)}{\sigma^2}$$

Where ρ represents the statistical significance we want from our results.

Step Four: Select the appropriate statistical testing model.

For testing experimental means a two tailed test has been chosen, the confidence interval for which is 95% (1-α).

Step Five: Collect the data and calculate the statistic (P-value).

With N trials worth of data, an experimental mean value for each individual can be calculated. The P-value is then determined as the percentage of the resulting means that fall within the 95% confidence interval. Once all trial data has been assessed, the P-value is compared against α to determine if a statistically significant result has occurred.

P-value < α H_0 is accepted as true and statistically significant

P-value > α H_0 is rejected

2 Benchmarking and Quality Assessment

In order to compare the quality of one system against another benchmarking can be employed. Benchmarking is used to measure system performance using specific metrics to quantify errors resulting in a performance evaluation which can then be used to compare similar systems [187, 188]. The table below outlines the specific chapters from this thesis with experiments that would be repeated using benchmarking and statistical analysis to gauge their effectiveness when being directly compared to industry standard systems.

Table E.2 Table outlining the chapters, suggested systems for comparison and metrics that would be used to benchmark using a statistical hypothesis test

Chapter – Measurement Basis (System A)	Suggested Systems / Sensors for Comparison (System B)	Indications of Accuracy
Two – Position Sensing	Video or infrared based tracking system	Absolute hand position inference
Three – Electrooculography	Ag-AgCl electrodes	Gaze position estimation
Four – Electroretinography	Ag-AgCl / DTL fibre electrodes	Implicit time measurements (L_a and L_b)
Five and Six – Electromyography	Ag-AgCl electrodes	Normalised SEMG amplitudes.

Power analysis is applied in order to determine an appropriate sample size and therefore the efficiency of the test with respect to the alternate hypothesis.

Power (efficiency) is determined by the following:

- Alpha level - level of significance (α)
- Effect Size – an estimation of the strength of a relationship (*d*)
- Sample size – number of experimental data sets required (N)
- Variance – squared standard deviation (σ^2)
- Chosen statistical testing model

The aim here is to detect a truly significant event, and there is always an associated risk that this significant event will be missed. The probability of this risk is called a Type II error, also known beta (β). In relation to Type II error, power is define as ($1 - \beta$). In other words, power is the probability of detecting a true significant difference; hence we must aim to design an experiment with a relatively high power ($\geq 80\%$). However, if the test is too powerful, even a trivial difference will be mistakenly reported as a significant one. This type of error is called Type I error (α), this type of error must be kept below 0.05.

For the systems discussed throughout this thesis, the methodology that was discussed in the previous section (Appendix E.1) is proposed. However, in this case, the means of two systems will be compared, such that we can define the following:

Step One: Formulate out null and alternative hypothesis (H_0 and H_a) in statistical terms.

H_0: experimental mean from system A is true ($\mu = \mu_A$)

H_a: experimental mean from system B is true ($\mu = \mu_B$)

Step Two: Set the level of significance, $\alpha = 0.05$.

Step Three: Determine the sample size (N), such that the power ($1- \beta$) will remain above 80%.

Step Four: Select the appropriate statistic testing model.

For testing the experimental means of two different systems or models, a two tailed t-test can be used, the confidence interval for which is 95% ($1-\alpha$).

Step Five: Collect the data and calculate our statistic (P value).

In this case the two systems, A and B, would be run at the same time on the same subject for direct comparison. Again, with N trials worth of data, the experimental mean values for each individual, ascertained with each system, can be calculated. The P-value is then determined as the percentage of the resulting means that fall within the 95% confidence in interval. The P-values of each system can then be compared against one another.

P-value system A < P-value system B H_0 is accepted as more accurate

P-value system A > P-value system B H_a is accepted as more accurate

3 Algorithm Performance Testing for Assistive Technology Applications

Two feature extraction algorithms have been presented in this thesis: first a hand position localisation algorithm in chapter two and second a temporal feature extraction algorithm for identifying and determining intentions based on eye movements was presented in chapter three. To further validate both of these systems an assessment would need to be made of the ability of the algorithms to extract the same information repeatedly from different users, in different scenarios for the same set of features. In other words the algorithm needs to be tested for effectiveness and accuracy. There are several different tests that can be used for this assessment [189, 190]; the F-measure is chosen due to its simplicity in design and interpretation [191]. The F-measure, the number of distinct test cases to detect the first program failure, is an effectiveness measure for program testing strategies. The F-measure considers both precision (*p*) and recall (*r*) of the test to compute the score: *p* is the number of correct events extracted from the algorithm divided by the number of events detected in total and *r* is the number of correct events extracted divided by the total number of events the should have been detected. The resulting F-measure will range between 0 and 1, representing a weighted average of the precision and recall.

In the cases of the position determination algorithm (chapter two) and the EOG feature extraction algorithm (chapter three), a group of subjects would be tested while carrying out the same series of actions; this would be done over a number of trails in order to correctly

validate the experiments. We can then define the following with respect to the output of the feature extraction algorithm observed for each individual under test:

True Positives (TP):	Where the feature has been identified correctly.
False Positives (FP):	Where the feature has been incorrectly identified.
False Negatives (FN):	Where a feature has occurred and not identified.

We can then define precision and recall:

$$p = \frac{TP}{TP + FP} \qquad r = \frac{TP}{TP + FN}$$

The F-measure is then calculated by:

$$F = 2 \times \frac{p \times r}{p + r}$$

An F-score close to one will indicate a high accuracy of the feature extraction algorithms capability to perform in a similar manner across a range of subjects.